12-2020

Chemical Modification and In Silico Validation of Medicinally Privileged Molecular Scaffolds as Kras and SARS-CoV-2 Protease Inhibitors

Precious M. Okwuchukwu
The University of Texas Rio Grande Valley

CHEMICAL MODIFICATION AND *IN SILICO* VALIDATION OF MEDICINALLY PRIVILEGED MOLECULAR SCAFFOLDS AS K-RAS AND SARS-COV-2 PROTEASE INHIBITORS

A Thesis

by

PRECIOUS M. OKWUCHUKWU

Submitted to the Graduate college of
The University of Texas Rio Grande Valley
In partial fulfillment of the requirements for the degree of

MASTER OF SCIENCE

December 2020

Major Subject: Chemistry

CHEMICAL MODIFICATION AND *IN SILICO* VALIDATION OF MEDICINALLY PRIVILEGED MOLECULAR SCAFFOLDS AS K-RAS AND SARS-COV-2 PROTEASE INHIBITORS

A Thesis
by
PRECIOUS M. OKWUCHUKWU

COMMITTEE MEMBERS

Dr. Debasish Bandyopadhyay
Chair of Committee

Dr. Javier Macossay-Torres
Committee Member

Dr. Ahmad Hassan
Committee Member

Dr. Tulay Atesin
Committee Member

December 2020

ABSTRACT

Okwuchukwu, Precious M., Chemical Modification and *In Silico* Validation of Medicinally Privileged Molecular Scaffolds as K-Ras and SARS-CoV-2 Spike Protease Inhibitors. Master of Science (MS), December 2020, 138 pp, 10 tables, 69 figures, references 95 titles.

Coronavirus disease was declared a global pandemic by WHO in March 2020, cancer is the second leading cause of death by a disease. Several scientists around the world are working relentlessly to discover an effective remedy to eradicate these deadly diseases. A natural polyphenol (magnolol) has been isolated from a tree *Magnolia grandiflora* (family *Magnoliaceae*) found on UTRGV campuses. This research is focused on design of a series of chemically modified sulfonyl derivatives based on the isolated magnolol framework and other medicinally privileged molecular scaffolds framework that can effectively bind to the COVID-19 main protease, SARS- CoV-2 3CL protease and K-Ras protease (PDB ID's: 6LU7, 6M2Q, 4EPV, respectively). In silico studies was conducted to identify lead compounds of the series, determine protein-ligand interactions, physicochemical properties and druggability of the new compounds. On appropriate biological evaluations, these novel compounds may possibly find pharmacological applications as antiviral agents against COVID-19 disease or as anticancer agents.

ACKNOWLEDGEMENT

I wish to express my sincere appreciation to the graduate college for presenting me with the Presidential graduate research assistantship (PGRA) award, to Dr. B. Connie Allen, Interim Chair, Chemistry Department for her relentless assistance during this project. I wish to express my deepest gratitude to my mentor, Dr. Debasish Bandyopadhyay for his invaluable support, guidance, constructive advice, patience, and encouragement throughout this research.

I would like to recognize my thesis committee members; Dr. Hassan Ahmad, Dr. Tulay Atesin, and Dr. Javier Macossay-Torres for their meaningful contribution and practical suggestions. I want to also thank Dr. Daniel Wherritt for helping me with running the NMR. Thanks to my family for all their support and encouragement. Thanks to my dad for being my daily inspiration.

Finally, I want to sincerely thank Omar Espino for all his valuable time spent helping with the 3D structures and teaching me how to perform molecular docking. To all my lab mates, you have all been amazing, Thank you for all your help!

TABLE OF CONTENTS

Page

LIST OF TABLES

Page

LIST OF FIGURES

Page

BACKGROUND

Medicinal plants possess a wide range of phytoceuticals which are commonly used for the treatment of several human ailments, this has kept them relevant for several decades. “Phyto” is a Greek word that means plant. Phytochemicals are described as a large group of compounds obtained from plants. Phytochemicals can be classified into nutraceuticals, toxins, addictives (narcotics), phytoceuticals, and biological inactive compounds.

Phytoceuticals and nutraceuticals are important molecules. They possess a positive therapeutic effect. Since the beginning of civilization, phytochemicals have played essential roles in the battle against several diseases as well as in promoting the health benefits of humans and animals. The structural and medicinal investigation of natural products has led to a surge in discovery, research, and development of final drug entities. Presently, about 25% of medicines are derived from nature. Between 1940 and 2014, FDA approved 175 anticancer small drug molecules. Out of 175, about 131 molecules (75%) were totally non-synthetic molecules. This suggests that the chemical investigation and modification of natural products are authentic routes for the and efficient in the efficient discovery of novel active pharmaceutical ingredients (APIs) (1). Several medicinal plants have been left unexploited due to the emergence of modern synthetic medicines. Given the rapid surge in the rate of fatalities and deterioration of human health, it has become obvious that modern medicine cannot be fully depended upon. Alternative sources need to be exploited to develop better pharmacological therapeutics that have improved efficacy and are

readily available. Accordingly, efforts have been made to evaluate the possible therapeutic effects of some biological compounds through the efficient exploitation, careful isolation, and characterization of their active agents. Of particular interest are the active compounds present or obtainable from two medicinal plants (*Magnolia grandiflora* and *Aloe barbardensis*). The chemical modification and *in silico* study of a polyphenol-magnolol and other medicinally privileged scaffolds 4- aminoquinoline and amantadine is reported herein.

CHAPTER I

INTRODUCTION

Plant polyphenols have gathered a lot of interest because of the valuable properties they possess. *Magnolia* species such as *Magnolia grandiflora*, *Magnolia acuminata*, *Magnolia officinalis* (Houpo in Chinese) (2), *Magnolia virginiana*, *Magnolia macrophylla*, all belonging to the *Magnoliaceae* family, the extracts and pure compounds obtained from parts (leaves and seeds) of this species, has been reported to have several ethnomedicinal uses in North America.(3) *Magnolia grandiflora* (belong to family *Magnoliaceae*, genus: *Magnolia)* is a medicinal plant with different species grown all over the world, its extracts have found various therapeutic applications such as anti-inflammation, antimicrobial, antioxidation, antispasmodic, antidiabetic, neuroprotective, antidepressant, anticancer properties etc (3). The magnolia plant family is popular in North America because of its numerous pharmacological properties, specifically, in a native tribe called *Talauma* in Mexico, *Magnolia* is frequently used to treat various anti-inflammatory diseases such as extreme fevers and rheumatism (3). In Asian countries, the ethanol extract of the bark of *Magnolia officinalis* usually the major constituent found in herbal formulations like the Saiboku-to and Banxia-houpo preparation, has found several therapeutic applications in traditional medicine for the treatment of depression, anxiety, neurosis, stroke allergies, and gastrointestinal disorders (4). Most importantly, in China's traditional and modern medical practice, it has been continuously prescribed for the treatment of asthmatic cough, pains, indigestion, and distention of the abdomen (2,5). *Magnolia species* are also currently in use in Japanese Kampo medicine as

anti-inflammatory agents (3). Additionally, Japan, Korea, China uses stomachic herb which constitutes of the methanolic extract obtained from the stem bark of *Magnolia obovata* as a traditional remedy for problems of the digestive system. The methanolic extract obtained from the stem bark of *Magnolia obovate* has also been evaluated for its antifungal activity against *Trichophyton mentagrophytes (*6*).* Thus, due to these numerous properties, particularly, their antioxidant property phenolic compounds (e.g. magnolol) obtained from magnolia species are largely exploited in pharmaceutical, agricultural, and cosmetic industries (7).

Cancer is the second leading cause of death globally, thus, a global health concern. According to WHO, Global cancer statistics, and GLOBOCAN there have been approximately 17 million new cancer cases and 9.5 million deaths (https://gco.iarc.fr/today/data/factsheets/cancers) due to various kinds of cancer in 2018 alone. This has led to a global driven investigation and research to discover promising treatment regimens and curative agents. Although several treatment modalities (surgery, chemotherapy, radiation) and chemotherapeutic agents have been developed to help combat cancer, the chemotherapeutic agents still pose several challenges and side effects such as renal dysfunction, destruction of bone marrow, vomiting, development of CVD's, and development of resistance. These adverse effects in most cases cause cancer resurgence and advancement, thus, limits the applications of these therapeutics (8). Hence, finding a treatment regimen or possibly a curative agent with fewer side effects and better efficacy is of utmost importance.

In March 2020, COVID-19 was declared a global pandemic by the center for disease control (CDC). As of December 12, 2020, approximately 288,000 deaths (cdc.gov) have been recorded in the United States alone. Coronaviruses are enveloped, single-stranded, positive-sense RNA viruses having large-scale viral genomes. In February 2020, the novel highly virulent strain

2019-nCoV was changed to severe acute respiratory syndrome coronavirus 2 (SARS-CoV-2), family *Coronaviridae*, genus *Betacoronavirus* (9). (SARS-CoV-2) enters the host by employing spike protein to bind to cell surface receptor angiotensin-converting enzyme (ACE2), to the host cell. The virus then fuses by proteolytic activation, causing the cleavage of the S1 subunit and conformational change of the S2 subunit of the spike protein. Thus, there is an urgent need for potential therapeutic antiviral agents to target SARS-CoV-2 structural proteins responsible for virion assembly, envelope formation, and pathogenesis (10).

CHAPTER II

LITERATURE REVIEW

Magnolol is commonly known as 5,5'-diallyl-[1,1'-biphenyl]-2,2'-diol (IUPAC name is 2-(2-hydroxy-5-prop-2-enylphenyl)-4-prop-2-enylphenol) is a neolignan, an organic compound which is one of the primary biologically active constituents found in *Magnolia grandiflora* matured green seed cones. Magnolol is a flexible, hydroxylated biphenyl whose pharmacophore consists of two aromatic rings bridged by one C-C bond (11,12). This characteristic structural feature contributes to the activation of diverse interactions with several active binding sites present on the protein surface thus, magnolol can act as an effective ligand for a variety of disease-causing molecules, through modulation of binding affinity in several proteins (13,14). This makes it a great chemical modification candidate. In addition, its structural features, two hydroxyl groups, and two allylic side chains attached to a biphenolic moiety could be the reason for its potent activity (15). Magnolol possesses several pharmacological applications such as antioxidant, smooth muscle relaxant, anti-epileptic, antidyspeptic, cardiovascular diseases, cytotoxic activities, hepatoprotective, anti-inflammatory, antiasthmatic, antidiabetic, antidepressant, Antimicrobial (16) etc.

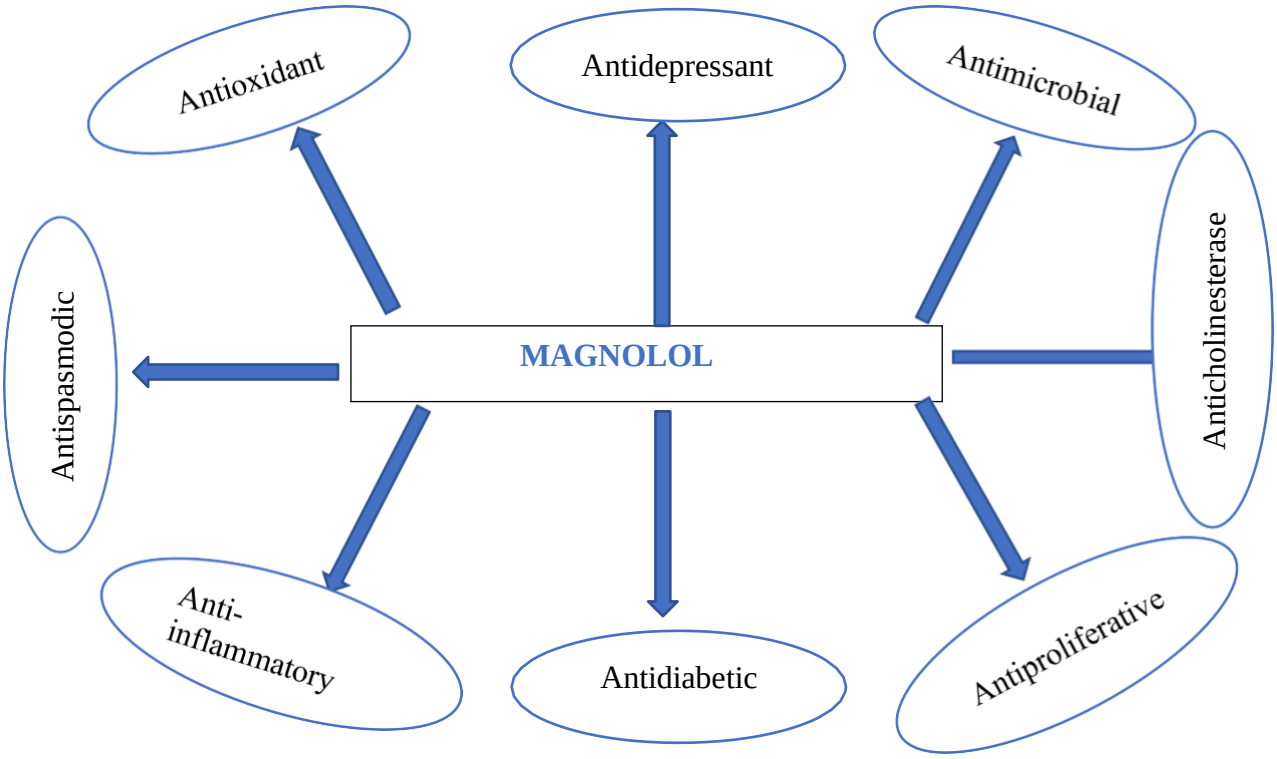

Figure 1. Different therapeutic applications of magnolol

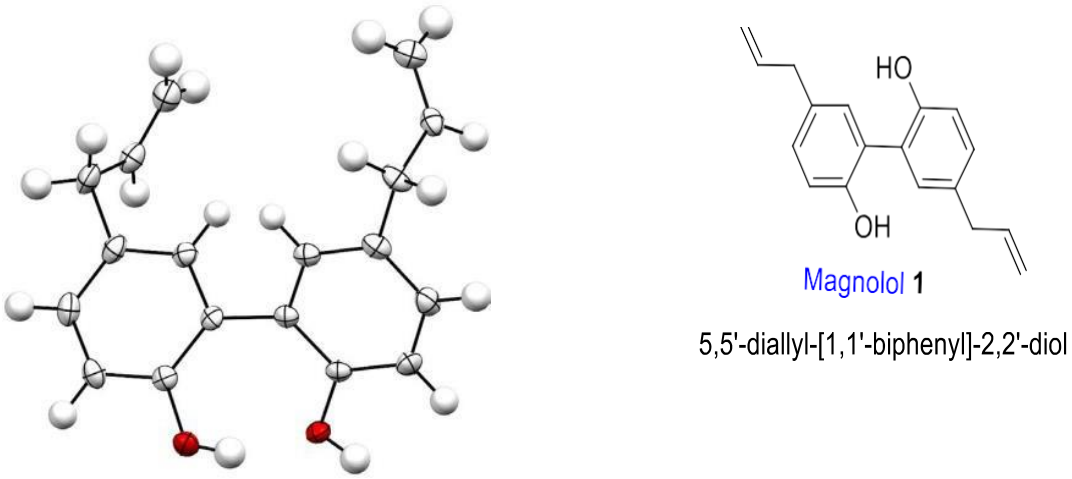

Figure 2. X-ray crystallographic structure of magnolol

Previous studies have shown the effects of magnolol when targeted to various molecular proteins involved in the regulation of the cell cycle and its cytotoxic activities (induces differentiation and apoptosis, suppresses angiogenesis, counters metastasis, and reverses multi-drug resistance). One study reported that magnolol has deleterious effects on gall bladder carcinoma cell lines. It works by blocking cell progression at the G0/G1 phase, inhibits GBC-SD cancer cell line with IC_{50} of 20.5± 6.8 µmol/L after 48 hours, it also activates mitochondrial related apoptosis by the up-regulation of p53 and p21 protein levels and downregulating cyclin D1, CDC25A, and cDk2 protein levels (17). In cholangiocarcinoma, magnolol effectively inhibits cell invasion, migration, cell growth, and downregulates expression of Cyclin D1, p-p65. It arrests cell cycle at G1 Phase and proliferates cell nuclear antigen, matrix metalloproteinases 2,7, and 9 (18). Although magnolol has a wide range of pharmacological activity, it has poor water solubility and poor bioavailability.

Thus, phytochemical investigation involving the chemical modification of magnolol is focused on carefully transforming the different reactive sites (primarily, the phenyl hydroxyl groups) present on magnolol with different ring sizes and substituents that could optimize drug-protein interaction, enhance efficacy, increase polarity, bioavailability, and hopefully, reduce side effects. The subsequent druggability of the novel magnolol analogs synthesized is determined by an energy docking technique known as molecular docking.

Amantadine, a synthetic tricyclic symmetric amine is an antiviral drug that inhibits viral replication especially myxoviruses such as influenza A viruses (19). It possesses an adamantane molecular scaffold (looks like a Packard structure). It is commonly known as adamantine, IUPAC name- adamantan-1-amine. Amantadine exerts its antiviral activity against influenza A viruses by binding directly to the viral M2 ion channel of the matrix protein, thereby inhibiting uncoating and

replication of the virus (20). Also, it has been reported that has a significant capacity to induce sustained biochemical antiviral activity in patients (18%) diagnosed with the hepatitis C virus but do not respond to monotherapy interferon (IFN)-α (21). The ability of amantadine to cross the endosomal membrane, disrupt the hydrogen bridges formed by Ala 30 and Gly 34, stop the inflow of proton into the virion thereby inhibiting the discharge of viral nucleus into the cell has made it a very important antiviral agent (22).

Amantadine and rimantadine are the first antiviral agents developed (in 1964) for humans. Some hypothesis studies report that amantadine and derivatives could be effective against the viral load of SARS-CoV-2 by inhibiting replication of the virus through down-regulation of cysteine endosomal proteases- Cathepsin L (CTSL) and breakdown of lysosomal pathway (23). Another hypothesis study suggests that amantadine inhibits the viroporine channel of coronavirus-19 (COVID-19) which impedes the discharge of the viral nucleus into the cytoplasm (22). Although, amantadine has great application, a great challenge associated with its use, is that the influenza virus becomes insensitive and then mutates, thereby causing the amino acid present on the ion channel of M2 protein to change thus, developing resistance. To fix this, solid-state NMR studies propose that compounds larger than rimantadine, could have better efficacy to block the amantadine-resistant influenza viruses. Another strategy would be to incorporate substituents having active functional group (amino acids, peptides, etc.) into amantadine scaffold, this could help disrupt protein transport (24). Thus, efforts are made to chemically modify the primary amine group and secondary alcohol group present on 3-amino adamantanol and molecular docking is performed to analyze protein-ligand binding affinity.

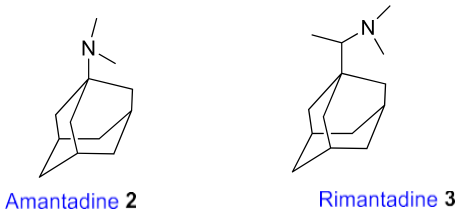

Figure 3. Structure of first commercially available adamantane derivatives

Chloroquine and hydroxychloroquine are 4-amino quinoline derivatives. They are synthetic drugs obtained from the bark of the cinchona tree and are most widely used as antimalarials in tropical countries (25). Chloroquine has also been reported to inhibit viral replication of influenza A virus (26), HIV-1 (currently in clinical trials), Herpes simplex virus (27). Recently, chloroquine was found to inhibit the replication of SARS-CoV-2 *in vitro* Vero E6 cells with IC50 8.8 µM (27). Hydroxychloroquine, an analog of chloroquine has less drug-drug interaction and fewer side effects (28). Results from *in vitro* studies of hydroxyquinoline show that hydroxyquinoline (EC_{50} 6.14, 0.72 µM for 24 and 48hours) has a better antiviral effect on SARS-CoV-2 than chloroquine (EC_{50} 23.90, 5.47 µM for 24 and 48hours) does (28). The mechanism of action of both drugs towards inhibition of SARS-CoV-2 has not been fully understood, previous studies propose that they alter PH at the cell surface, inhibit replication, the fusion of virus complex to host cells, virus assembly and release, etc (29). This suggests that both drugs possess antiviral activity against SARS-CoV-2. Although hydroxyquinolones have a better safety profile and lesser drug-drug interactions, the presence of the primary alcohol group poses challenges this has limited its use as a treatment for COVID-19. Such challenges include cardiotoxicity (25), retinopathy, and neuropathy. Thus, attempts have been made to chemically modify the primary alcohol group on the amino quinoline nucleus to mitigate these challenges and improve efficacy.

CHAPTER III

(A). CHEMICAL MODIFICATION OF POLYPHENOL MAGNOLOL

Novel magnolol derivatives having potent activity as anticancer agents

i. Non-small cell lung cancer (NSCLC)

Malignant lung cancer is one of the leading causes of death related to all cancers (30). NSCLC has a five-year survival rate of 16%, thus, a lot of focus has been directed to its treatment (31). To overcome the drawbacks associated with the use of magnolol, several magnolol derivatives were synthesized by reacting them with different heterocycle rings. Subsequently, an investigation for antiproliferative activity was carried out on NSCLC cell lines (HCC827, H1975, and H460) using MTT assay. Compounds **4**, **5** and **6** showed promising antiproliferative activity for all three cell lines- for HCC827 (IC_{5O} value- 6.80 µM 4.87 µM, 5.01 µM) for H1975 (IC_{5O} value- 7.12 µM, 4.82 µM, 5.61 µM) and for H460 (IC_{5O} value- 5.92 µM, 5.71 µM, 5.98 µM). showed better IC_{50} values than magnolol and honokiol which were used as control; respectively. Further, *in vitro* antiproliferative assay was conducted on EGFR wild type cell lines, EGFR mutation cell lines, and KRAS mutation cell lines, these compounds showed 4-8-fold better activity than magnolol. SAR studies suggest that substitution of the H-atom at C-3 position with a nitrogen heterocycle, for example, a piperazine ring having an oxyethyl group attached to a nitrogen atom or a piperidine ring having an amino group could improve broad-spectrum antiproliferative activity. Upon solubility evaluation, **4**, **5**, and **6** showed better solubility than piperitylmagnolol, thus could be formulated as an oral anticancer drug. This solves the problem of poor aqueous solubility. On the arrest of cell cycle and induction of apoptosis investigation in H1975 cells, the new compounds exhibited a concentration-dependent arrest at the G0/G1 phase of the cell cycle, and a dose-

dependent (0-20μM) cancer cell apoptosis was induced by **4**, **5**, **6** with apoptotic rates ranging from 16.49-76.20%, 16.49-97.60%, and 16.49-95.90% respectively in contrast to the apoptotic rate 51.77% exhibited by honokiol at 40 μM. *In vivo* evaluation using C26 xenograft model was conducted on all three compounds, **6** showed the best tumor growth inhibition (47.9%) at 100mg/kg oral administration with fewer to no side effects in contrast with honokiol which only showed tumor growth inhibition of 16.7% at the same dose. **6** on iv administration dissolved readily in pure water and produced no vascular irritation. **6** on per os (oral) treatment showed no significant decrease in the mice's body weight, less toxicity, no abnormality, and enhanced solubility. Thus, **6** has great potential as an oral antitumor agent. More investigation is highly recommended (32).

ii. Suppression of cancer cells by autophagy induction.

Deaths by cervical cancer and breast cancer are continuously on upward progression despite various advancements in chemotherapy and treatment regimens, this is majorly due to aggressive resistance of tumor cells and unpleasant side effects (33,34). Autophagy, also known as autophagocytosis is a cellular process that involves the breakdown of damaged/defective cytoplasmic components, organelles, cytoplasmic proteins in the lysosome. This aids in the renewal of certain vital organelles and helps the cell to achieve its metabolic needs (35). In this study, mannich base groups were incorporated at the ortho position of the phenolic OH group present on C-2' thus, the phenolic OH group is left untouched. *In vitro* antineoplastic activity, SAR, and mechanism of action by autophagy stimulation of the novel Mannich magnolol derivatives were investigated against human cell lines (T47D, A549, MCF-7), MTT assay was used and cisplatin was employed as a positive control. Of all the chemically modified compounds, **7** showed excellent antiproliferative activity especially on T47D cells (IC_{50} 0.91 μM) where its cytotoxicity activity greatly improved to 76.1 fold, this is in contrast to parent compound magnolol with IC_{50} 69.32 μM exhibited very low cytotoxic activity on T47D cells and almost no activity

(IC_{50} ≥80 μM) on A549, MCF-7 cells. Also, compound **7** showed better selectivity to carcinogenic cells over normal healthy cells than positive control cisplatin. SAR studies indicate that the morpholine ring and presence of 3,4,5 -tri-OCH_3 substituents are responsible for the potentiated antiproliferative activity of **7**. On further evaluation, **7** induced a dose dependent conversion of protein light chain 3-I to protein light chain 3-II (important for autophagy induction), also a sharp increase (57.94%) in autophagy dependent cell apoptosis is observed on co-administration of **7** and autophagy agonist rapamycin (RAPA). Compound **7** showed excellent anti-proliferative results thus, further investigation is encouraged as this could lead to the discovery of potent and selective anti-neoplastic agents (36).

As potent allosteric modulators of $GABA_A$ receptors

γ-aminobutyric acid (GABA) is one of the most inhibitory agents of the central nervous system (37). It is responsible for the activation of $GABA_A$ and $GABA_B$. $GABA_A$ acts as an ionotropic receptor responsible for controlling the influx of chloride ions, this makes it a great target of many antidepressants, anxiolytics, muscle relaxants, and anticonvulsive drugs (38). Recently, $GABA_A$ receptors have been discovered to possess binding sites for endocannabinoid 2-arachidonoylglycerol (2-AG) and the endocannabinoid metabolite N-arachidonoylglycine (NAGLY) (39,40). Magnolol and its metabolite tetrahydromagnolol act as potent partial agonists, they interact with cannabinoid receptors and potentiate $GABA_A$ currents. In this study, structural analogs of magnolol and honokiol were synthesized and investigated. Compound **8** having ethyl, and hexyl residue exhibited the most potentiation of $GABA_A$ receptor in the magnolol analog series. As a positive allosteric modulator (PAM), **8** showed concentration-dependent effects, with potentiation >1000% at a maximum concentration of 10μM. Due to its high lipophilicity, further concentrations could not be investigated. With a 2-6% maximal effect on GABA at 10μM, **8** was found to be a weak direct agonist of $GABA_A$ receptors thus, could be categorized as ago-allosteric

modulators. To search for allosteric binding sites, investigations on different subunits of $GABA_A$ receptors were conducted on magnolol analog **8**. A change in the α-subunit caused some significant changes in its potentiation activities, interchanging β_2 for β_1 (decrease) or β_3 (increase) affected the potentiation effects thus, the α-subunit and the nature of β-subunit are important for binding of the compound. The γ-subunit is not important for interaction with the allosteric moderator as no change in effects was observed when replaced/interchanged. After investigations, minor effects of **8** as potent allosteric modulators on BZD receptors showed that they do not interact with the benzodiazepine site. Compound **8** also exhibited an ancillary cannabinoid (CB_1) agonist activity of Ki CB1: 0.386 μM, these results qualify **8** for further investigations as an anti-convulsant or spasms treatment. SAR study suggests that one alkyl group (ideal group-propyl), a direct connection of phenyl rings, and a free phenolic group which is para to C2- or a C3- alkyl group is essential for activity, the pattern of substitution accounts for $GABA_A$ potentiating activity and selectivity of the CB receptors. Methylating the OH-groups present in magnolol led to a loss of activity irrespective of the position at which the methoxy group is placed. Encouraging results obtained from this potent allosteric modulator of $GABA_A$ receptors suggests further *in vivo* evaluation, could lead to the development of potential novel anxiolytics, hypnotics, and muscle relaxant drugs (41).

As anti-microbial agents

The surge in bacterial resistance has become a global concern especially the bacterial infections caused by *Vancomycin resistant enterococci* (VRE) and *Methicillin resistant staphylococcus aureus* (MRSA) (42–44). These causative agents are life-threatening especially to immunocompromised patients such as surgical patients, patients living with HIV, and other

diseases. Thus, it is important to develop novel classes of antimicrobials insusceptible to multidrug resistance (MDR). Magnolol derivatives were synthesized by Suzuki coupling reaction catalyzed by palladium and evaluated *in vitro* for antimicrobial and antiproliferative activity using ciprofloxacin and erythromycin as standards. Most of the derivatives showed outstanding antibacterial activity against Gram-positive bacteria S*taphylococcus aureus ATCC, MRSA 15187,* and *Vancomycin-resistant enterococci* (*VRE)* but compound **9** showed the highest activity with MIC of 2, 1 µg/ml for *S. aureus ATCC, MRSA 15187* respectively and 1 µg/ml for *VRE* and MBC values of 2, 1 µg/ml for *S. aureus ATCC, MRSA 15187* respectively and 2 µg/ml for *VRE.* This high activity could be attributed to the presence of alkyl groups such as butyl, propyl groups, and substitution of halogens on the phenyl rings (-dibromo substitutions show the highest activity). The novel magnolol derivatives were also evaluated for antifungal activity, **11** and **12** showed the best activity (MIC values 64 and 128 µg/ml) respectively against *Candida albicans ATCC 90029* and *Aspergillus fumigatus LSI-II* (MIC values 32 and 64 µg/ml). This significant result could be due to the presence of an allylic side chain. Upon anti-proliferative study, compound **10** possessing dihalo (-diiodo) and alkyl (butyl) substituents showed the best activity on MOLT-4, HL-60, and PC-3 cell lines (MIC values 10, 2, 2 µM respectively). On further investigation, the mechanism of action of these newly synthesized derivatives was discovered to be induced apoptotic cell death using DNA laddering and flow cytometric assay. Hence, alkylated halogen magnolol analogs synthesized showed outstanding antibacterial and antiproliferative activities greater than the parent compound magnolol (45).

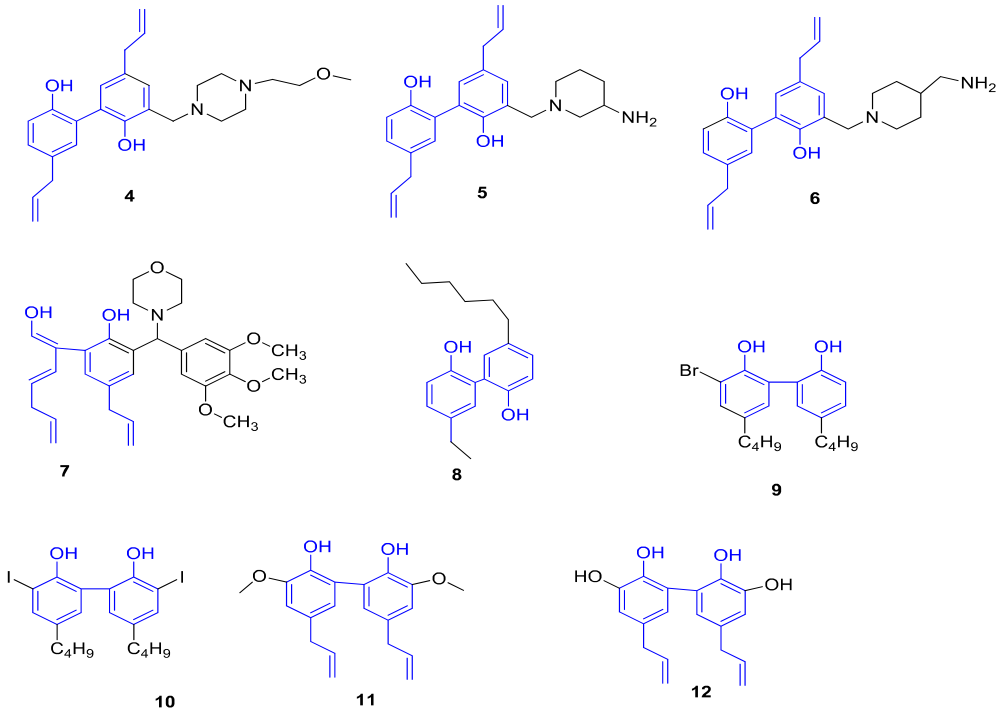

Figure 4. Diverse biologically active magnolol derivatives

CHAPTER III. (B). CHEMICAL MODIFICATION OF MEDICINALLY PRIVILEGED SCAFFOLD 4-AMINO QUINOLINE

Neurogenerative diseases

Uncommon infectious pathogen-prion protein (PrP) is the primary cause of neurogenerative diseases (transmissible spongiform encephalopathies) manifested in humans and animals. The progression of this disease depends on the conversion of PrP^{c} to its abnormal isoform, PrP scrapie PrP^{sc}. Therefore, novel compounds with the ability to prevent this conversion and inhibit PrP aggregation are important. Compound **13** (4-amino-7-chloroquinoline) and **14** (N-(7-chloro-4-quinolinyl)-1,2-ethanediamine) showed excellent inhibitory activity against $ShaPrP^{109-149}$, both compounds exhibited a 90% inhibitory activity (IC_{50} 8.4, 7.9% for compounds **13** and **14**

respectively) at concentration 1.0 µM. SAR analysis suggests that the presence of a primary amine group might be necessary for activity (46).

Anti-malarial

Malaria is a parasitic disease prevalent in tropical and subtropical regions. It is caused by protozoan parasites (genus *plasmodium*) *plasmodium falciparum, P. ovale P.vivax, P. malariae.* Approximately 1-3 million patients die from malaria (WHO) due to the lack of adequate treatment. Aminoquinolines such as chloroquine has been the first-line drug malaria treatment but due to the development of resistance and the adverse effects associated with them, their use has been limited (47). 4-amino-7-chloroquinolines were chemically modified by attaching substituents with small heterocyclic systems such as thiazolino-4-one to the lateral amino side chain, then their antimalarial activity is evaluated *in vitro* against *P. falciparum NF*-54 strain, their antimalarial properties were significantly improved. Compound **15**- 2,3-dihydro-benzo[e][1,3]thiazin-4-one having 4-chlorophenyl substitution on C-2 position showed the best activity (IC_{50}; 0.013 µM, MIC; 0.26 µM) higher than that of the chloroquine (IC_{50}; 0.039 µM, MIC; 4.72 µM). On *in vivo* evaluation against *P.yeoli* infection in swiss mice, compound **15** showed 81% suppression of *P.yeoli* infection after four days of administration at a dose of 30mg/kg. Biochemical studies show that **15** exhibits its antimalarial activity by forming a complex with hematin, thus, inhibiting hemozoin formation. These results open a novel strategy for developing new antimalarial drugs (47).

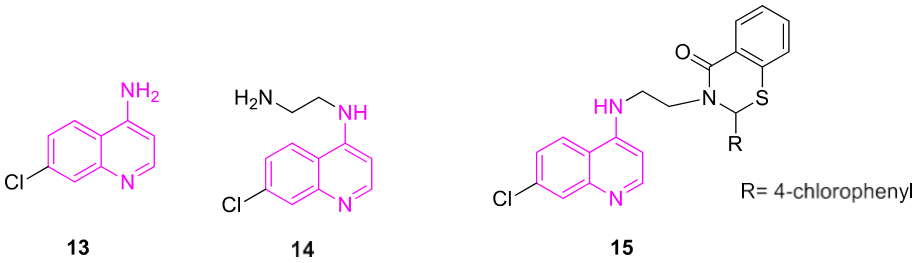

Figure 5. Diverse biologically active 4-aminoquinoline derivatives

CHAPTER III. (C). CHEMICAL MODIFICATION OF MEDICINALLY PRIVILEGED SCAFFOLD AMANTADINE

Trypanocidal activity

African trypanosomiasis (sleeping sickness) is a deadly disease prevalent in the sub-Saharan region of Africa, it is caused by protozoa *Trypanosoma brucei* (genus*; Trypanosoma*) and transmitted by a tsetse fly bite, blood transfusion, congenital transmission. This extracellular parasite could replicate and travel into the bloodstream of humans and animals, it advances to an acute stage when the parasite crosses the blood-brain barrier (BBB), this could cause irreversible neurological damage (can lead to coma or death). Clinical manifestation includes cardiac, kidney, and endocrine disorders, etc. Adamantane derivatives are widely known for their antiviral activities, thus more derivatives were synthesized and studied for their activity against *Trypanosoma brucei form* found in the bloodstream. Adamantane derivative, Compound **16** with a guanylhydrazone analog and a 1-alkyl side chain on C10 showed much better activity with IC_{50}; 0.009 µM and IC_{90}; 0.11 µM when compared to amantadine and rimantadine (IC_{50} and IC_{90}; >132.4 µM for amantadine and IC_{50}; 7.04 µM and IC_{90}; 13.97 µM for rimantadine). **16** is believed to work by disrupting a localized ion channel on the membrane of the parasite. With this excellent result,

exploration of adamantane derivatives could lead to new drugs for combating the lethal sleeping sickness disease (48).

Antiviral activities

Epizootic virus avian influenza A is responsible for several outbreaks in Southeast Asia, it causes an acute infection: pneumonia (inflammation of air sacs in the lungs). Amantadine and rimantadine are adamantane derivatives known for their specific activity against influenza A virus, they work by disrupting the M2 ion channel transport (49). Over the years, their use has been limited due to the development of resistance. Thus, there is a need for more amantadine derivatives with improved activity and insusceptible to resistance. 1,2-annulated adamantane derivatives with five-membered heterocyclic derivatives were synthesized and their *in vitro* anti-influenza virus A (H3N2) activity in MDCK cells was analyzed. Compound **17** with a pyrrolidine ring showed the best antiviral activity (IC_{50}; 0.46 µM, MCC; 94 µM) with a selectivity index (SI) of 200. **17** showed a 4-fold greater potency than amantadine and rimantadine (IC_{50}; 2.00 µM and 0.36 µM), respectively. SAR studies indicate that changing the position of the amine nitrogen from the 2-adamantyl carbon and having zero substitution on the pyrrolidine ring improves antiviral activity. Compound **17** has the same mechanism of action as amantadine and rimantadine (49).

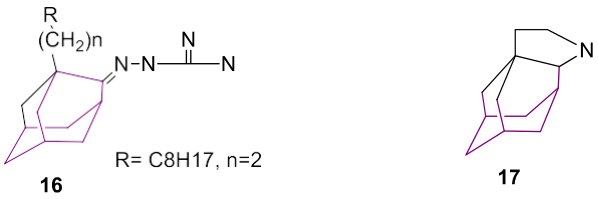

Figure 6. Diverse biologically active adamantane derivatives

CHAPTER IV

IN SILICO DESIGN OF MAGNOLOL DERIVATIVES

In silico design and the computational study was performed to predict the activities of the novel DBMGPO, DBADAPO, DBQPO, DBACPO series on severe acute respiratory syndrome coronavirus 2 (SARS-CoV-2) spike protein (PDB IDs- 6M2Q and 6LU7) and KRAS cancer protein. The ligands were prepared for docking by using Pymol, Avogadro, and AutoDock tools for energy minimization and conversion of the 3D PDB structures to pdqt files. Second, the target proteins, SARS-CoV-2 spike protein, and KRAS protein were prepared for docking (using Pymol and AutoDockTools-1.5.6) with the readied ligands. For the protein-ligand docking simulation, electrostatics was computed, the suitable grid box and potential docking parameters were determined manually with the guide of a chimera tool known as Advanced Poisson-Boltzman Solver (APBS). Finally, protein-ligand docking was performed using AutoDock Vina, a molecular mechanics force field (MMFF).

After the completion of the docking simulation, docking scores were exported from the log file, the best dock poses were extracted from the output file created by AutoDock vina, converted to pdb format, and then fused with the structure of the target proteins on Maestro 11.8, a docked protein-ligand complex in .pdb format was generated. Finally, the protein-ligand complex was used to determine the different hydrophobic interactions, non-covalent interactions like halogen-bond, hydrogen bond, etc. The Results seemed very promising, based on this there was heightened

interest for further modification. Different tables showing the binding affinity and diverse interaction seen in the protein-ligand complex of the proteins of interest are described below.

DBMGPO Series [PDB code 6LU7COVID-19 main protease in complex with an inhibitor N3

Code	**Structure**	**Binding energy (6LU7)**
Magnolol	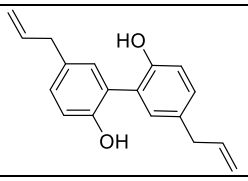	-6.4
DBMGPO-1	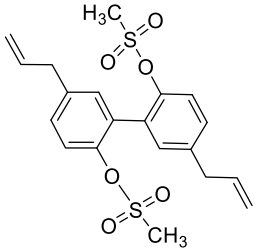	-5.8
DBMGPO-2	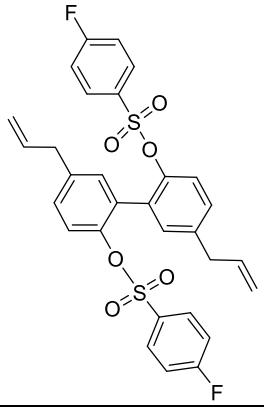	-5.9
DBMGPO-3	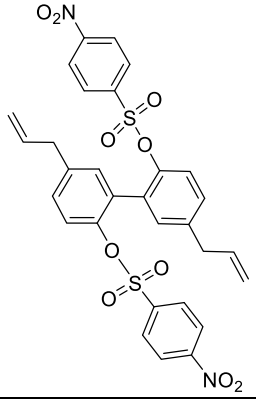	-6.5

DBMGPO-4	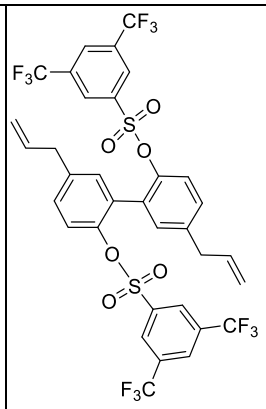	-7.5
DBMGPO-5 (This reaction did not give good yield, only 16 mg after three efforts).	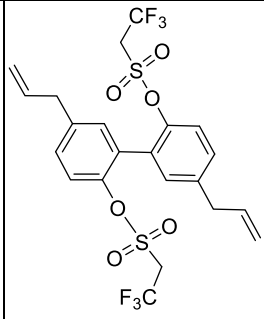	-5.9
DBMGPO-6	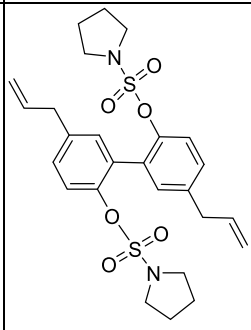	-5.9
DBMGPO-7	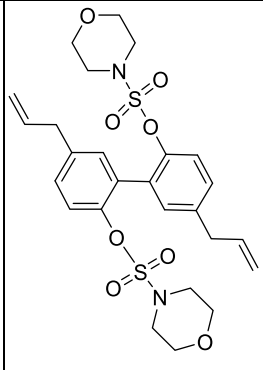	-6.6

DBMGPO-8	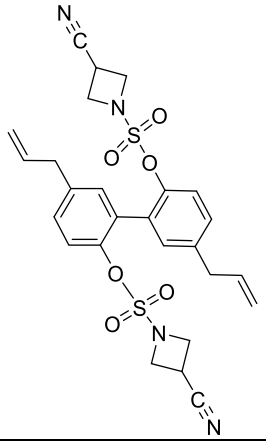	-7.2
DBADAPO-1A (3-Amino-1-adamantanol derived products)	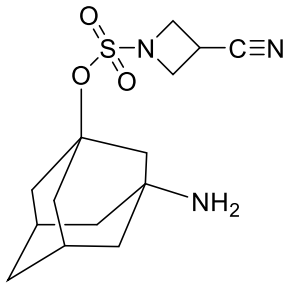	-6.7
DBADAPO-1B	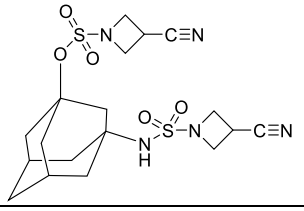	-7.3
DBADAPO-1C	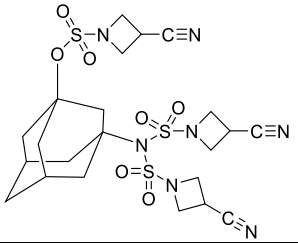	-7.6
DBQPO-1A	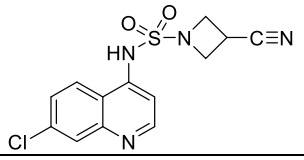	-6.9
DBQPO-1B	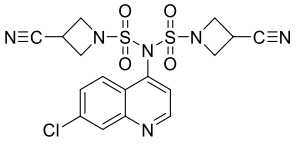	-7.2
DBQPO-2A	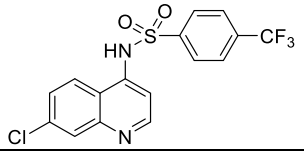	-7.3

DBQPO-2B	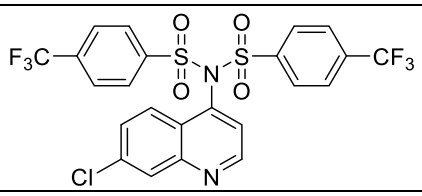	-8.0
Inhibitor N3	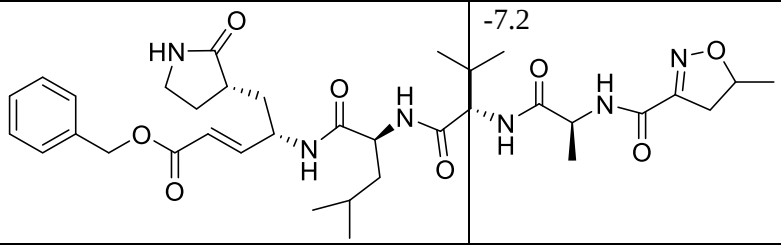	-7.2

Table 1. Code, structure, and binding energies of DBPO series against COVID-19 main protease in complex PDB code 6LU7.

Code	**Key residue interactions (ligand-receptor)**	
	H- Bond	**Pi stacking/ Pi-pi cation**
Magnolol	-	PHE 294
DBMGPO-1	SER 158 THR 111	-
DBMGPO-2	-	PHE 294
DBMGPO-3	HIS 246 PHE 294 GLN 110	-
DBMGPO-5	-	PHE 294
DBMGPO-6	PHE 291	PHE 294
DBMGPO-7	-	PHE 294
DBMGPO-8	-	PHE 294
DBADAPO-1B	SER 158 LYS 102	-
DBADAPO-1C	GLY 110	-
DBQPO-1A	GLU 166 GLY 143	HIS 41
DBQPO-1B	-	HIS 41
DBQPO-2B	GLN 110	-
Inhibitor N3	GLN 110	PHE 294

Table 2. Different ligand-receptor interactions of DBPO series against COVID-19 main protease in complex PDB code 6LU7.

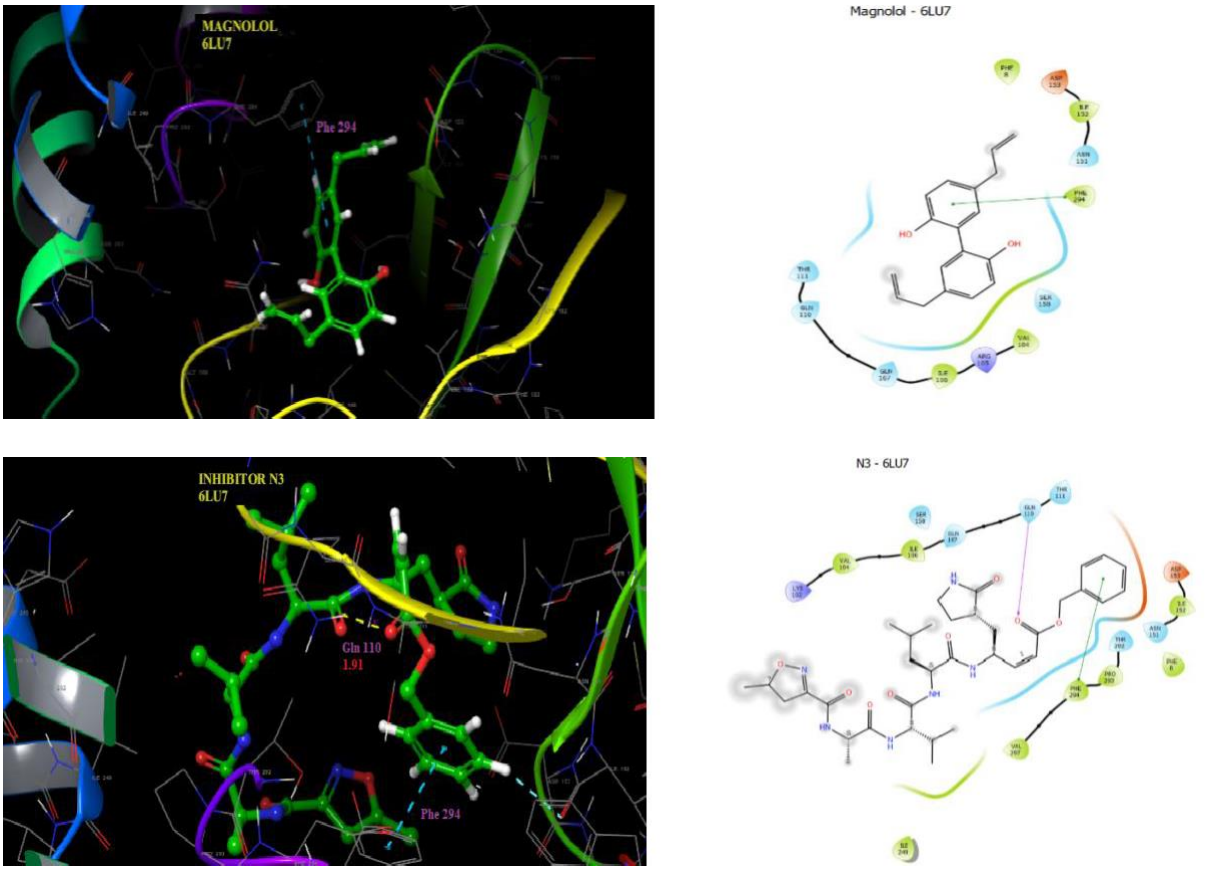

Figure 7. Binding modes of Magnolol and inhibitor N3 in the binding pocket of COVID-19 protein with PDB ID: 6LU7
The compounds are indicated in sticks; hydrogen bonds are shown as dashed yellow line; Pi-pi stacking/Pi-pi cation is shown as blue and green dashed lines.

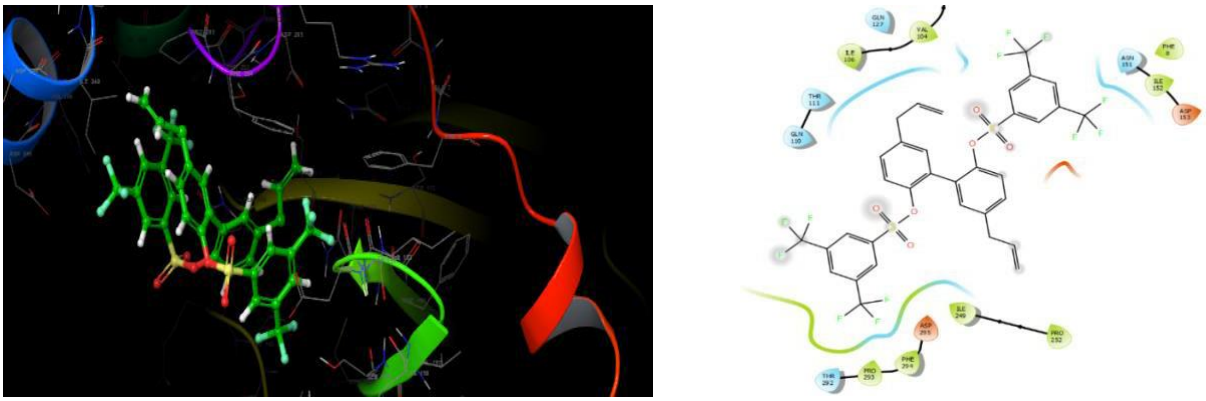

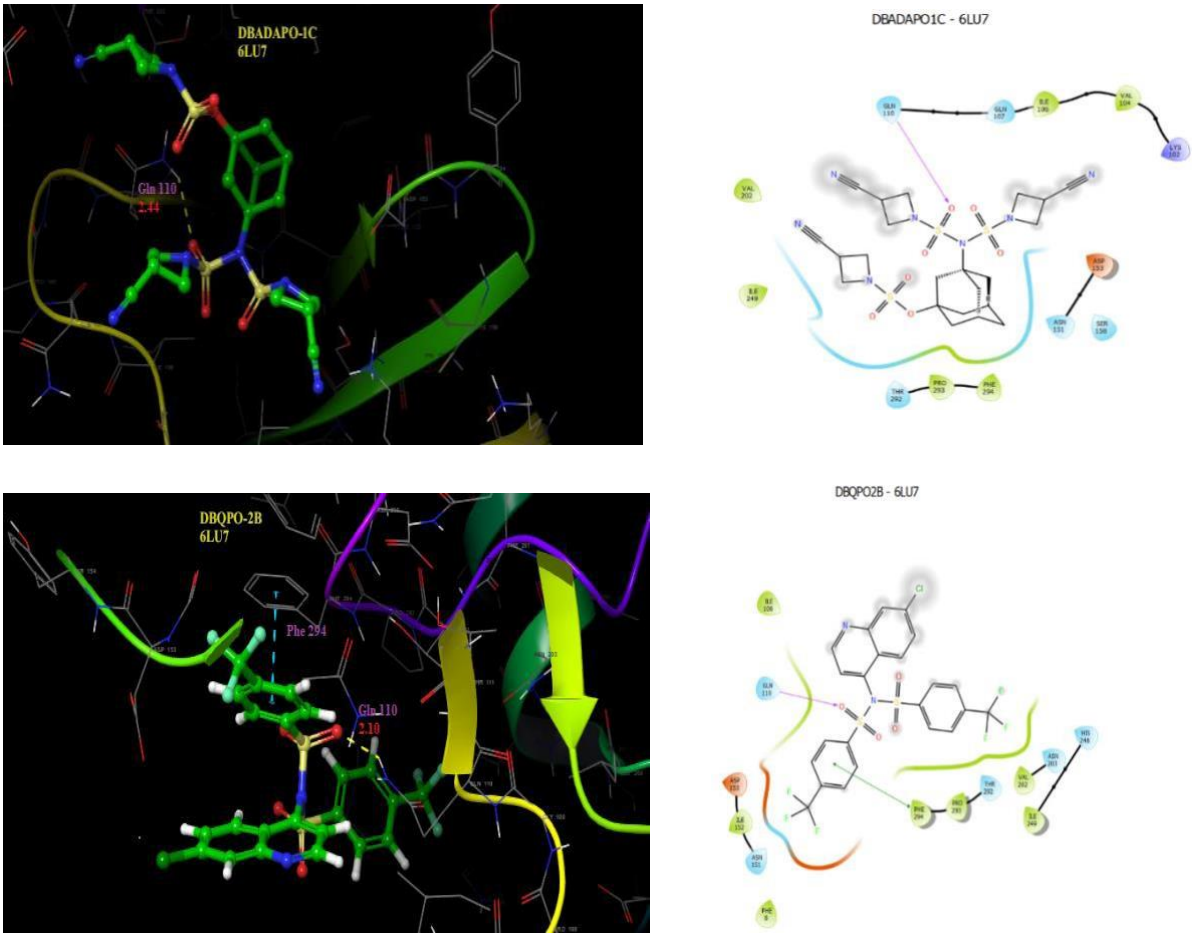

Figure 8. Protein-Ligand complex of DBPO series with top-scoring functions against COVID-19 main protease (PDB ID- 6LU7)
The compounds are indicated in sticks; hydrogen bonds are shown as a dashed yellow line; Pi-pi stacking/Pi-pi cation is shown as blue and green dashed lines.

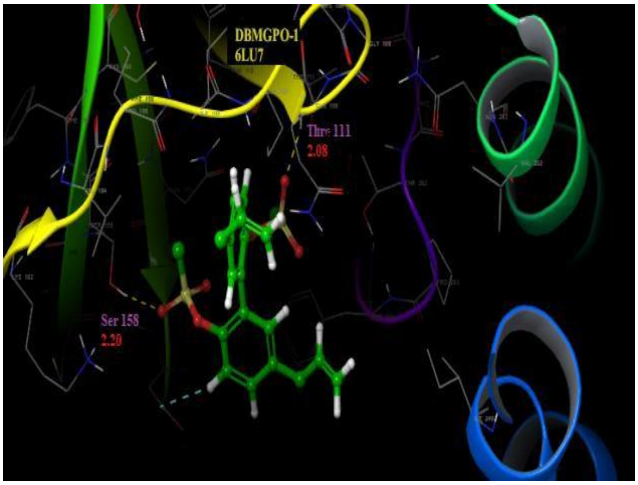
DBMGPO-1
6LU7
Thre 111
2.08
Ser 158
2.20

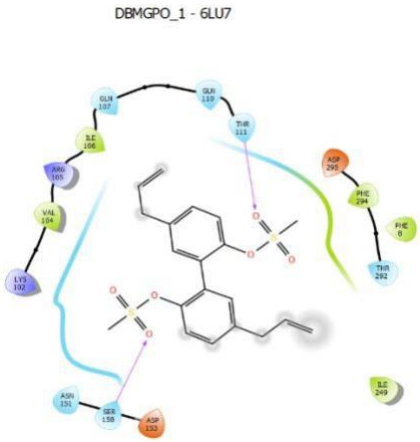
DBMGPO_1 - 6LU7

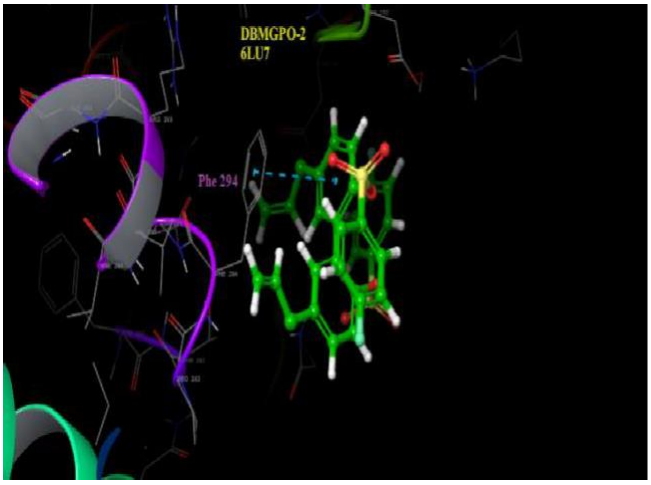
DBMGPO-2
6LU7
Phe 294

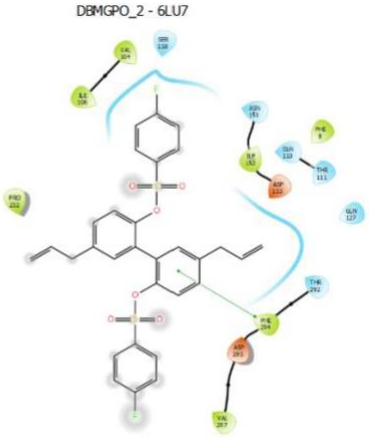
DBMGPO_2 - 6LU7

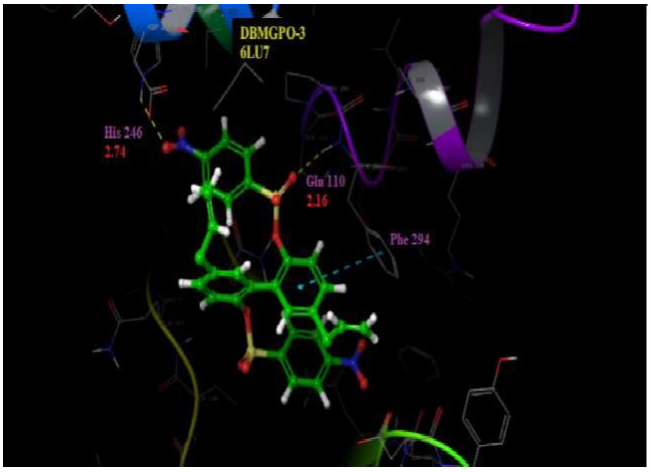
DBMGPO-3
6LU7
His 246
2.74
Gln 110
2.16
Phe 294

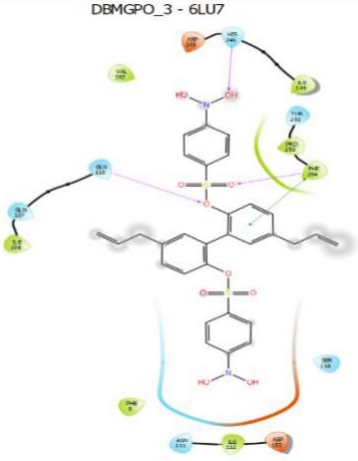
DBMGPO_3 - 6LU7

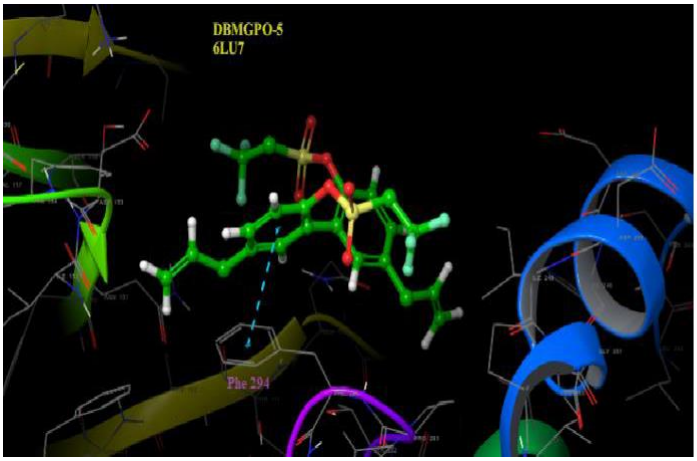
DBMGPO-5
6LU7
Phe 294

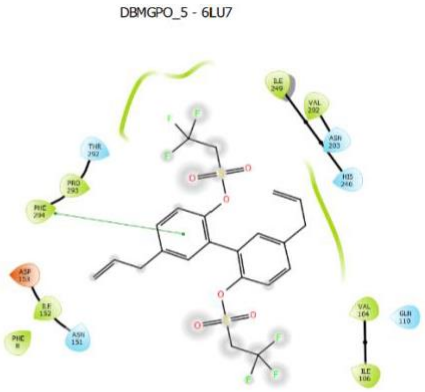
DBMGPO_5 - 6LU7

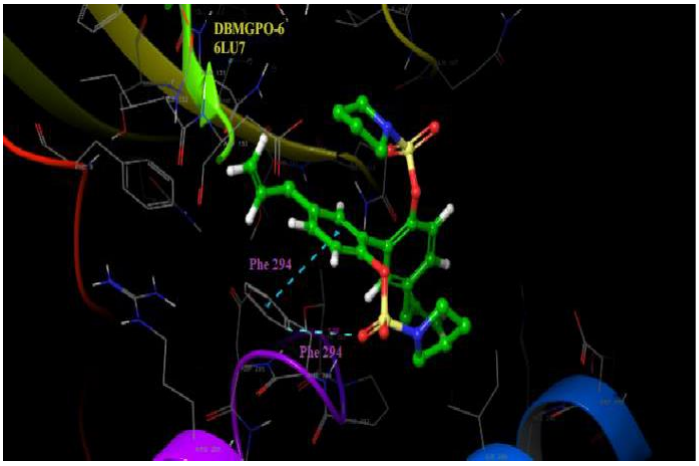
DBMGPO-6
6LU7
Phe 294
Phe 294

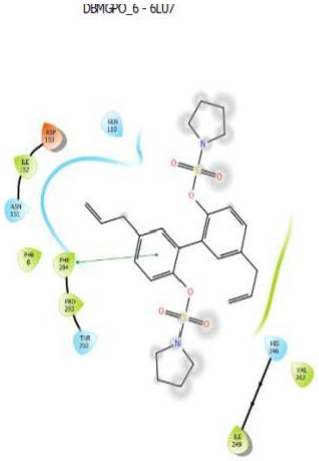
DBMGPO_6 - 6LU7

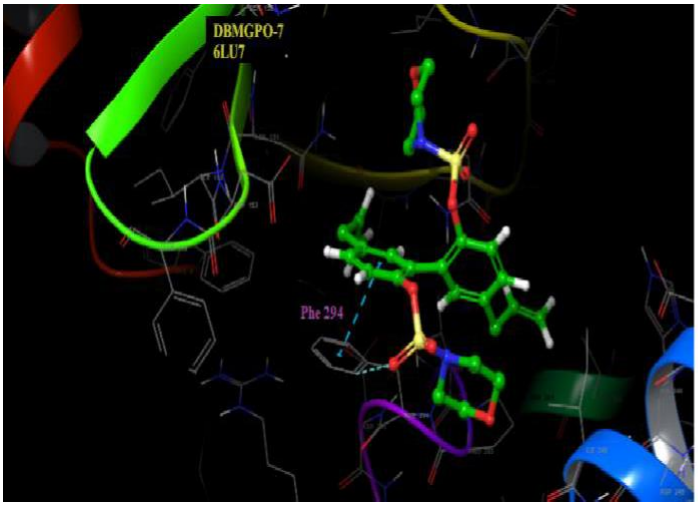
DBMGPO-7
6LU7
Phe 294

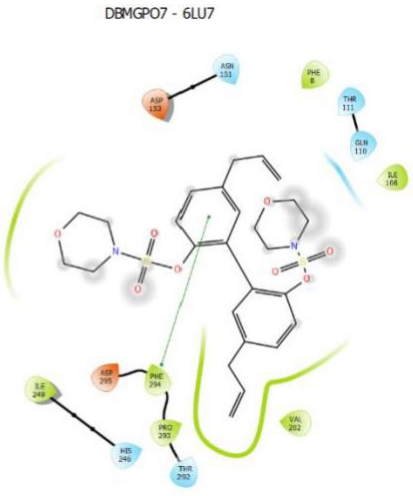
DBMGPO7 - 6LU7

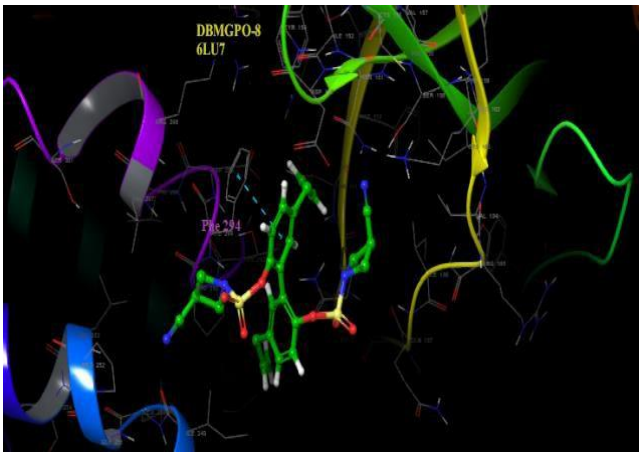

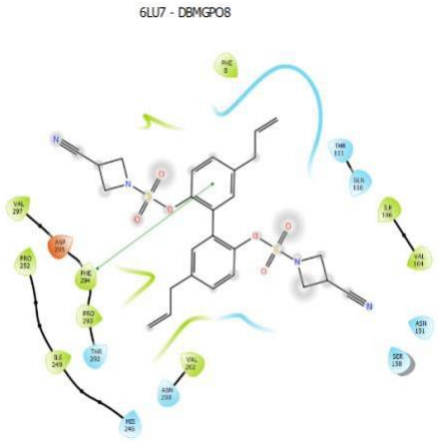

Figure 9. Protein-Ligand complex of DBMGPO series against COVID- 19 main protease (PDB ID- 6LU7)
The compounds are indicated in sticks; hydrogen bonds are shown as a dashed yellow line; Pi-pi stacking/Pi-pi cation is shown as blue and green dashed lines.

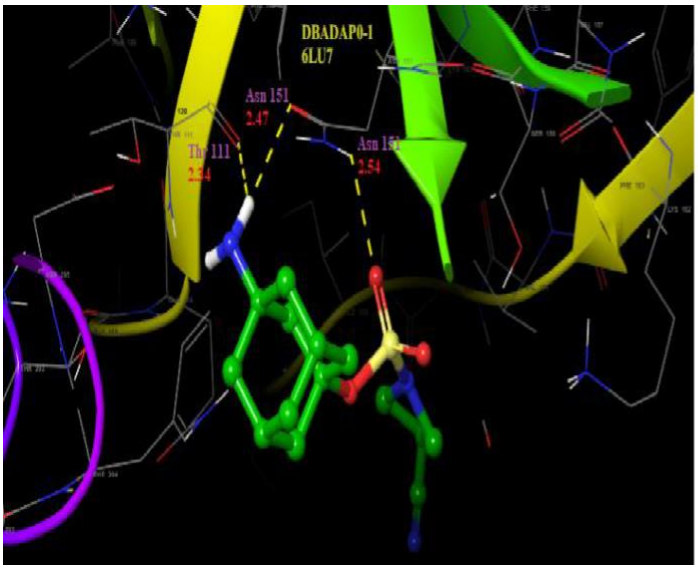

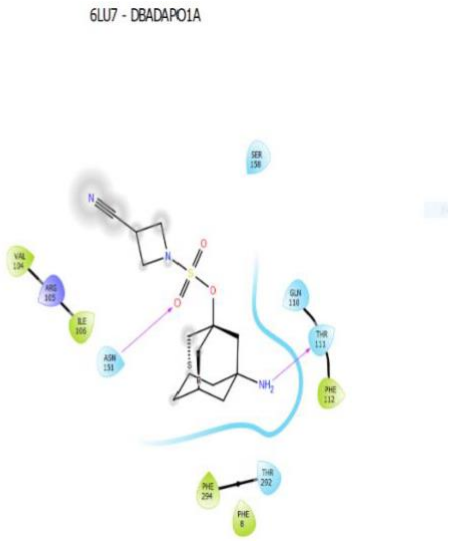

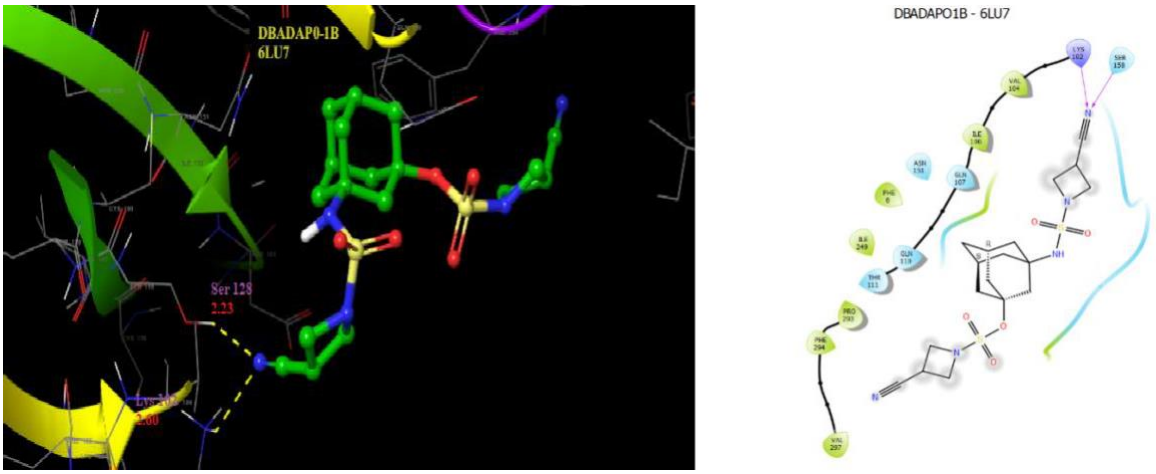

Figure 10. Protein-Ligand complex of DBADAPO series against COVID-19 main protease (PDB ID- 6LU7)
The compounds are indicated in sticks; hydrogen bonds are shown as dashed yellow line; Pi-pi stacking/Pi-pi cation is shown as blue and green dashed lines.

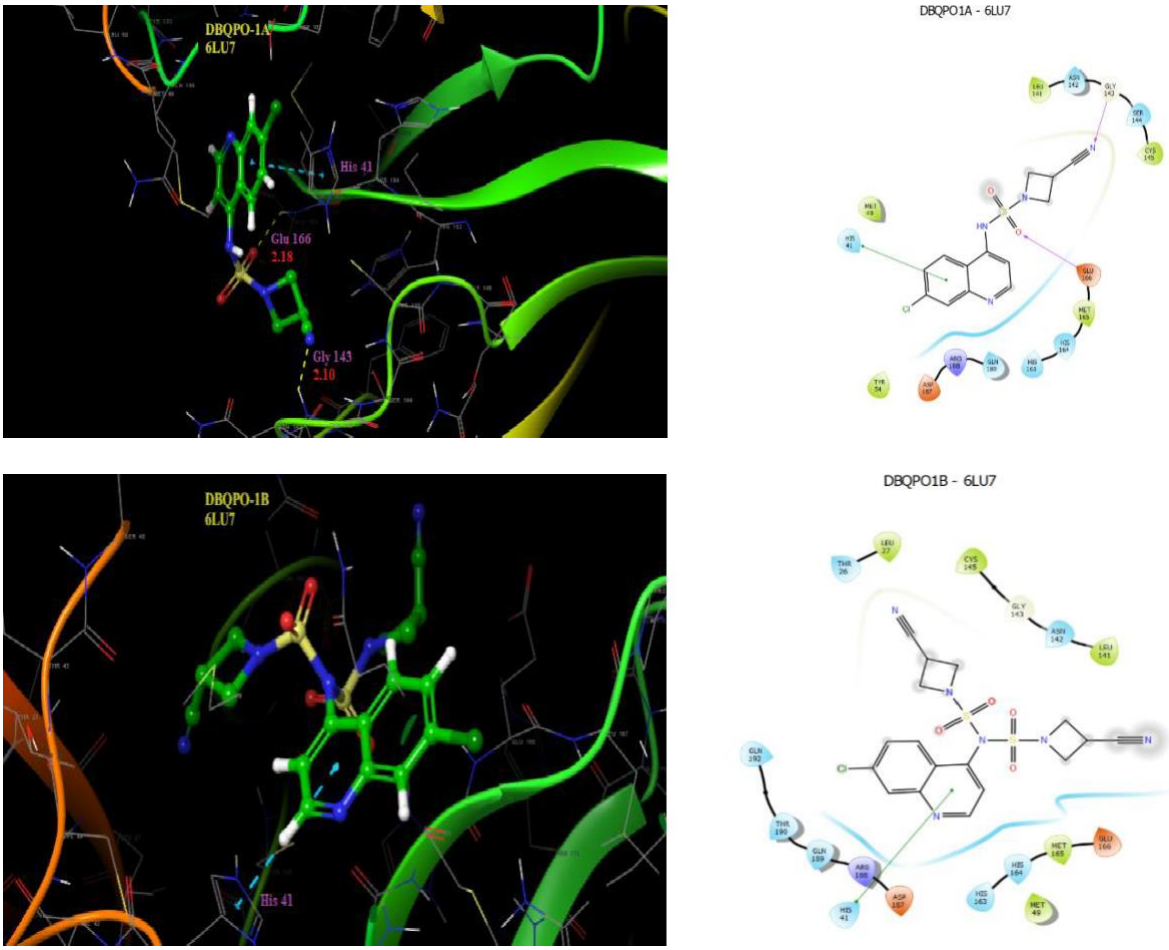

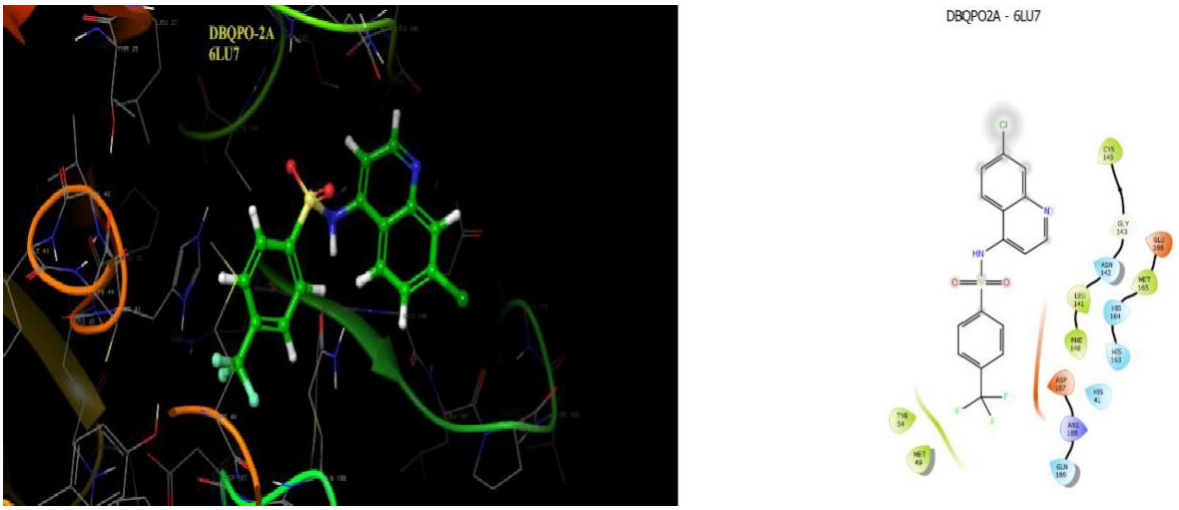

Figure 11. Protein-Ligand complex of DBQPO series against COVID-19 main protease (PDB ID- 6LU7)
The compounds are indicated in sticks; hydrogen bonds are shown as a dashed yellow line; Pi-pi stacking/Pi-pi cation is shown as blue and green dashed lines.

DBMGPO Series [PDB code 6M2Q, SARS-CoV-2 3CL protease in complex with an inhibitor N3]

Code	**Structure**	**Binding energy (6M2Q) Kcal/mol**
Magnolol	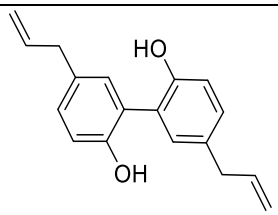	-7.2
DBMGPO-1	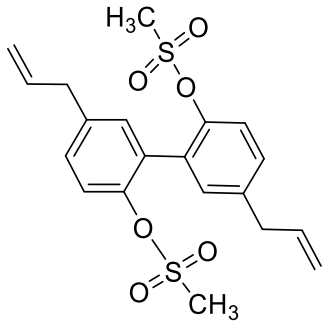	-6.0

DBMGPO-2	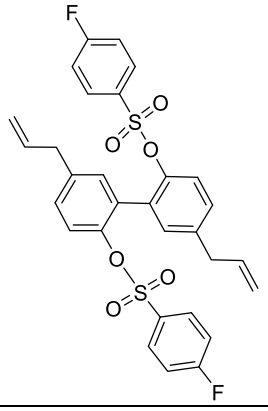	-7.1
DBMGPO-3	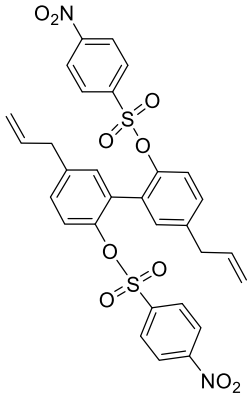	-7.1
DBMGPO-4	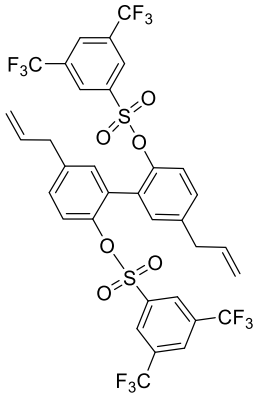	-5.8
DBMGPO-5 (This reaction did not give a good yield, only 16 mg after three efforts).	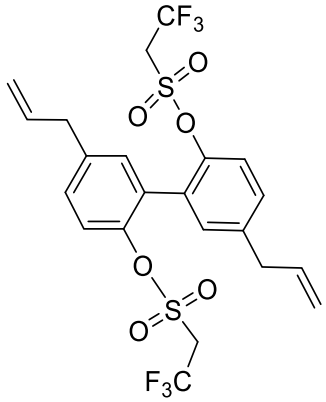	-6.3

DBMGPO-6	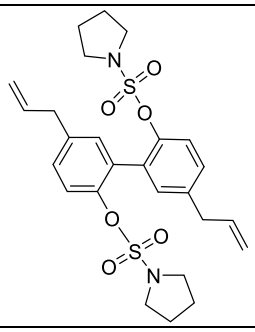	-6.6
DBMGPO-7	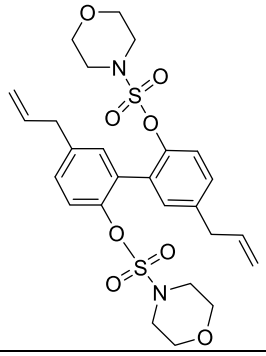	-5.6
DBMGPO-8	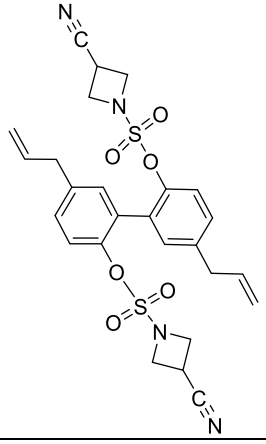	-7.2
DBADAPO-1A (3-Amino-1-adamantanol derived products)	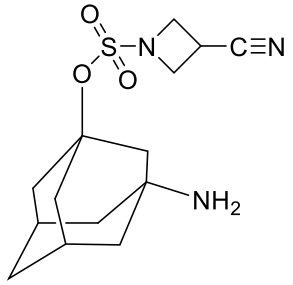	-7.6
DBADAPO-1B	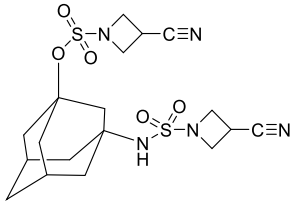	-9.1

DBADAPO-1C	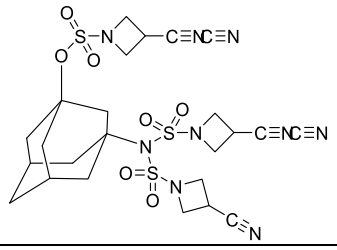	-7.6
DBQPO-1A	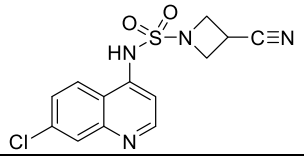	-7.3
DBQPO-1B	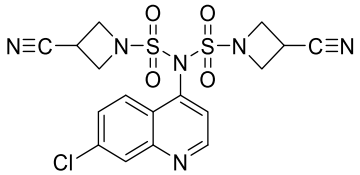	-6.8
DBQPO-2A	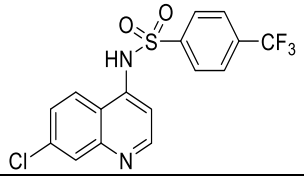	-7.6
DBQPO-2B	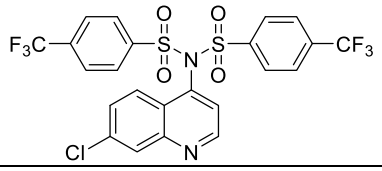	-7.3
Inhibitor N3	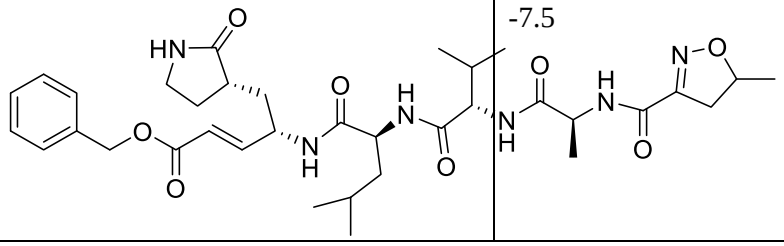	-7.5

Table 3. Code, structure, and binding energies of DBPO series against SARS CoV-2 3-CL protease (PDB ID- 6M2Q) complexed with inhibitor N3

Code	Key residue interactions (ligand-receptor)	
	H- Bond	**Pi-cation/ Pi-pi stacking**
Magnolol	THR 111	-
DBMGPO-2	-	PHE 294
DBMGPO-3	-	PHE 294
DBMGPO-5	-	PHE 294
DBMGPO-6	-	HID 246
DBMGPO-7	-	LYS 5

Table 4. Different ligand-receptor interactions DBPO series against SARS- CoV-2 3-CL protease (PDB ID- 6M2Q) complexed with inhibitor N3

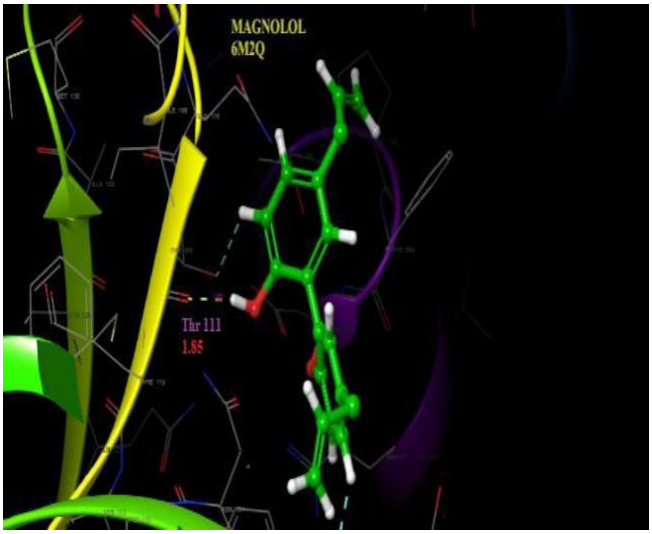

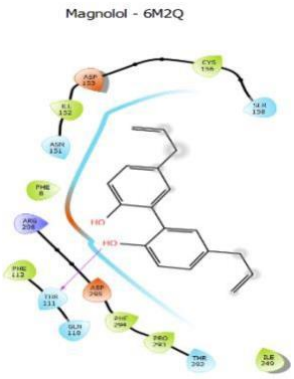

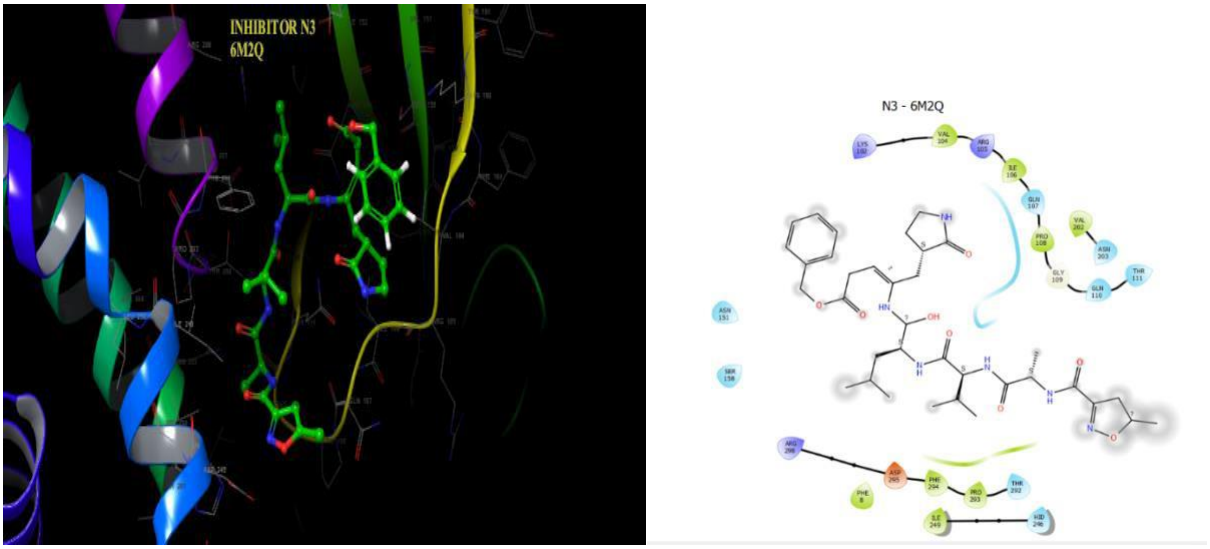

Figure 12. Binding modes of Magnolol and inhibitor N3 in the binding pocket of SARS-CoV-2 3CL protease (PDB ID: 6M2Q) complexed with an inhibitor N3.
The compounds are indicated in sticks; hydrogen bonds are shown as a dashed yellow line; Pi-pi stacking/Pi-pi cation is shown as blue and green dashed lines

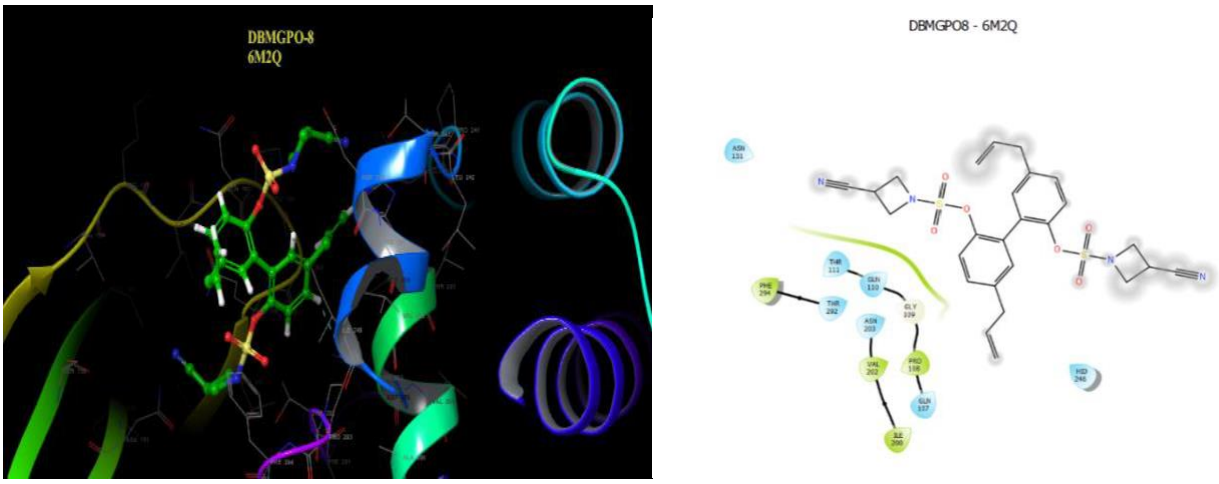

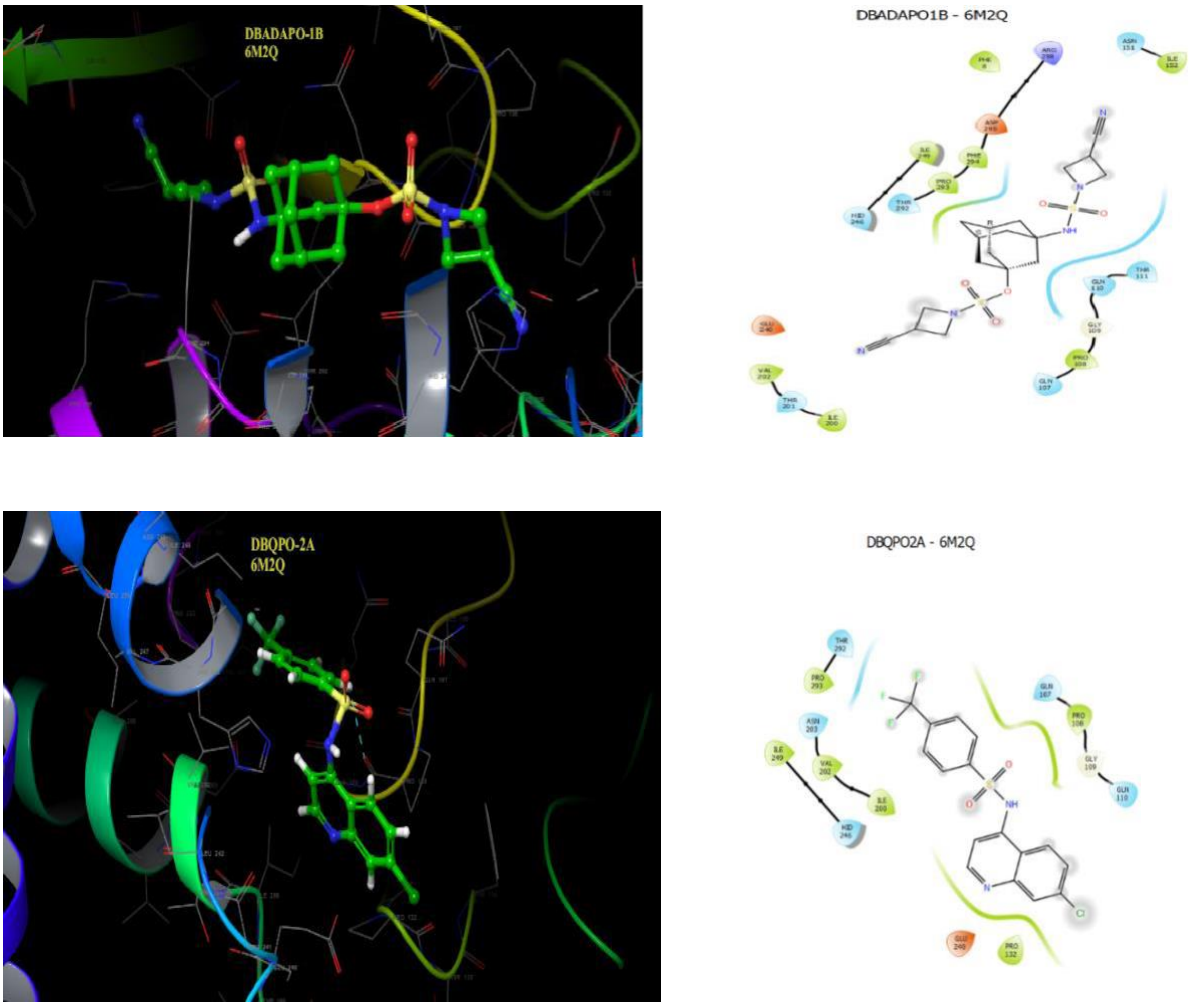

Figure 13. Protein-Ligand complex of DBPO series with top-scoring functions against SARS-CoV-2 3CL protease (PDB ID: 6M2Q) complexed with an inhibitor N3.
The compounds are indicated in sticks; hydrogen bonds are shown as a dashed yellow line; Pi-pi stacking/Pi-pi cation is shown as blue and green dashed lines

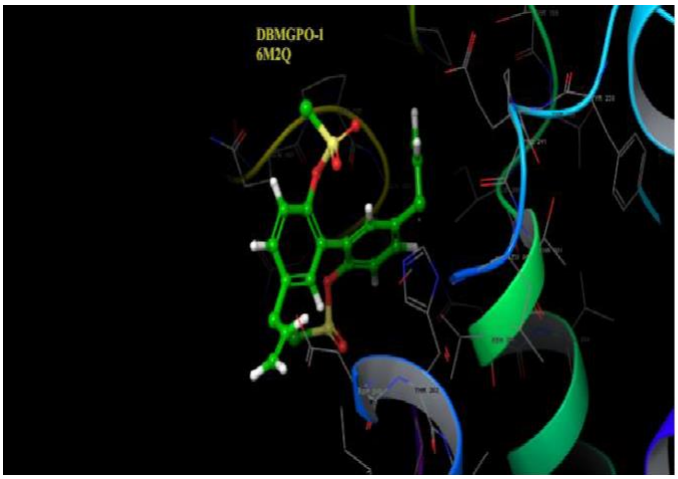
DBMGPO-1
6M2Q

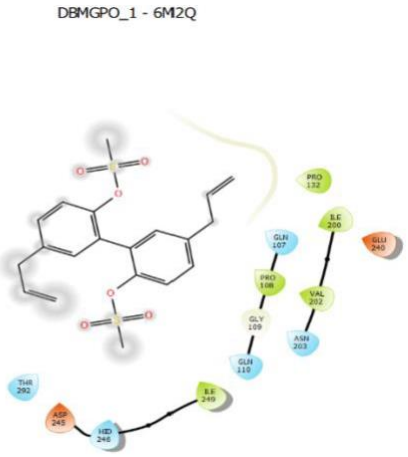
DBMGPO_1 - 6M2Q

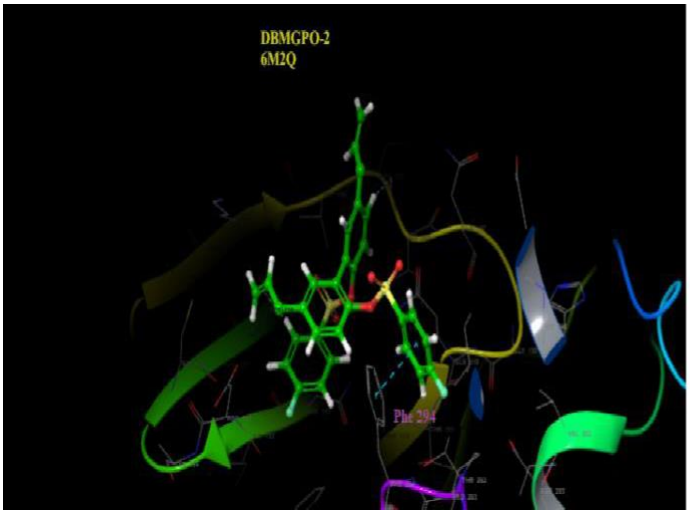
DBMGPO-2
6M2Q
Phe 294

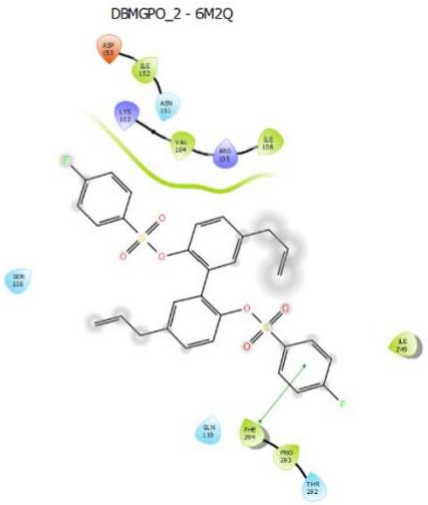
DBMGPO_2 - 6M2Q


DBMGPO-3
6M2Q
Phe 294

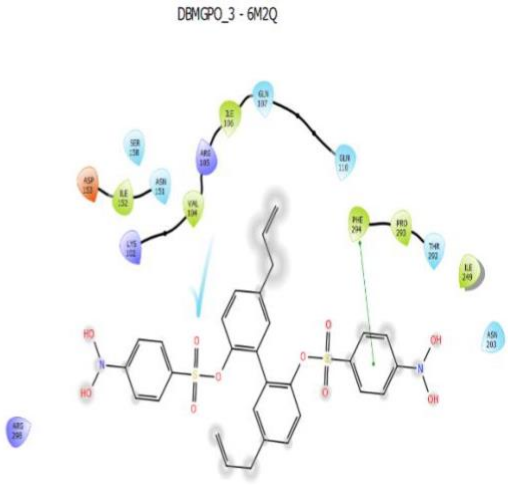
DBMGPO_3 - 6M2Q

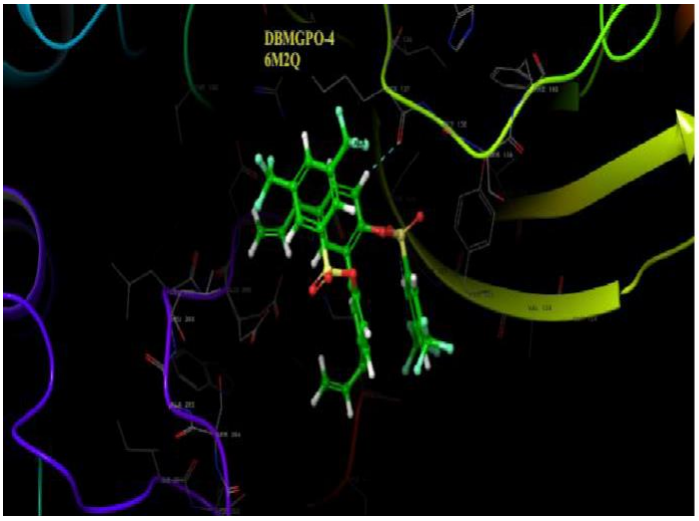
DBMGPO-4
6M2Q

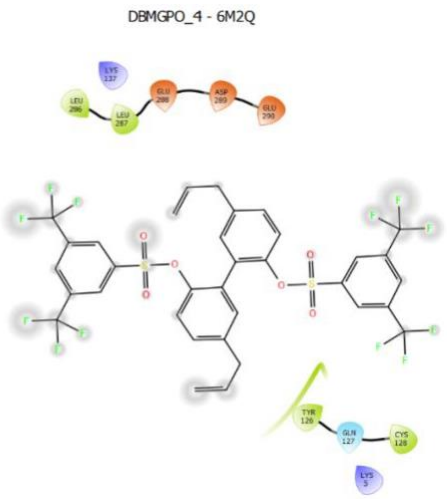
DBMGPO_4 - 6M2Q

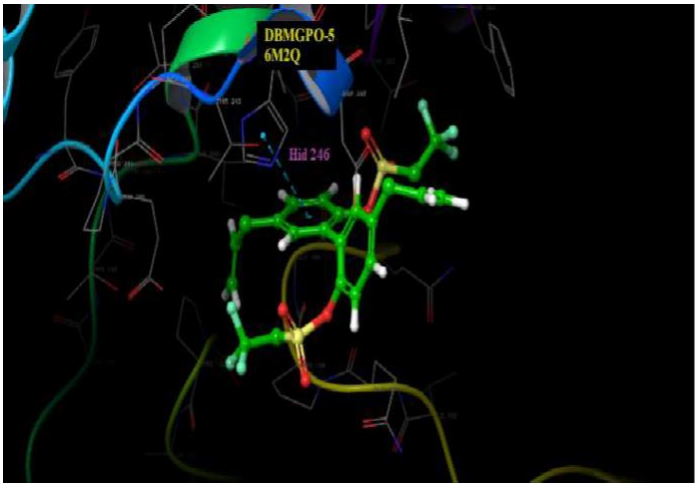
DBMGPO-5
6M2Q
His 246

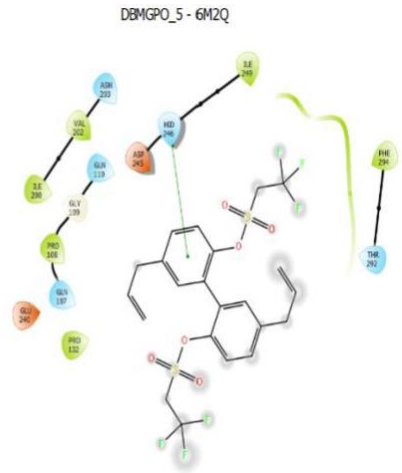
DBMGPO_5 - 6M2Q

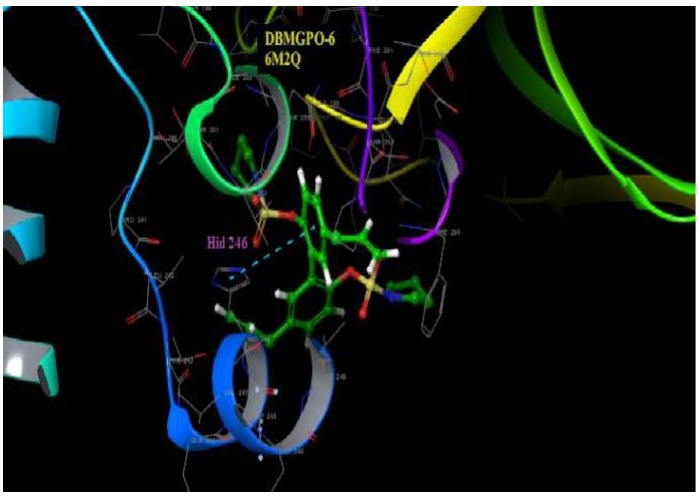
DBMGPO-6
6M2Q
His 246

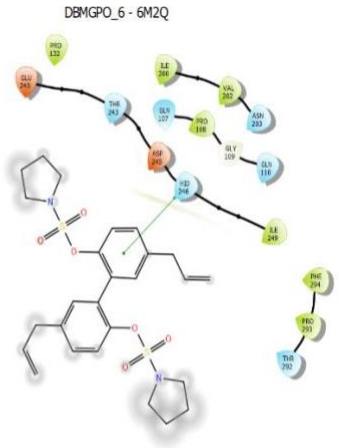
DBMGPO_6 - 6M2Q

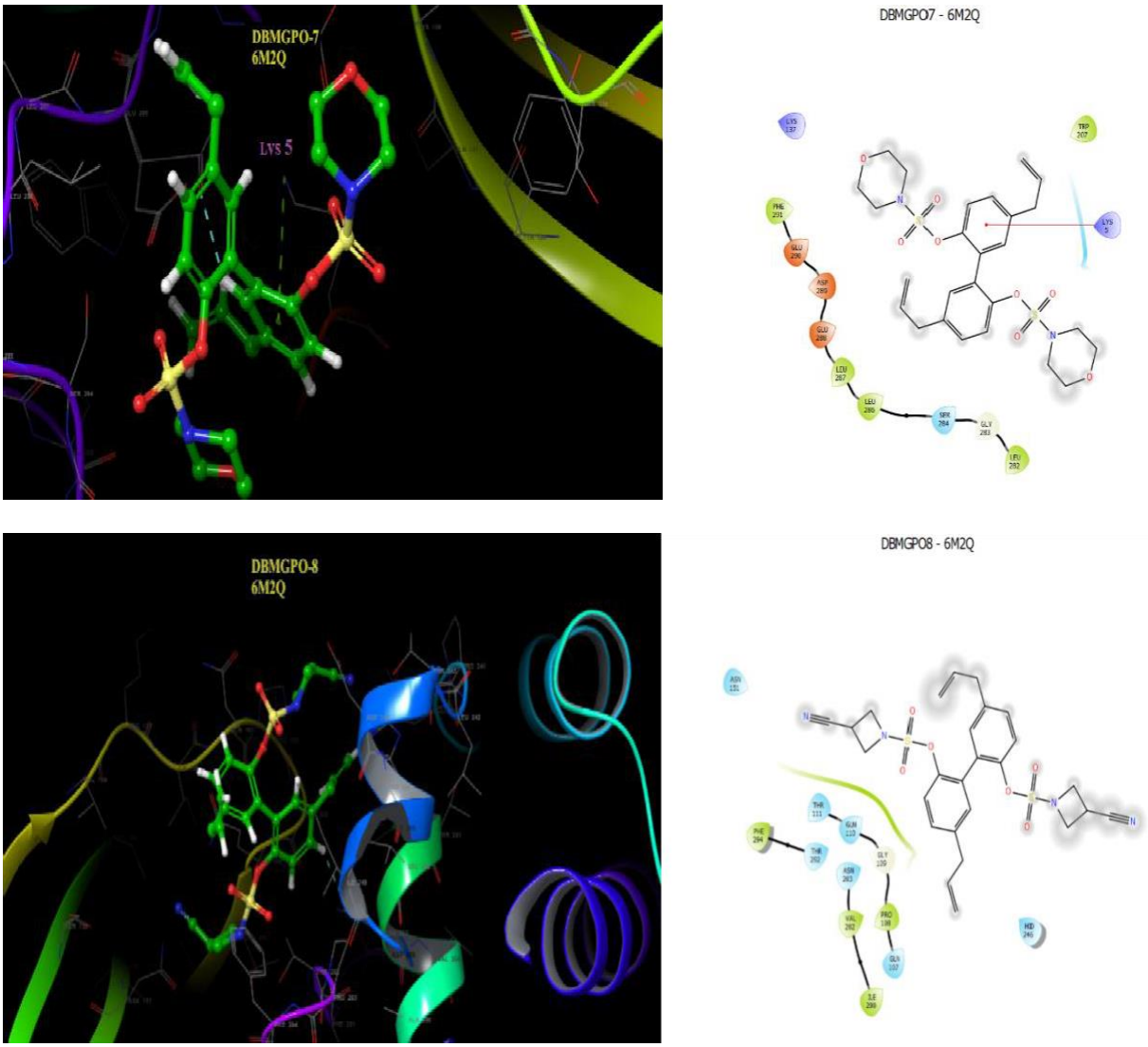

Figure 14. Protein-Ligand complex of DBMGPO series docked at the active site of SARS-CoV-2 3CL protease (PDB ID: 6M2Q) complexed with an inhibitor N3.
The compounds are indicated in sticks; hydrogen bonds are shown as a dashed yellow line; Pi-pi stacking/Pi-pi cation is shown as blue and green dashed lines

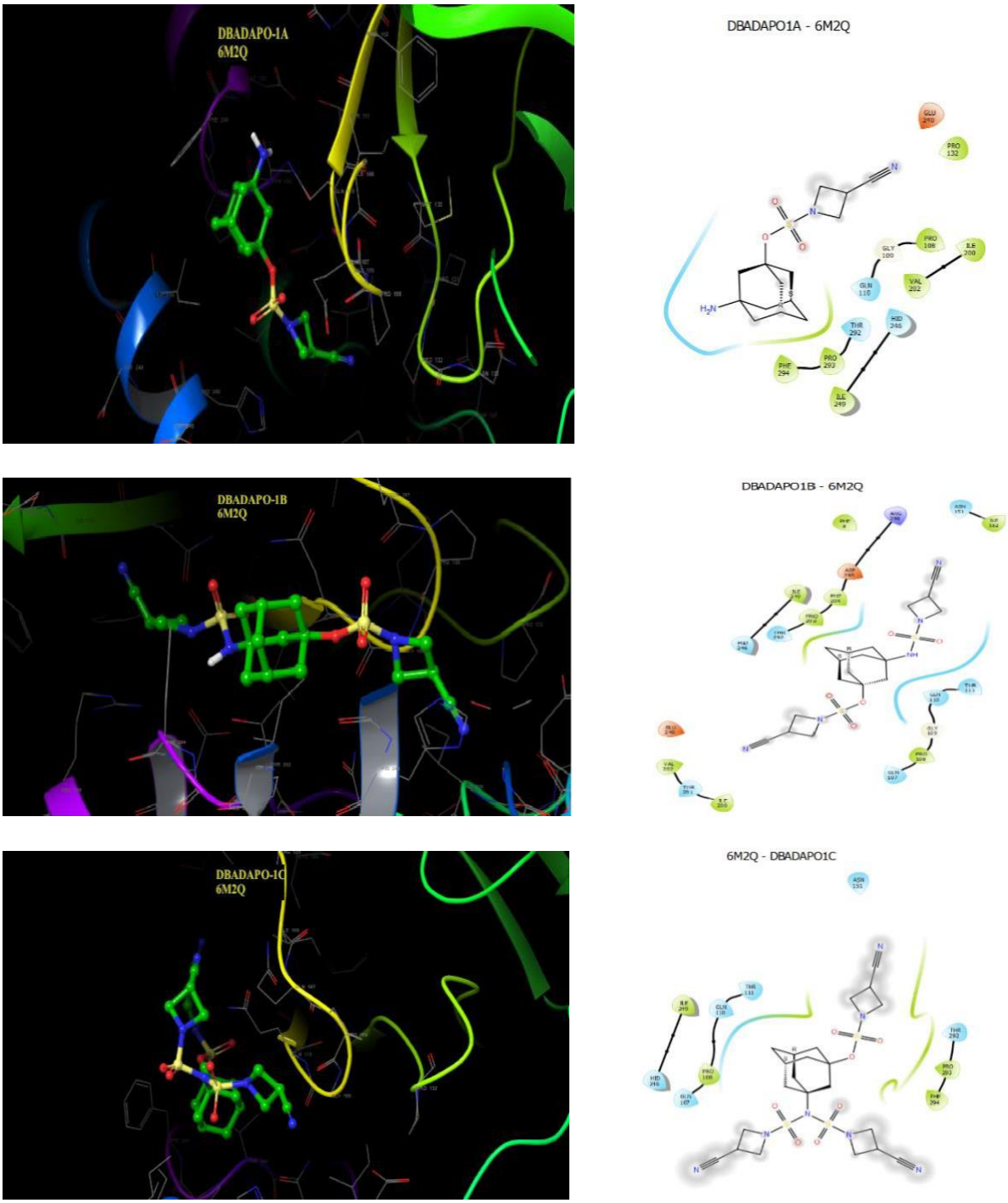

Figure 15. Protein-Ligand complex of DBADAPO series docked at the active site of SARS-CoV-2 3CL protease (PDB ID: 6M2Q) complexed with an inhibitor N3.
The compounds are indicated in sticks; hydrogen bonds are shown as a dashed yellow line; Pi-pi stacking/Pi-pi cation is shown as blue and green dashed lines

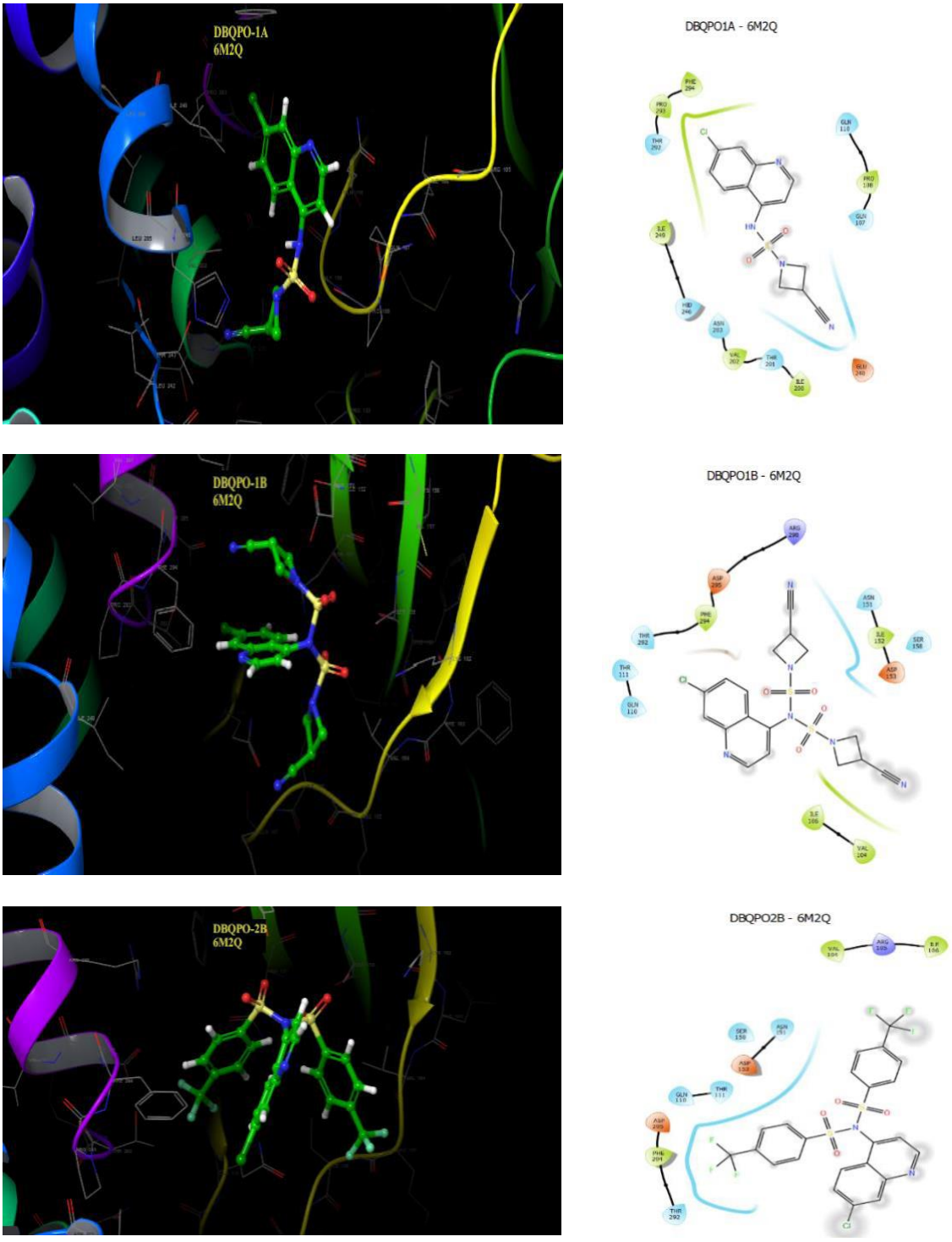

Figure 16. Protein-Ligand complex of DBQPO series docked at the active site of SARS-CoV-2 3CL protease (PDB ID: 6M2Q) complexed with an inhibitor N3.
The compounds are indicated in sticks; hydrogen bonds are shown as a dashed yellow line; Pi-pi stacking/Pi-pi cation is shown as blue and green dashed lines

DBMG Series [PDB code 4EPV, crystal structure of K-RAS cancer protein]

Code	**Structure**	**Binding energy (4EPV) Kcal/mol**
Magnolol	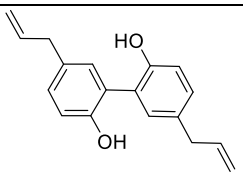	-7.3
DBMGPO-1	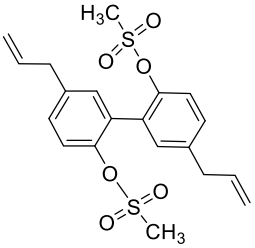	-4.8
DBMGPO-2	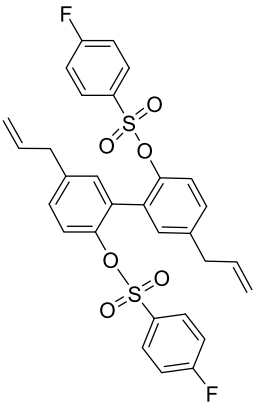	-5.3
DBMGPO-3	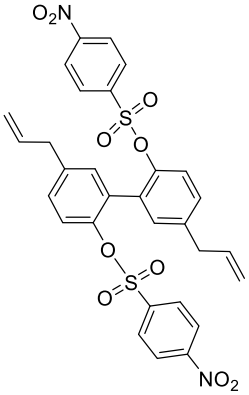	-4.7

DBMGPO-4	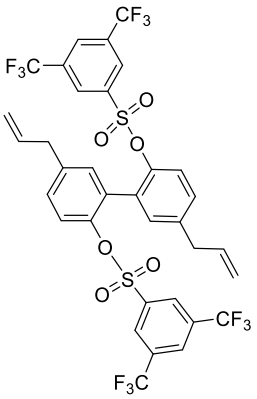	-5.8
DBMGPO-5	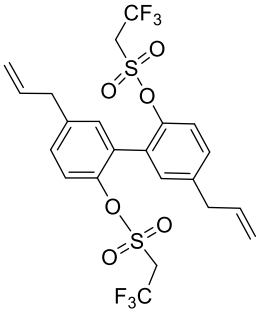	-4.8
DBMGPO-6	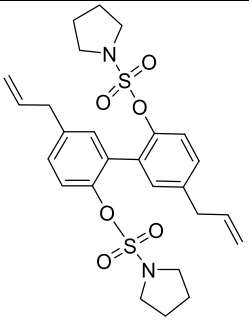	-4.4
DBMGPO-7	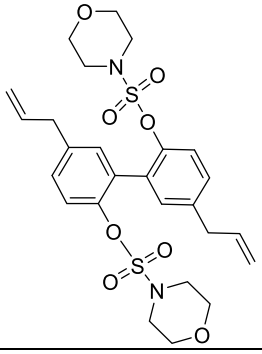	-6.9

DBMGPO-8	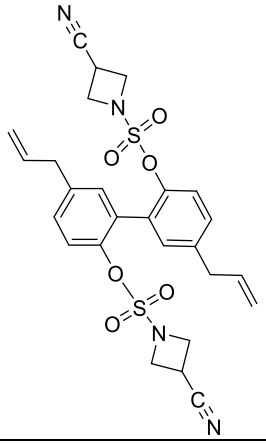	-7.6
DBADAPO-1A (3-Amino-1-adamantanol derived products)	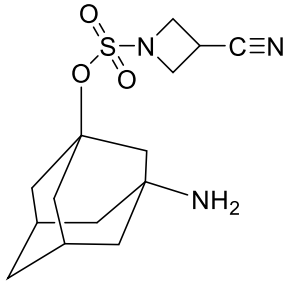	-7.6
DBADAPO-1B	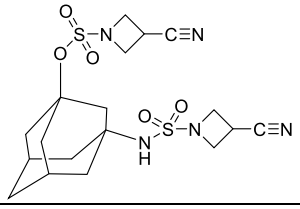	-5.6
DBADAPO-1C	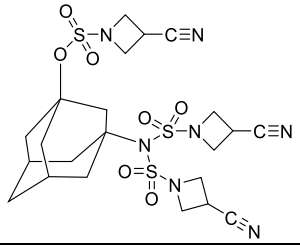	-7.7
DBQPO-1A	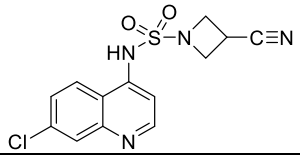	-8.2
DBQPO-1B	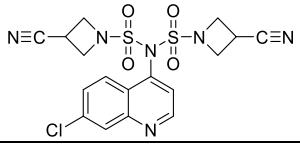	-8.2
DBQPO-2A	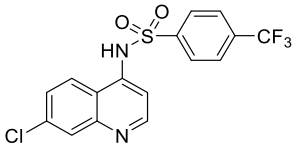	-8.4

DBQPO-2B	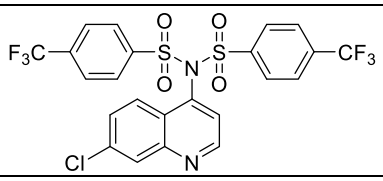	-5.4
Inhibitor N3	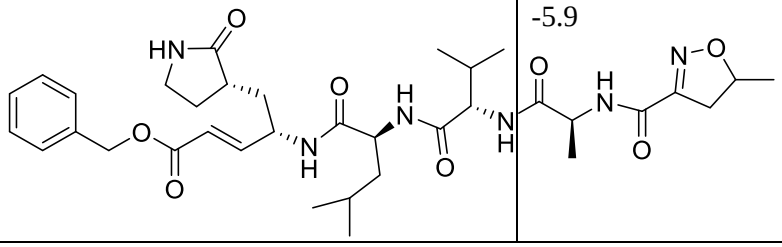	-5.9

Table 5. Structure, properties, and docking scores of DBPO series against crystal structure K-RAS protein complex (PDB ID- 4EPV)

DBMG Series [PDB code 4EPV, crystal structure of K-RAS cancer protein]

Code	**Key residue interactions (ligand-receptor)**	
	H-Bond	**Pi-pi stacking and Pi-cation**
Magnolol	-	PHE 298 LYS 117
DBMGPO-1	GLN 131	
DBMGPO-6	-	-
DBMGPO-7	ASP 30 VAL 29	LYS 117
DBQPO-1A	-	PHE 28 LYS 117
DBQPO-1B	ASP 30	PHE 28 LYS 117
DBQPO-2A	-	PHE 28 LYS 117

Table 6. Different ligand- receptor interactions DBPO series against crystal structure K-RAS protein complex (PDB ID- 4EPV)

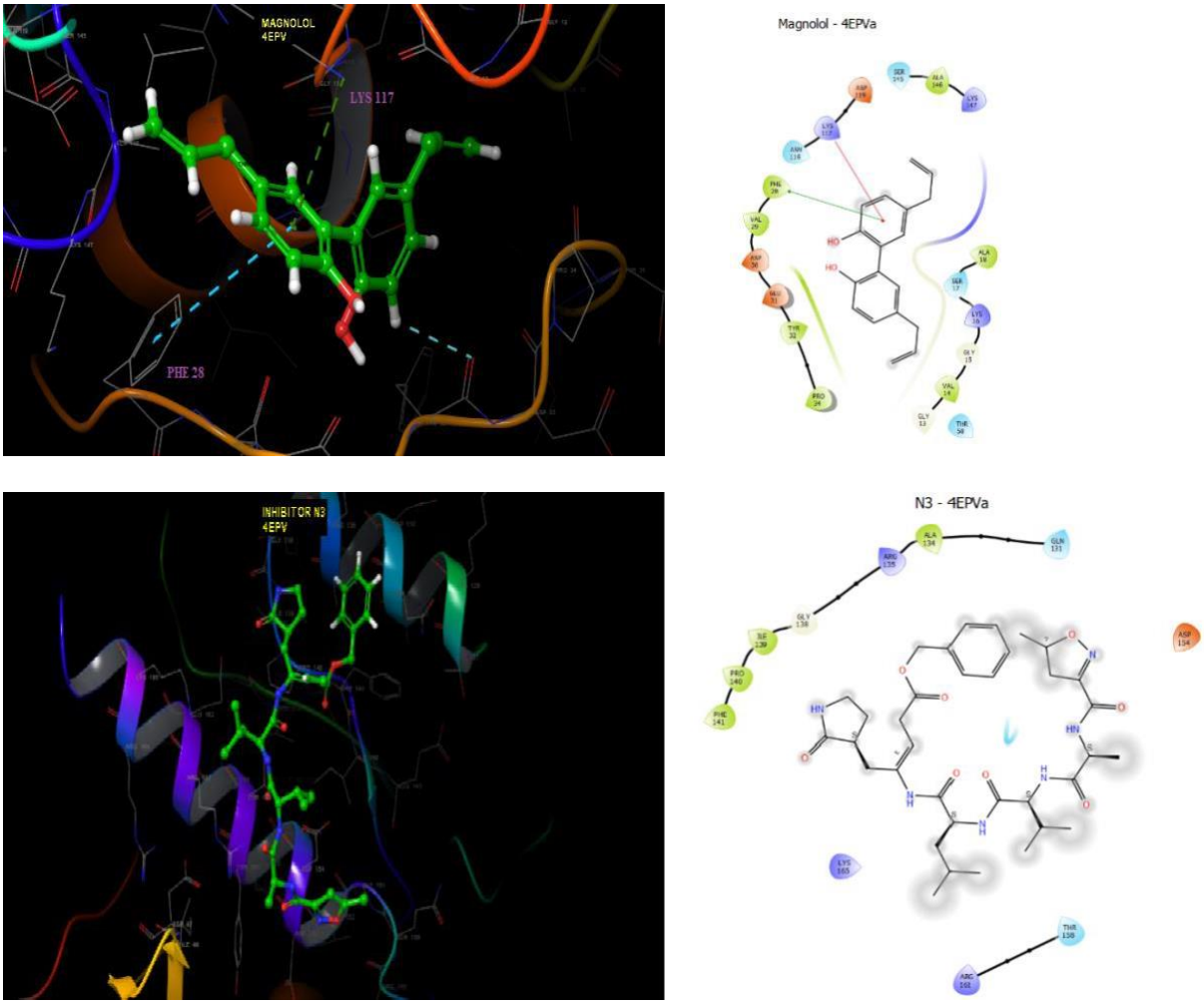

Figure 17. Binding modes of Magnolol and inhibitor N3 in the binding pocket of crystal structure K-RAS protein with PDB ID- 4EPV
The compounds are indicated in sticks; hydrogen bonds are shown as dashed yellow line; Pi-pi stacking/Pi-pi cation is shown as blue and green dashed lines

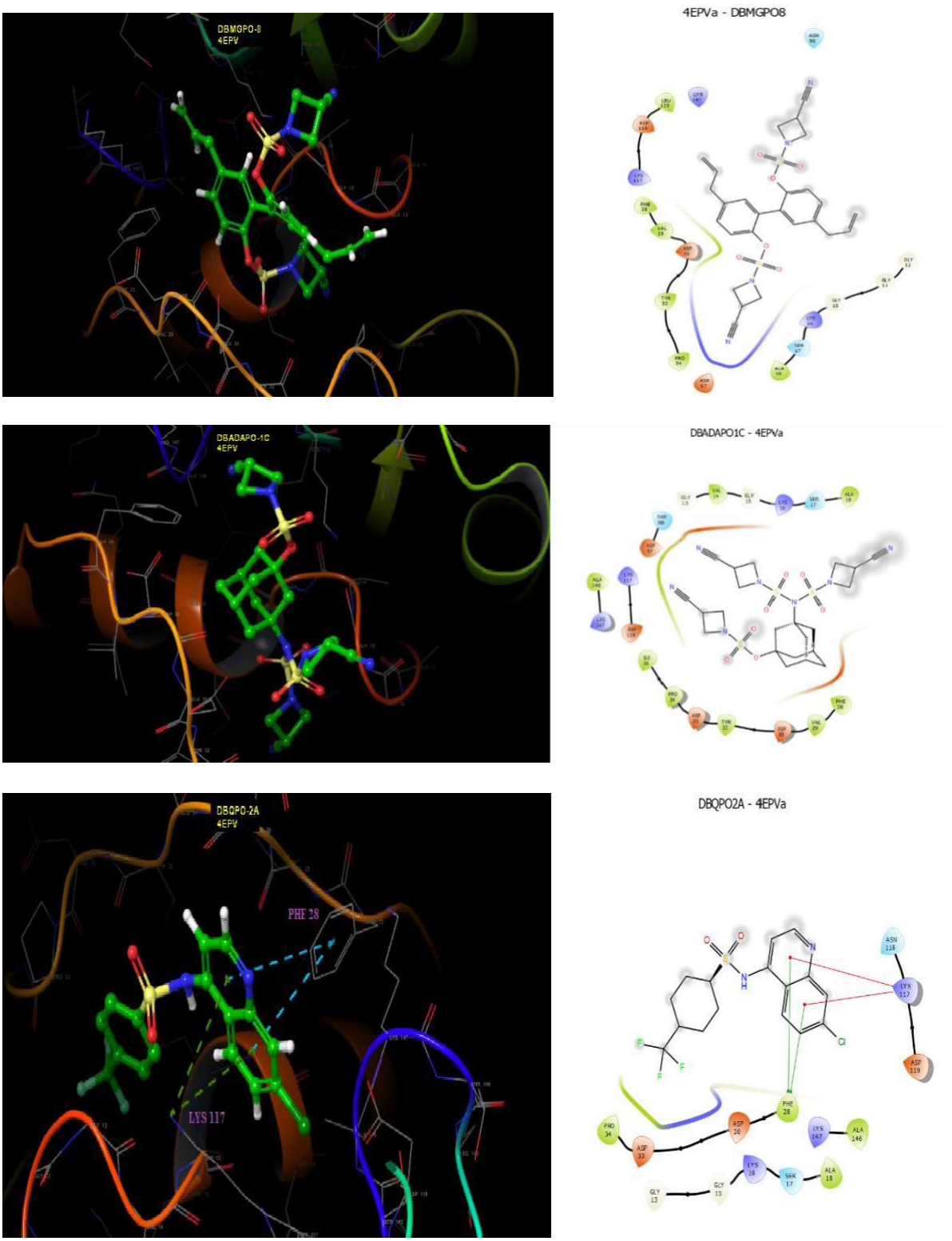

Figure 18. Protein-Ligand complex of DBPO series with top scoring functions crystal structure K-RAS protein with PDB ID- 4EPV.
The compounds are indicated in sticks; hydrogen bonds are shown as dashed yellow line; Pi-pi stacking/Pi-pi cation is shown as blue and green dashed lines

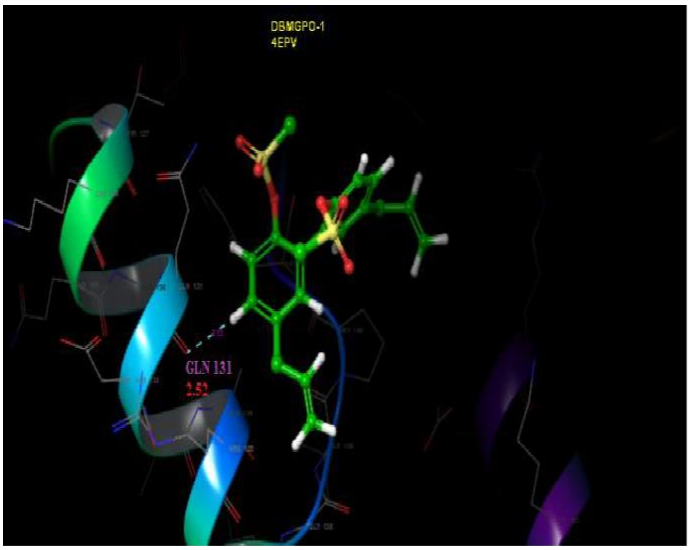

4EPVa - DBMGPO_1

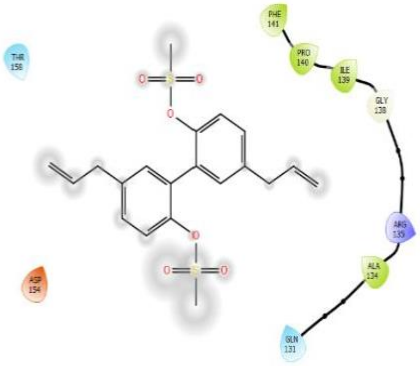

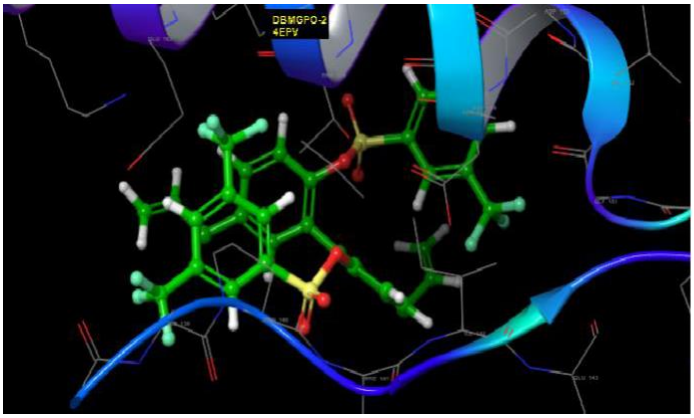

DBMGPO_2 - 4EPVa

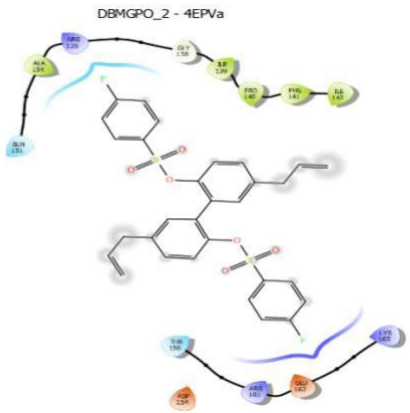

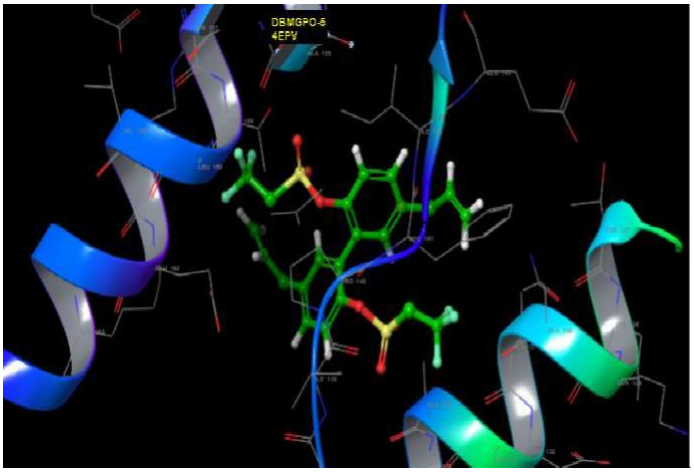

DBMGPO_5 - 4EPVa

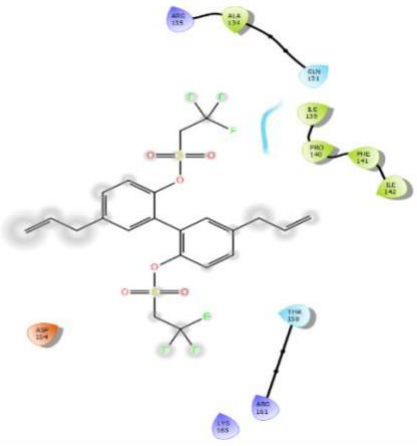

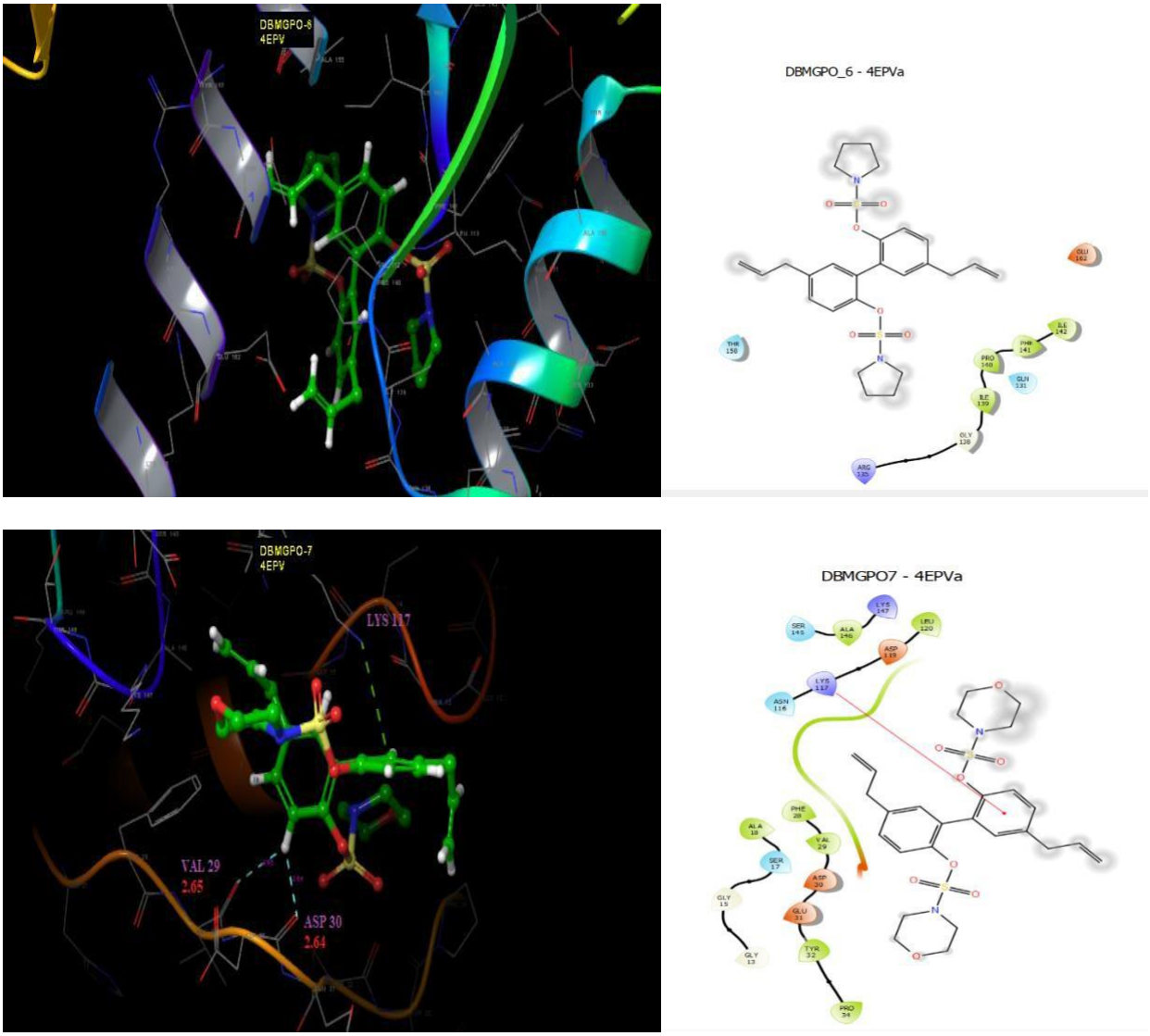

Figure 19. Protein-Ligand complex of DBMGPO series docked at the active site of crystal structure K-RAS protein with PDB ID- 4EPV
The compounds are indicated in sticks; hydrogen bonds are shown as dashed yellow line; Pi-pi stacking/Pi-pi cation is shown as blue and green dashed lines

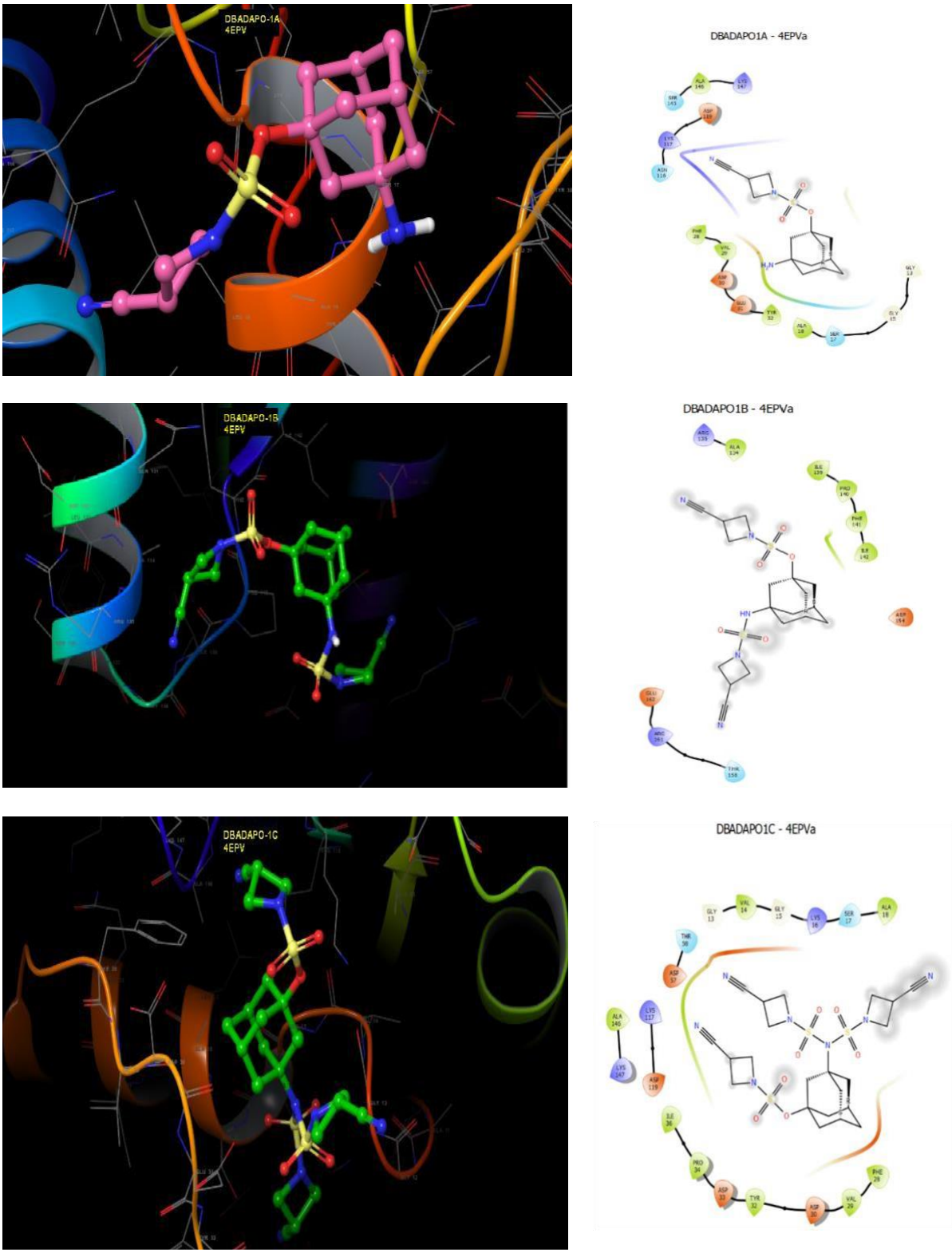

Figure 20. Protein-Ligand complex of DBADAPO series docked at the active site of crystal structure K- RAS protein with PDB ID- 4EPV.
The compounds are indicated in sticks; hydrogen bonds are shown as dashed yellow line; Pi-pi stacking/Pi-pi cation is shown as blue and green dashed lines

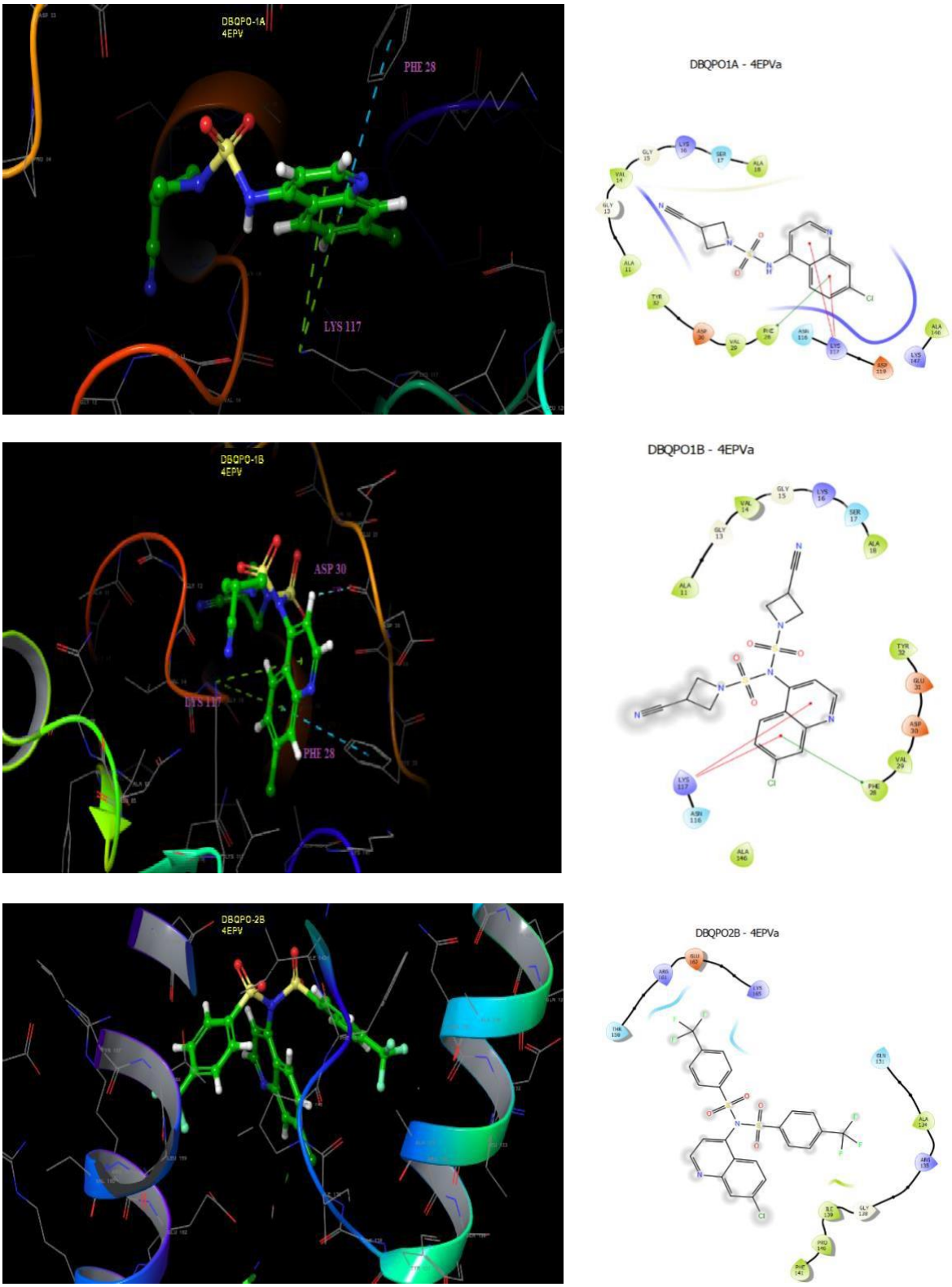

Figure 21. Protein-Ligand complex of DBQPO series docked at the active site of crystal structure K-RAS protein with PDB ID- 4EPV
The compounds are indicated in sticks; hydrogen bonds are shown as dashed yellow line; Pi-pi stacking/Pi-pi cation is shown as blue and green dashed lines

CHAPTER V

CHEMISTRY

Bioactivity-guided extraction of natural products

i. Diethyl ether magnolol extract

For this research, fresh mature green seed cones were collected from the *Magnolia grandiflora* tree, located at the University of Texas Rio Grande Valley. The seeds were purged, and the cones were chopped into several small fragments and air-dried. The dried seeds were crushed into small particulates and immersed completely in diethyl ether for 48 hours and sonicated at 25ºC for 21 hours (cold extraction method). The extract is filtered, and the filtrate is evaporated under reduced pressure using a rotavapor (Buchi Rotavapor R114). The gummy mass obtained is first dried using a heating mantle for 72hours, for further drying it is placed in a desiccator for an additional 48 hours. The resultant dried mass (85gm) is chromatographed over silica gel. Isolation is carried out by slowly increasing the polarity using hexanes/ethyl acetate as solvents. Magnolol (compound I) eluted at 97:3 ratio, on crystallization white needle-shaped crystals is collected (8.18gm >95% yield. Pure magnolol is expensive to obtain, 10mg of ≥95% Magnolol costs $140 on Sigma Aldrich. The extracted yield has an estimated value of about $11,452, thus, saving the lab a lot of money. Honokiol was also obtained at a 96:4 ratio from the same column using solvents hexanes/ethyl acetate as eluents. On crystallization, the reddish-brown powder was obtained (5.4gm). The characterization of both compounds was conducted. Melting

point, IR, 1D, and 2D NMR was carried out to determine both structures, X-ray crystallography was conducted to confirm the chemical structures.

Figure 22. Fresh matured green seed cones of *magnolia grandiflora*

ii. Aloe Rind

Aloe Vera L. (*Aloe barbadensis Miller*) belongs to the *Liliaceae* family. The major purpose of this bioactivity guided extraction is to regenerate waste to obtain precious chemicals which could ultimately lead to discovery of authentic small drug-like molecules. Aloe Vera contains several chemical constituents such as tannins, sterols, amino acids, flavonoids, and lipids, thus, it has found several applications in the treatment of inflammation, skin disorders, wounds, burns etc. Currently, there is an exhaustive literature on aloe gel but very few on aloe rinds. Aloe leaves were freshly collected (127gm) and washed with distilled water. Each leaf was scraped to separate the rinds from the gel, the rinds were left to dry at room temperature in the laboratory for 8 days. The semi-dried rinds were submerged completely in distilled water and sonicated for 72 hours. The resultant mixture was filtered, and the solvent was evaporated under reduced pressure. A resultant thick gummy mass was obtained, then transferred to a porcelain dish and placed on a heating mantle for further drying at 30^{o}C. The dried mass was collected, weighed, and transferred to a

stoppered Erlenmeyer flask, which was placed in a desiccator for 48 hours to ensure maximum drying. After the stipulated time, the flask was taken out and the final weight was taken (93.93gm). Currently, a research is being conducted on the dried mass of the aloe rind water extract using HRMS.

iii. Magnolol water extract

Fresh mature green seed cones were collected from the *Magnolia grandiflora* tree, located at the University of Texas Rio Grande Valley. The seeds were purged, and the cones were chopped into several small fragments and air-dried. The dried seeds were crushed into small particulates and immersed completely in water for 48 hours and sonicated at 25ºC for 21 hours (cold extraction method). The extract is filtered, and the filtrate is evaporated under reduced pressure using a rotavapor (Buchi Rotavapor R114). The gummy mass obtained is first dried using a heating mantle for 72hours, for further drying it is placed in a desiccator for an additional 48 hours. The resultant dried mass (85gm) is chromatographed over silica gel. HPLC/MS-MS was conducted.

Synthetic procedure for the chemical modification of DBPO series

Reaction 1: Semisynthetic procedure for DBMGPO-1

All glassware and metal wares used must be oven-dried, add magnolol (0.376mmol), dry DCM (7 mL), and dry triethylamine (TEA) (1 mL) are added to a 25ml round bottom flask containing a magnetic stirrer. The round bottom flask is sealed, and the solution is placed in an ice bath (0-5ºC) and stirred for 20-25 minutes under argon. The methane sulfonyl chloride (0.6ml) is added to the solution and stoppered immediately, the reaction mixture is stirred vigorously until the reaction is complete (TLC monitoring). Reaction time- 14 hours. The resultant reaction mixture was extracted (liquid-liquid extraction) in a separatory funnel with dichloromethane (DCM), the

organic phase was washed with brine solution (saturated saltwater), then dried for about 10-15 minutes with a sufficient amount of anhydrous sodium sulfate, the mixture is filtered, concentrated under reduced pressure with a rotavapor using Buchi Rotavapor R114. The resultant reaction mixture was purified by column chromatography on silica gel to yield pure products. Ethyl acetate and hexanes were used as a solvent.

Reaction 2: Semisynthetic procedure for DBMGPO-2

Magnolol (0.5mmol, 133mg), dry DCM (7 mL), and dry triethylamine (TEA) (1 mL) are added to a 25ml round bottom flask containing a magnetic stirrer. The round bottom flask is sealed, and the solution is placed in an ice bath (0-5^{o}C) and stirred for 20-25 minutes under argon. The 4 fluorobenzene sulfonyl chloride (195 mg) is added to the solution and stoppered immediately, the reaction mixture is stirred vigorously until the reaction is complete (TLC monitoring). Reaction time: 16 hours. The resultant reaction mixture was extracted (liquid-liquid extraction) in a separatory funnel with dichloromethane (DCM), the organic phase was washed with brine solution (saturated saltwater), then dried for about 10-15 minutes with a sufficient amount of anhydrous sodium sulfate, the mixture is filtered, concentrated under reduced pressure with a rotavapor using Buchi Rotavapor R114. The resultant reaction mixture was purified by column chromatography on silica gel to yield pure products. Ethyl acetate and hexanes were used as a solvent.

Reaction 3: Semisynthetic procedure for DBMGPO-3

Magnolol (0.5mmol, 133mg), dry DCM (7 mL), and dry triethylamine (TEA) (1 mL) are added to a 25ml round bottom flask containing a magnetic stirrer. The round bottom flask is sealed, and the solution is placed in an ice bath (0-5^{o}C) and stirred for 20-25 minutes under argon. The 4-

nitrobenzene sulfonyl chloride (222 mg) is added to the solution and stoppered immediately; the reaction mixture is stirred vigorously until the reaction is complete (TLC monitoring). Reaction time: 14 hours. The resultant reaction mixture was extracted (liquid-liquid extraction) in a separatory funnel with dichloromethane (DCM), the organic phase was washed with brine solution (saturated saltwater), then dried for about 10-15 minutes with a sufficient amount of anhydrous sodium sulfate, the mixture is filtered, concentrated under reduced pressure with a rotavapor using Buchi Rotavapor R114. The resultant reaction mixture was purified by column chromatography on silica gel to yield pure products. Ethyl acetate and hexanes were used as a solvent.

Reaction 4: Semisynthetic procedure for DBMGPO-4

Magnolol (0.5mmol, 133mg), dry DCM (7 mL), and dry triethylamine (TEA) (1 mL) are added to a 25ml round bottom flask containing a magnetic stirrer. The round bottom flask is sealed, and the solution is placed in an ice bath (0-5^{o}C) and stirred for 20-25 minutes under argon. The 3,5- Bis (trifluoromethyl benzenesulfonyl chloride) (1.2 mmol, 375 mg) is added to the solution and stoppered immediately, the reaction mixture is stirred vigorously until the reaction is complete (TLC monitoring). Reaction time: 15 hours. The resultant reaction mixture was extracted (liquid-liquid extraction) in a separatory funnel with dichloromethane (DCM), the organic phase was washed with brine solution (saturated saltwater), then dried for about 10-15 minutes with a sufficient amount of anhydrous sodium sulfate, the mixture is filtered, concentrated under reduced pressure with a rotavapor using Buchi Rotavapor R114. The resultant reaction mixture was purified by column chromatography on silica gel to yield pure products. Ethyl acetate and hexanes were used as a solvent.

Reaction 5: Semisynthetic procedure for DBMGPO-5

Magnolol (0.5mmol, 133mg), dry DCM (7 mL), and dry triethylamine (TEA) (1 mL) are added to a 25ml round bottom flask containing a magnetic stirrer. The round bottom flask is sealed, and the solution is placed in an ice bath (0-5^{o}C) and stirred for 20-25 minutes under argon. The 2,2,2-trifluoroethane sulfonyl chloride (1.2 mmol, 0.14ml) is added to the solution and stoppered immediately, the reaction mixture is stirred vigorously until the reaction is complete (TLC monitoring). Reaction time: 14 hours. The resultant reaction mixture was extracted (liquid-liquid extraction) in a separatory funnel with dichloromethane (DCM), the organic phase was washed with brine solution (saturated saltwater), then dried for about 10-15 minutes with a sufficient amount of anhydrous sodium sulfate, the mixture is filtered, concentrated under reduced pressure with a rotavapor using Buchi Rotavapor R114. The resultant reaction mixture was purified by column chromatography on silica gel to yield pure products. Ethyl acetate and hexanes were used as a solvent.

Reaction 6: Semisynthetic procedure for DBMGPO-6

Magnolol (0.5mmol, 133mg), dry DCM (7 mL), and dry triethylamine (TEA) (0.7 mL) are added to a 25ml round bottom flask containing a magnetic stirrer. The round bottom flask is sealed, and the solution is placed in an ice bath (0-5^{o}C) and stirred for 20-25 minutes under argon. The pyrrolidine -1- sulfonyl chloride (2.4 mmol, 0.28 ml) is added to the solution and stoppered immediately; the reaction mixture is stirred vigorously until the reaction is complete (TLC monitoring). Reaction time: 51 hours. The resultant reaction mixture was extracted (liquid-liquid extraction) in a separatory funnel with dichloromethane (DCM), the organic phase was washed with brine solution (saturated saltwater), then dried for about 10-15 minutes with a sufficient

amount of anhydrous sodium sulfate, the mixture is filtered, concentrated under reduced pressure with a rotavapor using Buchi Rotavapor R114. The resultant reaction mixture was purified by column chromatography on silica gel to yield pure products. Ethyl acetate and hexanes were used as a solvent.

Reaction 7: Semisynthetic procedure for DBMGPO-7

Magnolol (0.5mmol, 133mg), dry DCM (7 mL), and dry triethylamine (TEA) (0.7 mL) are added to a 25ml round bottom flask containing a magnetic stirrer. The round bottom flask is sealed, and the solution is placed in an ice bath (0-5^{o}C) and stirred for 20-25 minutes under argon. The morpholine -4- sulfonyl chloride (3 mmol, 0.364ml) is added to the solution and stoppered immediately, the reaction mixture is stirred vigorously until the reaction is complete (TLC monitoring). Reaction time: 25 hours. The resultant reaction mixture was extracted (liquid-liquid extraction) in a separatory funnel with dichloromethane (DCM), the organic phase was washed with brine solution (saturated saltwater), then dried for about 10-15 minutes with a sufficient amount of anhydrous sodium sulfate, the mixture is filtered, concentrated under reduced pressure with a rotavapor using Buchi Rotavapor R114. The resultant reaction mixture was purified by column chromatography on silica gel to yield pure products. Ethyl acetate and hexanes were used as a solvent.

Reaction 8: Semisynthetic procedure for DBMGPO-8

Magnolol (1 mmol, 266 mg), dry DCM (10 mL), and dry triethylamine (TEA) (6 mmol, 0.84mL) are added to a 25ml round bottom flask containing a magnetic stirrer. The round bottom flask is sealed, and the solution is placed in an ice bath (0-5^{o}C) and stirred for 20-25 minutes under

argon. The 3- cyanoazetidine -1- sulfonyl chloride (3 mmol, 542 mg) is added to the solution and stoppered immediately; the reaction mixture is stirred vigorously until the reaction is complete (TLC monitoring). Reaction time: 3 days. The resultant reaction mixture was extracted (liquid-liquid extraction) in a separatory funnel with dichloromethane (DCM), the organic phase was washed with brine solution (saturated saltwater), then dried for about 10-15 minutes with a sufficient amount of anhydrous sodium sulfate, the mixture is filtered, concentrated under reduced pressure with a rotavapor using Buchi Rotavapor R114. The resultant reaction mixture was purified by column chromatography on silica gel to yield pure products. Ethyl acetate and hexanes were used as a solvent.

Reaction 9: Semisynthetic procedure for DBADAPO-1A-1C

3-amino adamantan-1-ol (2 mmol, 334.5 mg), dry DCM (20 mL), and dry triethylamine (TEA) (18 mmol, 2.51 mL) are added to a 25ml round bottom flask containing a magnetic stirrer. The round bottom flask is sealed, and the solution is placed in an ice bath (0-5^{o}C) and stirred for 20-25 minutes under argon. The 3- cyanoazetidine -1- sulfonyl chloride (9.6 mmol, 1.73 grams) is added to the solution and stoppered immediately; the reaction mixture is stirred vigorously until the reaction is complete (TLC monitoring). Reaction time: 9 days. The resultant reaction mixture was extracted (liquid-liquid extraction) in a separatory funnel with dichloromethane (DCM), the organic phase was washed with brine solution (saturated saltwater), then dried for about 10-15 minutes with a sufficient amount of anhydrous sodium sulfate, the mixture is filtered, concentrated under reduced pressure with a rotavapor using Buchi Rotavapor R114. The resultant reaction mixture was purified by column chromatography on silica gel to yield pure products. Ethyl acetate

and hexanes were used as a solvent. Each compound of the DBADAPO-1 series eluted at different solvent ratios.

Reaction 10: Semisynthetic procedure for DBQPO-1A-1B

4-amino -7- chloro quinoline (2 mmol, 357 mg), dry DCM (15 mL), and dry triethylamine (TEA) (12 mmol, 1.673 mL) are added to a 25ml round bottom flask containing a magnetic stirrer. The round bottom flask is sealed, and the solution is placed in an ice bath (0-5^{o}C) and stirred for 20-25 minutes under argon. The 3- cyanoazetidine -1- sulfonyl chloride (6 mmol, 1.084 grams) is added to the solution and stoppered immediately; the reaction mixture is stirred vigorously until the reaction is complete (TLC monitoring). Reaction time: 4 days. The resultant reaction mixture was extracted (liquid-liquid extraction) in a separatory funnel with dichloromethane (DCM), the organic phase was washed with brine solution (saturated saltwater), then dried for about 10-15 minutes with a sufficient amount of anhydrous sodium sulfate, the mixture is filtered, concentrated under reduced pressure with a rotavapor using Buchi Rotavapor R114. The resultant reaction mixture was purified by column chromatography on silica gel to yield pure products. Ethyl acetate and hexanes were used as a solvent. Each compound of the DBQPO- 1 series eluted at different solvent ratios.

Reaction 11: Semisynthetic procedure for DBQPO-2A-2B

4-amino -7- chloro quinoline (2 mmol, 357 mg), dry DCM (15 mL), and dry triethylamine (TEA) (12 mmol, 1.673 mL) is added to a 25ml round bottom flask containing a magnetic stirrer. The round bottom flask is sealed, and the solution is placed in an ice bath (0-5^{o}C) and stirred for 20-25 minutes under argon. The para- trifluoro methyl benzene sulfonyl chloride (6 mmol, 1.468

grams) is added to the solution and stoppered immediately; the reaction mixture is stirred vigorously until the reaction is complete (TLC monitoring). Reaction time: 3 days. The resultant reaction mixture was extracted (liquid-liquid extraction) in a separatory funnel with dichloromethane (DCM), the organic phase was washed with brine solution (saturated saltwater), then dried for about 10-15 minutes with a sufficient amount of anhydrous sodium sulfate, the mixture is filtered, concentrated under reduced pressure with a rotavapor using Buchi Rotavapor R114. The resultant reaction mixture was purified by column chromatography on silica gel to yield pure products. Ethyl acetate and hexanes were used as a solvent. Each compound of the DBQPO-2 series eluted at different solvent ratios.

Reagent grade chemicals and solvents were used for all experimental procedures unless otherwise stated, UltraPure Silica Gels (Silicycle) was procured from 2500, boul. du Parc-Technologique, Québec (Québec) G1P 4S6 CANADA. All solvents for entire experimental procedures were purchased from Fisher-Scientific (Pittsburgh, PA). Additional chemicals were procured from Sigma-Aldrich Corporation (St. Louis, MO). Deionized water was used for the preparation of all aqueous solutions. All columns used were purchased from Sigma-Aldrich. Different column sizes and length was used for column chromatography to ensure an efficient separation. Air pressure was used in running the column.

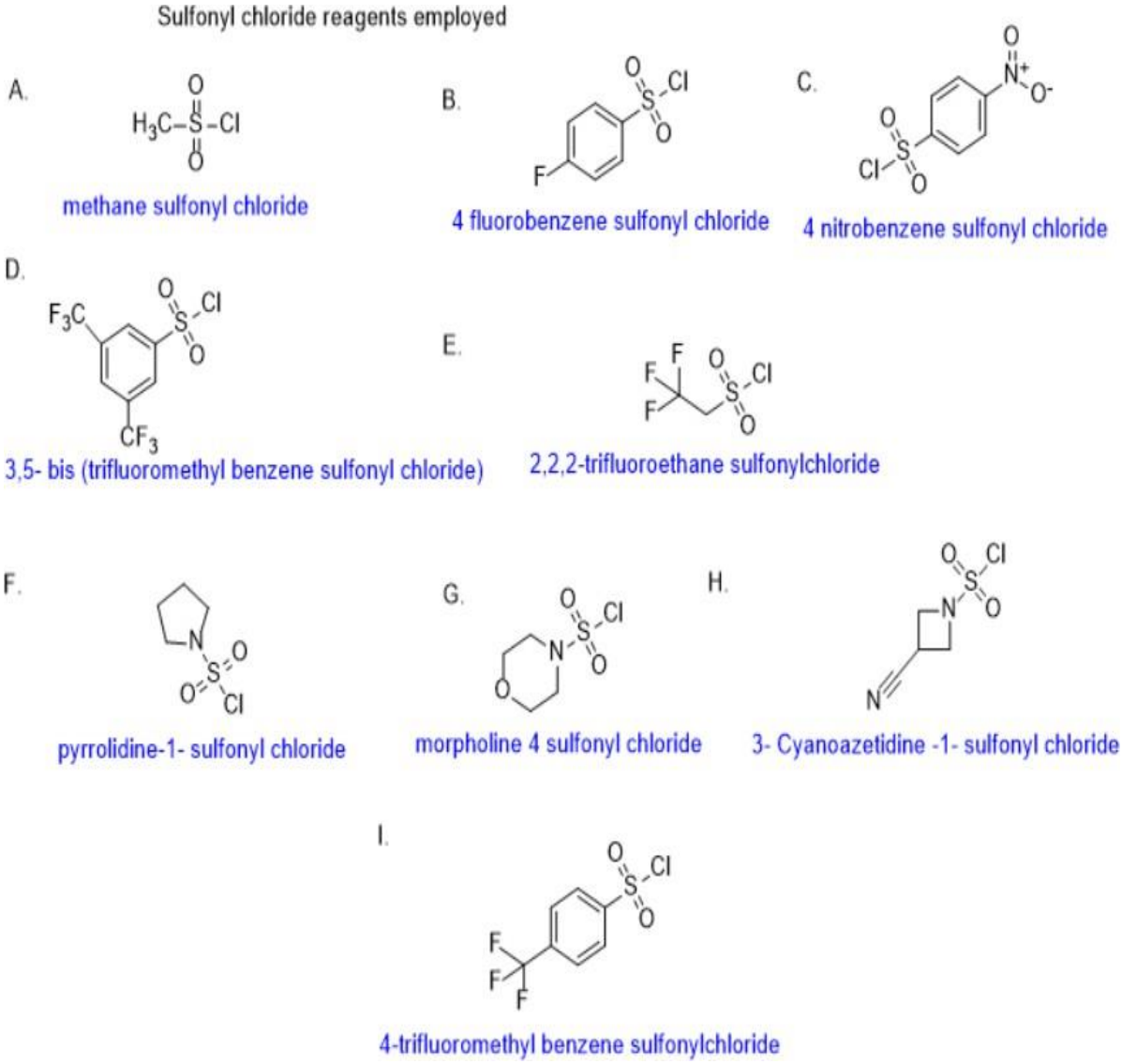

Figure 23. Different sulfonyl chloride reagents used.

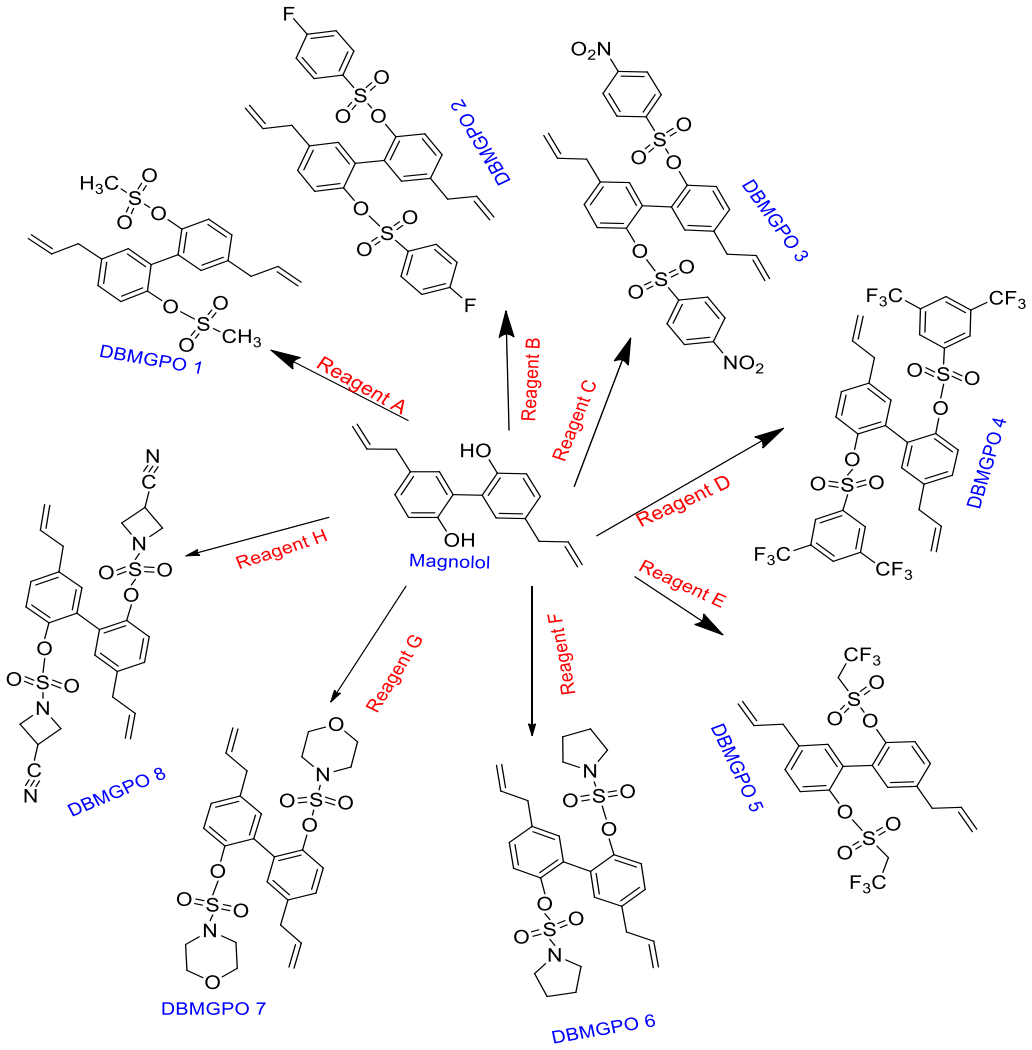

Figure 24. Novel chemically modified magnolol derivatives (DBMGPO 1-8)

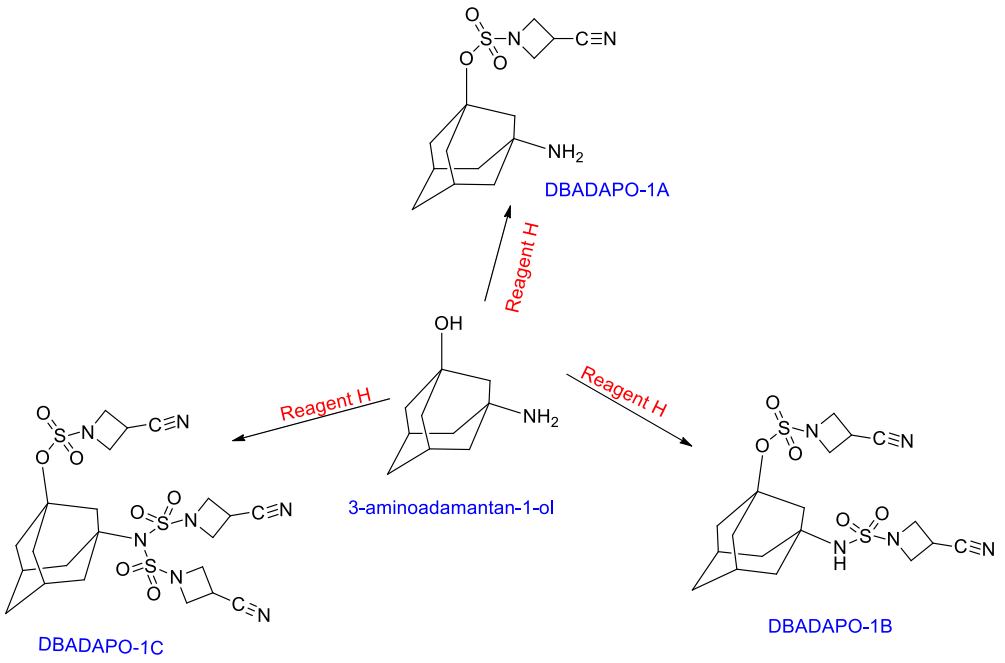

Figure 25. Novel chemically modified 3-aminoadamantan-1-ol derivatives (DBADAPO 1A-1C)

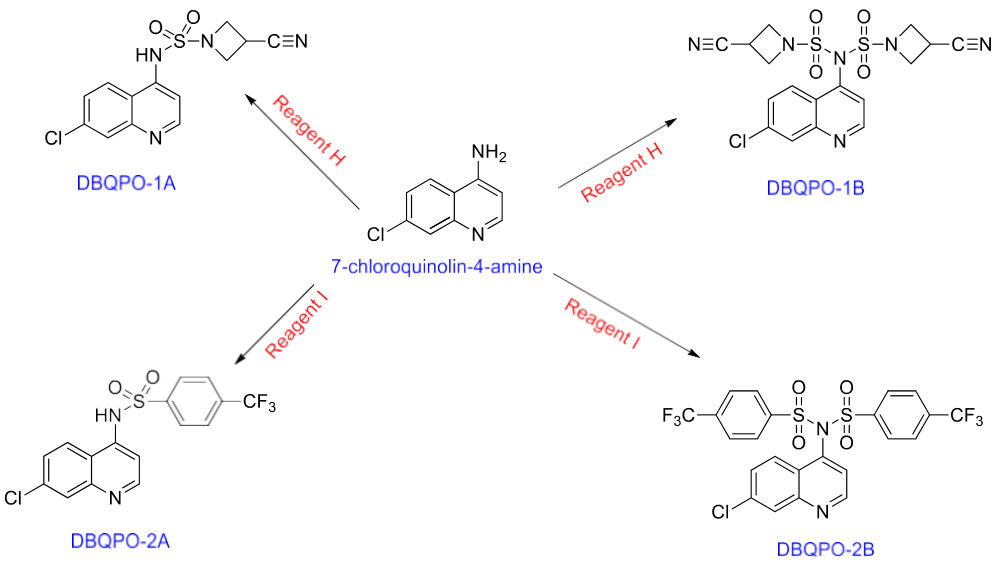

Figure 26. Novel chemically modified 4-amino-7-chloroquinoline derivatives (DBQPO 1A-1B, 2A-2B)

Code	Structure	IUPAC Name	MW (g/mol)	M.F
Magnolol	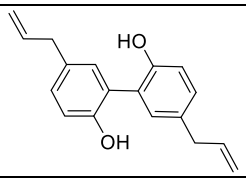	5,5'-diallyl-[1,1'-biphenyl]-2,2'-diol	266.4	$C_{18}H_{18}O_2$
DBMGPO-1	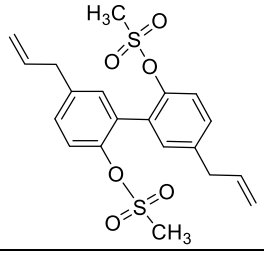	5,5'-diallyl-[1,1'-biphenyl]-2,2'-diyl dimethanesulfonate	422.52	$C_{20}H_{22}O_6S_2$
DBMGPO-2	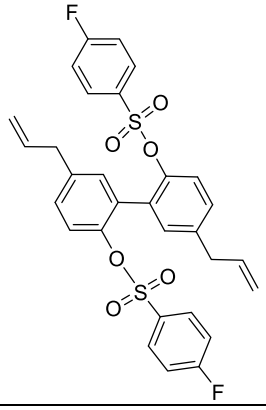	5,5'-diallyl-[1,1'-biphenyl]-2,2'-diyl bis(4-fluorobenzenesulfonate)	582.64	$C_{30}H_{24}O_6F_2S_2$
DBMGPO-3	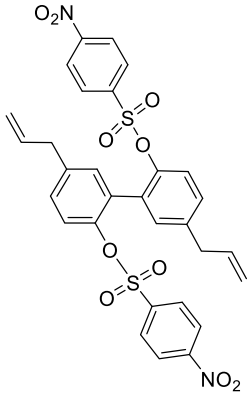	5,5'-diallyl-[1,1'-biphenyl]-2,2'-diyl bis(4-nitrobenzenesulfonate)	636.66	$C_{30}H_{24}N_2O_{10}S_2$
DBMGPO-4	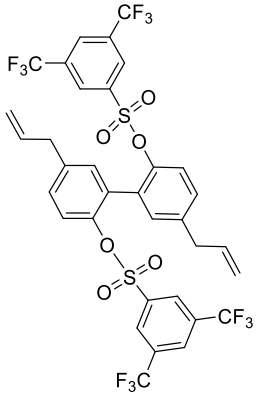	5,5'-diallyl-[1,1'-biphenyl]-2,2'-diyl bis(3,5-bis(trifluoromethyl)benzenesulfonate)	818.65	$C_{34}H_{22}O_6F_{12}S_2$

DBMGPO-5 (This reaction did not give a good yield, only 16 mg after three efforts).	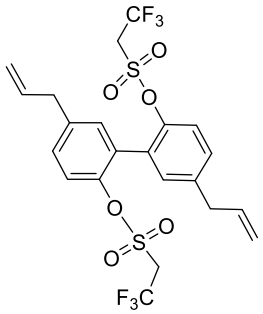	5,5'-diallyl-[1,1'-biphenyl]-2,2'-diyl bis(2,2,2-trifluoroethanesulfonate)	558.51	$C_{22}H_{20}O_6F_6S_2$
DBMGPO-6	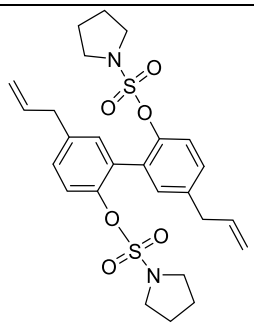	5,5'-diallyl-[1,1'-biphenyl]-2,2'-diyl bis(pyrrolidine-1-sulfonate)	532.68	$C_{26}H_{32}N_2O_6S_2$
DBMGPO-7	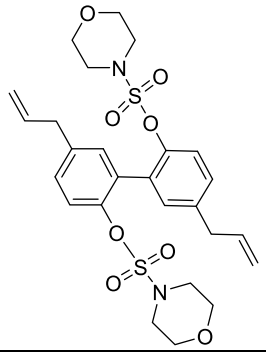	5,5'-diallyl-[1,1'-biphenyl]-2,2'-diyl bis(morpholine-4-sulfonate)	564.68	$C_{26}H_{32}N_2O_8S_2$
DBMGPO-8	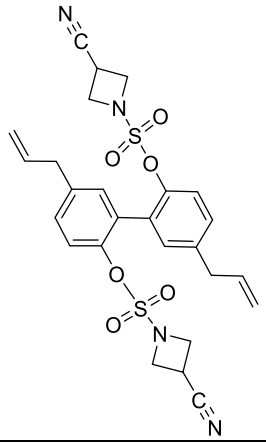	5,5'-diallyl-[1,1'-biphenyl]-2,2'-diyl bis(3-cyanoazetidine-1-sulfonate)	554.65	$C_{26}H_{26}N_4O_6S_2$
DBADAPO-1A (3-Amino-1-adamantanol derived products)	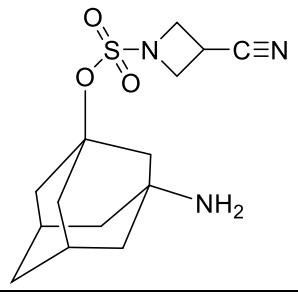	(1s,3r,5R,7S)-3-aminoadamantan-1-yl 3-cyanoazetidine-1-sulfonate	311.40	$C_{14}H_{21}N_3O_3S$

DBADAPO-1B	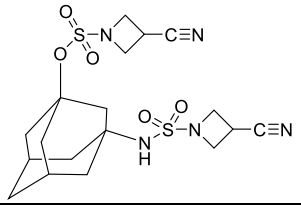	(1s,3r,5R,7S)-3-(3-cyanoazetidine-1-sulfonamido) adamantan-1-yl 3-cyanoazetidine-1-sulfonate	455.56	$C_{18}H_{25}N_5O_5S_2$
DBADAPO-1C	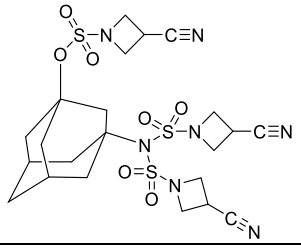	(1s,3r,5R,7S)-3-(3-cyano-N-((3-cyanoazetidin-1-yl)sulfonyl)azetidine-1-sulfonamido)adamantan-1-yl 3-cyanoazetidine-1-sulfonate	599.71	$C_{22}H_{29}N_7O_7S_3$
DBQPO-1A	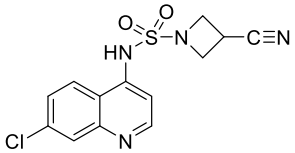	N-(7-chloroquinolin-4-yl)-3-cyanoazetidine-1-sulfonamide	322.78	$C_{13}H_{11}N_4O_2ClS$
DBQPO-1B	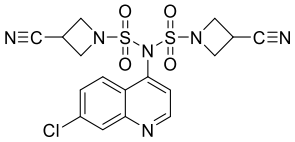	N-(7-chloroquinolin-4-yl)-3-cyano-N-((3-cyanoazetidin-1-yl)sulfonyl)azetidine-1-sulfonamide	466.93	$C_{17}H_{15}N_6O_4ClS_2$
DBQPO-2A	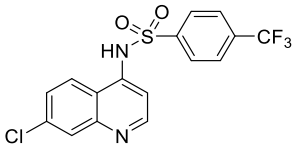	N-(7-chloroquinolin-4-yl)-4-(trifluoromethyl)benzenesulfonamide	386.78	$C_{16}H_{10}N_2O_2ClF_3S_2$
DBQPO-2B	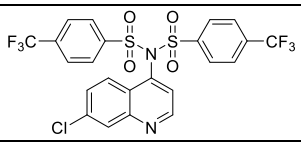	N-(7-chloroquinolin-4-yl)-4-(trifluoromethyl)-N-((4-(trifluoromethyl)phenyl)sulfonyl)benzenesulfonamide	594.94	$C_{23}H_{13}N_2O_4ClF_6S_2$

Table 7. IUPAC name, molecular formula and molecular weight of novel DBPO series

Code	Eluting solvent	MP (°C)	Yield (mg)	Percentage yield	Color and description
Magnolol	3%EA/HEX	101.5-102	818	-	White crystalline solid
DBMGPO-1	5-20% EA/HEX	-	53	33.42%	Yellow semi-solid

DBMGPO-2 (Please note this is a different compound than before. Initially it was DBMGPO-4)	5-6% EA/HEX	107.1-107.8	156	53.6%	White short needle shaped flaky crystals
DBMGPO-3	8% EA/HEX	160.3-161.4	146	51.9%	White flaky amorphous solid
DBMGPO-4	2-4% EA/HEX	122.2-123.5	206	61.9%	White ball and needle shaped crystals
DBMGPO-5 (This reaction did not give a good yield, only 16 mg after three efforts).	20-30% EA/HEX	-	16	5.7%	Milky yellow crystals
DBMGPO-6	1%, 4-5% EA/HEX	173.3-183.1	204	76.7%	Transparent white solid shape (boxy) crystal
DBMGPO-7	11% EA/HEX	-	30	10.6%	Yellow semisolid
DBMGPO-8	26% EA/HEX	89.4-90.5	440	79.4%	White flaky amorphous solid
DBADAPO-1A (3-Amino-1-adamantanol derived products)	50% EA/HEX	152.4-153.7	18	TBD	White short narrow crystals
DBADAPO-1B	50% EA/HEX	144.4-147.8b	54	TBD	White solid crystals

DBADAPO-1C	50-75% EA/HEX	151.0-152.0	141	TBD	Yellow solid crystals
DBQPO-1A	50% EA/HEX	151.8-155.2	95	TBD	Light yellow amorphous solid
DBQPO-1B	80-85% EA/HEX	105.1-107.8	75	TBD	Orange amorphous solid
DBQPO-2A	75% EA/HEX	252-254	623	TBD	Milky white flaky amorphous solid
DBQPO-2B	50% MEOH/EA	210-214 (decomposed)	375	TBD	Brown amorphous solid

Table 8. Characterization of DBPO series showing yield, melting points, description, and elution percentage.

Characterization of novel pure compounds obtained in the DBPO series

FT-IR spectra of all the DBPO series were performed on a Bruker Alpha modular Platinum-ATR FT-IR spectrometer with OPUS software, using the samples directly. NMR spectra analysis was performed using Bruker Ascend 500 MHz with a cold probe for better resolution and Bruker 600 MHz. Spectras were generated using TopSpin software.

5,5'-diallyl-[1,1'-biphenyl]-2,2'-diol **(Magnolol)**

FTIR shows a broad strong peak from 2919-3075 cm^{-1} this indicates the presence of an alkene group (unsaturation), 731-1135 cm^{-1} indicates presence of aromatic compound, sharp narrow peak at 704 cm^{-1} - indicates benzene derivative. DEPTs 90 and 135 were used to identify methine, methylene and methyl carbons. ^{1}H NMR (500 MHz, $CDCl_3$, 7.5 ppm), ^{1}H-NMR ppm

δ7.1245 (2H, dd, J=2.1), 7.0760 (d, 2H, J=2.1), 6.9406 (d, J=8.28, 2H), 5.9906-5.9232 (m, 2H), 5.65 (s, 4H), 5.1041-5.0499 (m, 4H), 3.3642 (d, J=6.72, 4H); ^{13}C (150 MHz, $CDCl_3$) ppm δ 151.12 (q), 137.51 (≡CH), 133.25 (q), 131.22 (≡CH), 130.00 (≡CH), 123.75(q), 116.6 (≡CH), 115.84 (-CH_2-), 39.96 (-CH_2-).

5,5'-diallyl-[1,1'-biphenyl]-2,2'-diyl dimethanesulfonate **DBMGPO-1**

FTIR shows a sharp strong peak from 2847-2914 cm^{-1} this indicates the presence of an alkene group, Strong peak at 1310- 1367 cm^{-1} (S=O stretch) indicates sulfonate derivative, sharp narrow peak at 1165 indicates C-O stretch. DEPTs 90 and 135 were used to identify methine, methylene and methyl carbons. ^{1}H NMR (600 MHz, $CDCl_3$), ^{1}H-NMR ppm δ7.2894 (dd, J=2.22Hz, 2H), 7.2277 (d, J = 2.16 Hz, 2H), 7.0534 (dd, J= 7.56 Hz, 2H), 6.9604 (d, J= 8.34, 2H), 6.9051 (d, J=8.16, 1H), 6.0075-5.9634 (m, 2H), 5.3475 (d, J = 2.76 Hz, 2H), 5.0698 (m, 4H), 3.8743(s, 3H), 3.4318 (dd J=6.66, 2H), ^{13}C (150 MHz, $CDCl_3$) ppm δ 157.09 (q), 150.85 (q), 137.81 (≡CH), 136.52 (≡CH), 132.17 (q), 130.51 (≡CH), 115.82 (≡CH), 115.9 (-CH_2-), 39.4 (-CH_2-), 27.23 (-CH_3-).

5,5'-diallyl-[1,1'-biphenyl]-2,2'-diyl bis(4-fluorobenzenesulfonate) **DBMGPO-2**

FT-IR spectra of DBMG(OFBS)PO shows strong peak at 1489 cm^{-1}- indicates presence of a fluoro compound, Strong peak at 1371 cm^{-1} - indicates presence of sulfonate group (S=O stretch), sharp broad peak at 1173 cm^{-1} - Indicates C-F stretch, sharp narrow peak at 704 cm^{-1} - indicates benzene derivative, peaks from 704-1131 cm^{-1} indicates presence of aromatic compound. . DEPTs 90 and 135 were used to identify methine, methylene and methyl carbons. ^{1}H NMR(500 MHz, DMSO), ^{1}H-NMR ppm δ 7.3800-7.3523 (m, 4H), 7.2605 (q, J =9 Hz, 2H), 6.6292 (d, J=4.25 Hz, 2H), 6.1288-6.0500 (m, 4H), 5.2929 (dd, J=5.6, 4H), 5.1433 (d, J=1.35, 2H), 5.1274 (d, J=10.2, 2H), 3.3326 (t, J = 13.1 Hz, 4H). ^{13}C (150 MHz, DMSO) ppm δ 166.70 (q), 164.68 (q), 152.35 (q), 144.5(q), 139.72(q), 137.0(≡CH), 131.44(≡CH), 131.13(≡CH), 131.05(≡CH), 129.97(≡CH), 123.10(≡CH), 117.40(≡CH), 117.22(≡CH), 117.21 9 (-CH_2-), 38.829 (-CH_2-). 19F

(470 MHz, DMSO) -102.87- -102.92 (Ar- 2F)

5,5'-diallyl-[1,1'-biphenyl]-2,2'-diyl bis*(4-nitrobenzenesulfonate)* **DBMGPO-3**

FT-IR spectra of DBMG(ONBS)PO shows a narrow sharp peak at 1527 cm^{-1} - Indicates presence of a Nitro compound (N-O stretch), Peak at 1375 cm^{-1} shows presence of Sulfonate (S=O stretch), Peak at 1168 cm^{-1} indicates C-O stretch, Peak at 701-741- Benzene derivative, narrow sharp peaks from 823- 1104 cm^{-1} indicates presence of an aromatic compound. . DEPTs 90 and 135 were used to identify methine, methylene and methyl carbons. ^{1}H NMR (500 MHz, DMSO), ^{1}H-NMR ppm δ 8.2578(d, J=8.7, 4H), 7.6803 (d, J =8.55 Hz, 4H), 7.6632 (d, J=21.8 Hz, 2H), 7.2569 (dd, J=1.6, 4H), 6.6065 (s, 2H), 5.8862-5.8372 (m, 2H), 5.0592-4.9525 (m, 4H), 3.3329(d, J= 6.40, 2H). ^{13}C (150 MHz, DMSO) ppm δ 152.96 (q), 150.91(q), 148.08 (q), 144.41 (q), 140.25 (q), 140.14 (q), 136.87 (≡CH), 131.70(≡CH), 130.24(≡CH), 129.61(≡CH), 125.11(≡CH), 123.34(≡CH), 117.20 (≡CH), 117.0 (-CH_2-), 38.67 (-CH_2-).

5,5'-diallyl-[1,1'-biphenyl]-2,2'-diyl bis(3,5-bis(trifluoromethyl)benzenesulfonate) **DBMGPO-4**

FT-IR spectra of DBMG(TFMBS)PO: Strong narrow peak at 590 cm^{-1} indicates the presence of halo compound, sharp peak at 1389 cm^{-1} indicates C-F stretch, Strong peak at 710 indicates benzene derivative, Peak at 1335 cm^{-1} (S=O stretch) indicates presence of a Sulfonate derivative. . DEPTs 90 and 135 were used to identify methine, methylene and methyl carbons. ^{1}H NMR (500 MHz, DMSO), ^{1}H-NMR ppm δ 8.6449 (s, 4H), 7.8910 (s, 2H), 7.2478 (s, 2H), 5.8936-5.8395 (m, 2H), 5.8463-5.7621 (m, 4H), 5.0314 (d, J=1.3 Hz, 4H), 4.9071 (s, 2H), 3.3322 (s, 4H). ^{13}C (150 MHz, DMSO) 143.96 (q), 140.25 (q), 137.44 (q), 136.78 (≡CH), 132.30 (q), 131.48 (≡CH), 130.74 (≡CH), 129.47 (≡CH), 128.31 (≡CH), 125.77 (q), 125.77 (q), 123.25 (≡CH), 121.42 (q), 119.24 (q), 119.24(q), 117.11 (-CH_2-), 38.67 (-CH_2-). 19F NMR (-61.48)

5,5'-diallyl-[1,1'-biphenyl]-2,2'-diyl bis(pyrrolidine-1-sulfonate) **DBMGPO-6**

FT-IR spectra of DBMG(OPSC)PO: medium broad peak at 2996 cm^{-1} (N-H) stretch indicates presence of an amine salt, medium narrow peak at 1378 cm^{-1} indicates presence of a sulfonate (S=O stretch), broad peak from 1241 cm^{-1} shows C-N stretch, narrow peaks from 661-1186 cm^{-1} indicates presence of an aromatic compound.

5,5'-diallyl-[1,1'-biphenyl]-2,2'-diyl bis(morpholine-4-sulfonate) **DBMGPO-7**

The slightly broadened peaks at about 2862- 2976 cm^{-1} clearly indicates presence of C–H stretching bands, Strong narrow peak at 1372 cm^{-1} (S=O stretch), narrow sharp peaks from 641-1195 cm^{-1} indicates presence of an aromatic compound. DEPTs 90 and 135 were used to identify methine, methylene and methyl carbon. ^{1}H NMR (600 MHz, $CDCl_3$), ^{1}H-NMR ppm δ 7.5195 (d, J=8.4 Hz, 2H), 7.3048 (d, J = 1.9 Hz, 2H), 6.9560 (d, J= 8.25 Hz, 2H), 6.0085-5.9265 (m, 2H), 5.1664-5.0656 (m, 4H), 3.5962 (t, J = 4.75 Hz, 4H), 3.5962 (t, J = 4.75 Hz, 4H), 3.4574(dd, J=6.8, 4H), 2.9921 (t, 4.75 J=4.75, 4H), 2.9826 (t, 4.75 J=4.75, 4H). ^{13}C (150 MHz, $CDCl_3$) ppm δ 151.46 (q), 136.45 (q), 136.3 (≡CH), 132.28 (≡CH), 130.0 (≡CH), 127.10 (q), 116.2 (≡CH), 115.73 (-CH_2-), 65.73 (-CH_2-), 65.73 (-CH_2-), 46.37(-CH_2-), 46.37 (-CH_2-), 39.8 (-CH_2-).

5,5'-diallyl-[1,1'-biphenyl]-2,2'-diyl bis(3-cyanoazetidine-1-sulfonate) **DBMGPO- 8**

Slightly broad peaks at about 2890 cm^{-1} clearly indicates presence of C–H stretching bands. Weak narrow sharp peak at 2251 cm^{-1} indicates presence of (−C≡N stretching) nitrile group, strong narrow peak at 1378 cm^{-1} (S=O stretch) indicates presence of a sulfonate, narrow sharp peaks from 635- 1128 cm^{-1} indicates presence of an aromatic compound. DEPTs 90 and 135 were used to identify methine, methylene and methyl carbons. ^{1}H NMR (500 MHz, DMSO),

^{1}H-NMR ppm δ 7.3963 (d, J =1.95 Hz, 2H), 7.3795 (d, J=2 Hz, 2H), 7.2968 (dd, J=1.85, 2H), 6.0449 (m, 2H), 5.1509-5.0859 (m, 4H), 3.1476 (d, J=6.7, 4H), 3.7580 (m, 8H), 3.7580 (s, 2H). ^{13}C (150 MHz, DMSO) ppm δ 146.82(q), 145.15(q), 143.15(q), 139.56(q), 138.95(q), 137.53(≡CH), 130.40 (≡CH), 121.83(≡CH), 132.28(≡CH), 116.93(-CH_2-), 54.82(-CH_2-), 39.03(-CH_2-), 17.43(-CH_2-).

(1s,3r,5R,7S)-3-aminoadamantan-1-yl 3-cyanoazetidine-1-sulfonate **DBADAPO-1A**

FTIR shows slightly broad weak peaks at about 2890- 3006 cm^{-1} indicates the presence of C–H stretching bands, sharp peak at 2246 cm^{-1} shows (−C≡N stretching) nitrile group, strong narrow sharp peak at 1378 cm^{-1} (S=O stretch) indicates the presence of a sulfonate moiety.

(1s,3r,5R,7S)-3-(3-cyanoazetidine-1-sulfonamido) adamantan-1-yl 3-cyanoazetidine-1-sulfonate **DBADAPO-1B**

FTIR shows slightly broad weak peaks at about 2895- 3006 cm^{-1} indicates the presence of C–H stretching bands, sharp peak at 2246 cm^{-1} shows (−C≡N stretching) nitrile group, strong narrow sharp peak at 1346 cm^{-1} (S=O stretch) indicates the presence of sulfonate and sulfonamide.

(*1s,3r,5R,7S)-3-(3-cyano-N-((3-cyanoazetidin-1-yl)sulfonyl)azetidine-1-sulfonamido) adamantan-1-yl 3-cyanoazetidine-1-sulfonate* **DBADAPO-1C**

FTIR shows a slightly broad weak peak at about 2902 cm^{-1} indicates the presence of C–H stretching bands, a sharp peak at 2240 cm^{-1} shows the presence of (−C≡N stretching) nitrile group, strong narrow sharp peak at 1349cm^{-1} (S=O stretch) indicates the presence of sulfonate and sulfonamide.

N-(7-chloroquinolin-4-yl)-3-cyanoazetidine-1-sulfonamide **DBQPO-1A**

FTIR shows a weak narrow peak at about 2223 cm^{-1} shows presence of (−C≡N stretching) nitrile group, strong narrow sharp peak at 1335 cm^{-1} (S=O stretch) indicates the presence of a sulfonate, narrow sharp peaks from 1275-1323 cm^{-1} indicates the presence of an aromatic amine group, narrow sharp peaks from 1048-1200 cm^{-1} indicates the presence of (-C-N stretch) of an amine group, strong narrow sharp peaks from 551-605 cm^{-1} indicates the presence of (-C-Cl stretch) halo compound. . DEPTs 90 and 135 were used to identify methine, methylene and methyl carbons. ^{1}H NMR (500 MHz, DMSO), ^{1}H-NMR ppm δ 8.3696 (d, J =8.95 Hz, 1H), 8.1858 (d, J=7.1 Hz, 1H), 7.7111 (s, 1H), 7.5183 (dd, J=1.9Hz, 1H), 7.0772 (d, J=7.25 Hz, 1H), 6.0960 (d, J=15.85, 1H), 4.2025 (dd, J=8.25 Hz 4H), 3.7745-3.7683 (m, 1H). ^{13}C (150 MHz, DMSO) ppm δ 145.02 (≡CH), 140.60 (q), 139.50 (q), 137.27 (q), 133.14 (≡CH), 127.65 (≡CH), 125.80 (≡CH), 120.34 (q), 119.55 (q), 105.36 (≡CH), 48.83 (-CH_2-), 45.89 (-CH_2-), 20.72 (≡CH).

N-(7-chloroquinolin-4-yl)-3-cyano-N-((3-cyanoazetidin-1-yl)sulfonyl)azetidine-1-sulfonamide

DBQPO-1B

FTIR shows a weak narrow peak at about 2229 cm^{-1} shows presence of (−C≡N stretching) nitrile group, strong narrow sharp peak at 1358 cm^{-1} (S=O stretch) indicates the presence of a sulfonate, narrow sharp peaks from 1278-1320 cm^{-1} indicates the presence of an aromatic amine group, narrow sharp peaks from 1078-1209 cm^{-1} indicates the presence of (-C-N stretch) of an amine group, strong narrow sharp peaks from 568 cm^{-1} indicates the presence of (-C-Cl stretch) halo compound.

N-(7-chloroquinolin-4-yl)-4-(trifluoromethyl)benzenesulfonamide **DBQPO- 2A**

FTIR shows a strong narrow sharp peak at 1367 cm^{-1} (S=O stretch) indicates the presence of a sulfonate, narrow sharp peaks from 1283-1320 cm^{-1} indicates the presence of an aromatic amine group, narrow sharp peaks from 1071-1205 cm^{-1} indicates the presence of (-C-N stretch) of an amine group, strong narrow sharp peaks from 593 cm^{-1} indicates the presence of (-C-Cl stretch) halo compound, a sharp narrow peak from 1086-1410 (-C-F stretch) indicates the presence of carbon-fluorine bond.

N-(7-chloroquinolin-4-yl)-4-(trifluoromethyl)-N-((4-(trifluoromethyl)phenyl)sulfonyl) benzenesulfonamide **DBQPO- 2B**

FTIR shows a strong narrow sharp peak at 1322 cm^{-1} (S=O stretch) indicates the presence of a sulfonate, narrow sharp peaks from 1297 cm^{-1} indicates the presence of an aromatic amine group, narrow sharp peaks from 1061-1233 cm^{-1} indicates the presence of (-C-N stretch) of an amine group, strong narrow sharp peaks from 601 cm^{-1} indicates the presence of (-C-Cl stretch) halo compound, a sharp narrow peak from 1404 (-C-F stretch) indicates the presence of carbon-fluorine bond.

1.7 Liquid chromatography-tandem mass spectroscopy analysis of magnolol water extract

LC-MS of magnolol water extract was done by another lab- Lifeasible™. A systematic process was followed.

i. Sample preparation

25 mg of sample was weighed and dissolved in 300 µL of water, mix well and then 100 µL sample was mixed with 300 µL methanol (containing 5 µg/mL 2-Chloro-L-phenylalanine as internal

standard). The mixture was mixed by a vortex mixer for 1 min. Then the mixture was further mixed using a vortex mixer for about 1 min. Then centrifuged at 13,000 rpm, 4°C for 10 min. The supernatant was transferred to sampler vials for detection. An in-house quality control (QC) was prepared by mixing an equal amount of each sample.

Agilent 1290 Infinity II UHPLC system coupled to an Agilent 6545 UHD and Accurate-Mass Q-TOF/MS was used for LC-MS analysis. The chromatographic column used was Waters XSelect HSS T3 (2.5 μm 100*2.1 mm). Mass spectrometry was operated in both positive and negative ion modes. The parameters optimized were as follows. Capillary voltage: 3.5 kV. Drying gas flow: 10 L/min. Gas temperature: 325°C. Nebulizer pressure, 20 psig. Fragmentor voltage: 120 V. Skimmer voltage: 45 V. Mass range: m/z 50–3000.

ii. Metabolites identification

A qualitative method was employed in identifying various metabolites seen in the sample. An online database was used for accurate molecular weight comparison. Adduct manner; [M+H]+ and [M+Na]+ was selected in positive mode, [M-H]- in negative mode.

About 2577 compounds were detected in positive mode and 1119 compounds were detected in negative mode. The detected compounds were identified using HMDB online database, and their relative concentration was calculated as well. 20 compounds with the highest concentration (descending order) have been selected, their chemical and biological properties have been identified.

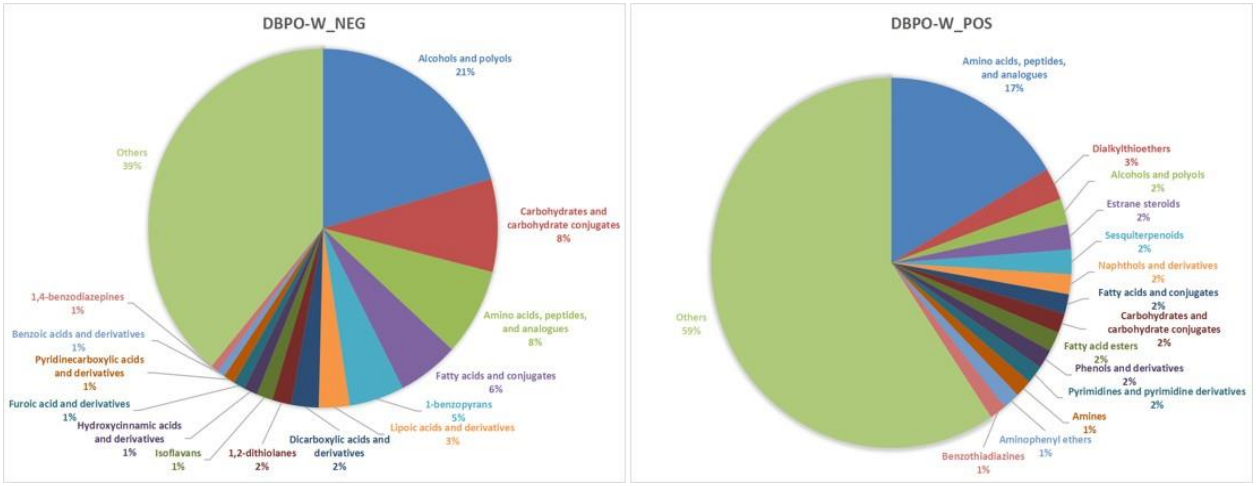

Figure 27. Metabolite Classification Diagram of DBPO-Water sample by available percentage; Left: Negative Mode; Right: Positive Mode

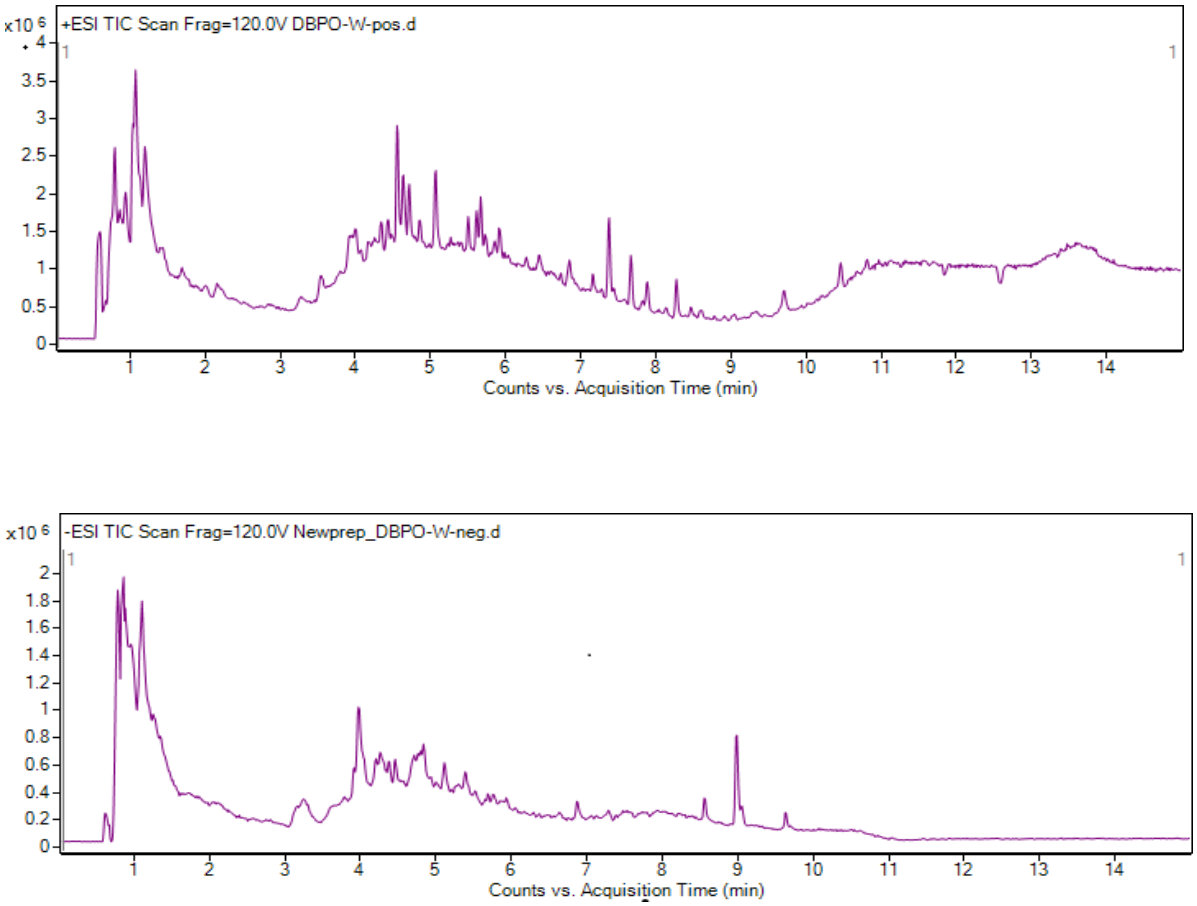

Figure 28. Magnolol water extract scan. Top- Positive; down- Negative

LC-MS NEGATIVE

S. No	Compound Name	RT (min)	M.Z	Mol. Formula	M.W. (g/mol)	Peak Area %	Biological Activity
1	s-Triazine, 2-methyl-4-methylamino-6-(trifluoromethyl)-	0.983	191.06	$C_6H_7F_3N_4$	192.06	260.1	Used for the marine xenobiotic metabolite of xenobiotic compound. (50)
2	Tri-tert-butyl(dichloromethyl)silane	3.983	281.13	$C_{13}H_{28}Cl_2SI$	282.13	60.6	Used as a catalyst in different reactions. (51)
3	Gibberellin 29	0.806	383.12	$C_{19}H_{24}O_6$	348.16	53.4	Used as a plant hormone. For growth regulation, and modulates the formation of steams, leaves, and flowers. (52)
4	Phosphinic acid, bis(1-aziridinyl)-, methyl ester	1.359	161.05	$C_5H_{11}N_2O_2P$	162.06	52.9	Improves the rate of sterility in insects (pink bollworm) when fumigating in a closed system. (53)
5	Pyroglutamic acid	1.116	128.04	$C_5H_7NO_3$	129.04	37.3	Used to improve blood circulation in the brain. Reduce the risk of cognitive decline and support memory. (54)
6	3-Methoxypropanesulphonic acid	3.258	153.02	$C_4H_{10}O_4S$	154.03	35.8	Valuable in research and analytics. (55)
7	1,1'-[4-(4-Methylphenyl)but-1-ene-1,1-diyl]bis(4-chlorobenzene)	0.959	365.09	$C_{23}H_{20}Cl_2$	366.09	29.2	Effective as a homoallylic alcohol derivative. (56)
8	N-Benzooxazol-2-yl-guanidine	4.284	175.06	$C_8H_8N_4O$	176.07	27.4	Imperative in proteomics research. (57)

9	1,3,8-Trihydroxy-4-methyl-2,7-diprenylxanthone	5.388	393.17	$C_{24}H_{26}O_5$	394.18	27.2	Plant metabolite, for conifers, and other gymnosperms. (58)
10	6H-Purin-6-one	0.984	133.02	$C_5H_2N_4O$	134.02	22.3	Efficient in research in the reaction and treatment of the different virus. (59)
11	2-Methyl-3-(4-nitrophenyl)prop-2-enoate	1.147	205.04	$C_{10}H_8NO_4$	206.05	20.9	Effective as a liquid crystal alignment agent. (60)
12	3,3-Dimethyl-3-silathietane	1.27	117.02	$C_4H_{10}SSi$	118.03	19.5	Used in research analysis. (61)
13	Thioxanthene, 9-(3-(4-methylpiperazinyl) propyl)-, dihydrochloride	4.702	409.13	$C_{21}H_{28}Cl_2N_2S$	410.14	18.9	Used in the production of preventive drugs. Antidepressants for obesity patients. (62)
14	Diethyl(4-methylphenyl) arsane	0.817	223.05	$C_{11}H_{17}As$	224.05	18.0	Used as a catalyst in different reactions. [63]
15	NSC370380	0.916	263.08	$C_{11}H_{12}N_4O_4$	264.09	17.5	Used in research treatment for cancer. (64)
16	Acetic acid--10-(methyldisulfanyl) decan-1-ol (1/1)	4.801	295.14	$C_{13}H_{28}O_3S_2$	296.15	15.3	Can be used to study different reactions of bacteria and fungi in the soil. (65)
17	2-Methyl-3-(4-nitrophenyl)prop-2-enoate	1.827	205.04	$C_{10}H_8NO_4$	206.05	15.1	Can be used as a liquid crystal alignment agent. (66)
18	Gossypol acetate	5.116	769.25	$C_{42}H_{42}O_{14}$	770.26	14.6	A model drug in the treatment of different illnesses for example tumors. (67)

19	1-Methyl-1-{2-[(1-phenylcyclohexane-1-carbonyl)oxy]ethyl}piperidin-1-ium	6.879	329.24	$C_{21}H_{32}NO_2$	330.24	14.5	Used in the study of si-heterocycles conformational preferences. (68)
20	D-Glucopyranuronic acid, ion(1-)	1.028	192.03	$C_6H_9O_7$	193.03	14.0	Available for different research purposes. Can be used as glucose absorption inhibiting agents. (69)

Table 9. Chemical and bioactive properties of substances of interest found in negative mode of LC-MS of magnolol water extract

LC-MS POSITIVE

S/No.	Compound Name	RT (min)	M/Z ratio	Mol. Formula	M.W. (g/mol)	Peak Area %	Biological Activity
1	6-Fluoro-1-(2-fluorophenyl)-3-(1-methylpiperidin-4-yl)-1H-indazole	4.571	328.16	$C_{19}H_{19}F_2N_3$	327.15	7.2	a) Antitumor Activity. (70) b) Antimicrobial Activity. (71) c) Anti-Diabetic Agents d) Anti-Inflammatory Activity. (72) e) Treatment of Parkinson's Disease. (73)
2	3-(Trimethoxysilyl)-N-[3-(trimethoxysilyl)propyl]propan-1-amine	4.648	342.18	$C_{12}H_{31}NO_6Si_2$	341.17	4.4	Salination reagent for polymer synthesis. [74]
3	Metaboranilide	1.204	121.07	C_6H_7BNO	120.06	4.2	Production of hydroxyboroxin-amine salt. (75)
4	N-Methyl-N,N-dipropylpropan-1-	4.727	330.21	$C_{17}H_{31}NO_3S$	329.20	3.2	General reaction

	aminium 4-methylbenzene-1-sulfonate						
5	Voglibose	5.069	268.14	$C_{10}H_{21}NO_7$	267.13	2.8	Treatment of type 2 diabetes mellitus. (76)
6	3,3-Dimethyl-2,3-dihydro-1H-3lambda(5)-benzo(e)phosphin Dole	3.542	216.11	$C_{14}H_{16}P$	215.10	2.7	Treatment of insomnia, contraception, and certain breast cancers. (77)
7	1,3,5,2,4,6-Trioxatriborinane-2,4,6-triamine	0.941	130.08	$B_3H_6N_3O_3$	129.07	2.7	A catalyst in the production of olefin polymer (78)
8	Flupirtine	0.788	305.14	$C_{15}H_{17}FN_4O_2$	304.13	2.6	Analgesic, skeletal muscle relaxant[79]
9	Carboxy-N,N,N-trimethylmethanaminium fluoride	1.204	138.10	$C_5H_{12}FNO_2$	137.09	2.5	Used as a catalyst for hierarchical reduction of CO_2. (80)
10	4-oxo 2-Nonenal-d3	1.082	180.11	$C_9H_{11}D_3O_2$	157.12	2.5	Lipid peroxidation marker, cytotoxic, genotoxic, chemotactic, protein alteration/modification, growth inhibition. (81-85)
11	6-({[tert-Butyl(dimethyl)silyl]oxy}methyl)-3-methyl-3H-imidazo[4,5-b]pyridine	1.145	300.15	$C_{14}H_{23}N_3OSi$	277.16	2.4	Used in different methods for treating IRAK4-mediated conditions and other diseases (86)
12	3-Nitro-5-(trifluoromethyl)pyridin-2(1H)-one	0.895	231.00	$C_6H_3F_3N_{23}$	208.01	2.4	Modulate specific receptor activity in vivo or in vitro and in the treatment of pathological receptors (87)
13	N-(2-Chloroethyl)dodecan-1-amine--	5.499	284.19	$C_{14}H_{31}Cl_2N$	283.18	2.3	A powerful adrenergic blocking agent is

	hydrogen chloride (1/1) **N-(2-Chloroethyl) dibenzylamine hydrochloride** is also referred as Dibenamine						known to modify the pharmacological effects of epinephrine (88,89)
14	2-Cyanoethylphosphine	0.587	110.01	C_3H_6NP	87.02	2.2	Used as reagent for the desulfurization of organic disulfides[90]
15	3-Hydroxy-2,3-dimethylbutan-2-yl hydrogen [2-(piperazin-1-yl)-1,3-thiazol-4-yl]boronate	4.337	314.17	$C_{13}H24BN3O3S$	313.16	2.0	Used in the treatment or prophylaxis of a disease (91)
16	Guanidine, N-nitro-N-nitroso-N-nonyl-	5.675	282.15	$C_{10}H_{21}N_5O_3$	259.16	2.0	<u>Other Name</u>: Methylnitronitrosoguanidine Used experimentally as a carcinogen and mutagen. (92)
17	Propanoic acid, 3-[[(hydrazinocarbonyl)amino]oxy]-, hydrazide	1.691	178.09	$C_4H_{11}N_5O_3$	177.09	2.0	Used in the analysis of some carboxylic acids in food samples and the environment. (93)
18	SCHEMBL8892039	1.026	241.20	$C_{13}H_{25}BO_3$	240.19	1.9	General reactions
19	2-{[4-(Dimethylamino) butanoyl]oxy}-N,N,N-trimethylethan-1-aminium chloride--hydrogen chloride (1/1/1)	1.060	289.14	$C_{11}H_{26}Cl_2N_2O_2$	288.14	1.7	Used to form lipid nanoparticles with oligonucleotides. (94)

20	Triacsin C	3.916	230.13	$C_{11}H_{17}N_3O$	207.14	1.7	Inhibition of lipid metabolism. Reduction or removal of lipid droplets. Blocks de novo synthesis of glycerolipids and cholesterol esters. (95)

Table 10. Chemical and bioactive properties of substances of interest found in the positive mode of LC-MS of magnolol water extract

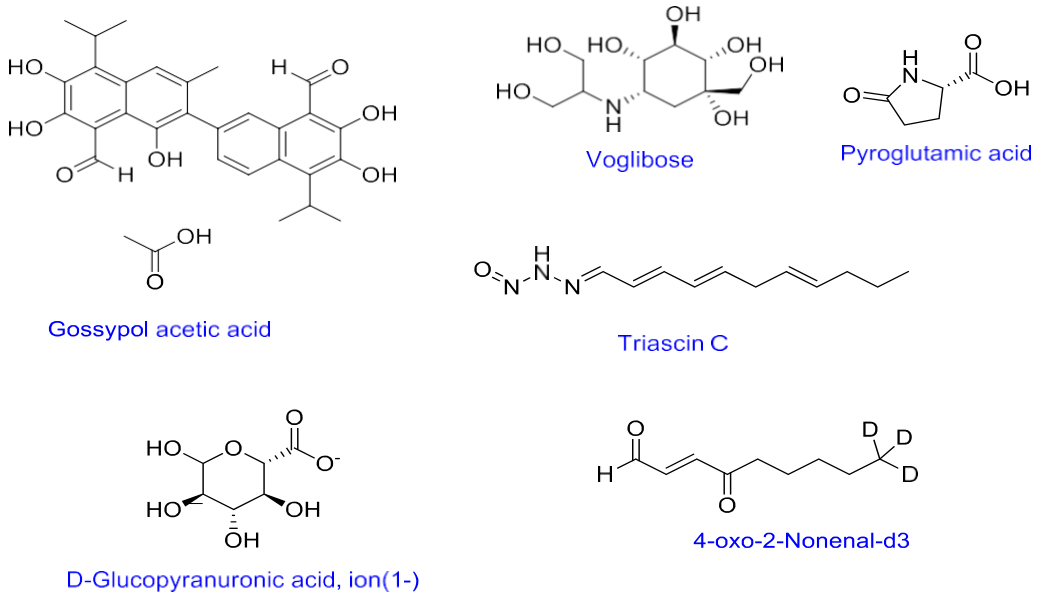

Figure 29. Notable structures of some compounds found in both negative and positive mode of magnolol water extract

CHAPTER VI

CONCLUSION AND FUTURE ASPECTS

SARS-CoV-2 and cancer are very deadly diseases with very high mortality rates. Thus, there is a desperate need for novel compounds and medicines that can effectively inactivate the proteases that are responsible for the fatal clinical manifestation often associated with the disease. Magnolol a natural polyphenol was successfully collected and extracted utilizing cost-effective bioactivity guided extraction method, this gave magnolol in good yield. The magnolol obtained was chemically modified using a diversity-oriented chemical modification to give a series of novel semisynthetic magnolol derivatives (DBMGPO 1-8). Also, chemical modification of 3-aminoadamantanol, a potent antiviral pharmacophore with a puckered structure and 7-chloro 4-amino quinoline pharmacophore was carried out to give DBADAPO- 1A-1C and DBQPO-1A, 1B, 2A, 2B derivatives were successfully synthesized. Diverse ring sizes were used to optimize protein-drug interaction and simultaneously improve bioavailability which is an important area of drug research. *In silico* evaluation of these series against KRAS cancer (PDB ID- 4EPV), SARS-CoV-2 3CL protease (PDB ID-6M2Q), and COVID-19 main protease (PDB ID- 6LU7) was carried out. Of the DBPO series, DBADAPO- 1B had the top-scoring function (-9.1) for COVID-19 protease, PDB ID -6M2Q and DBQPO- 2B showed top-scoring function (-8.0) for COVID-19 protease, PDB ID- 6LU7 score in comparison to Inhibitor N3 (-7.2, -7.5 for 6LU7 and 6M2Q, respectively). For Kras protein, DBMGPO-8 showed the best docking score (-7.6) of the DBMGPO series, and DBQPO-2A showed the best overall docking score in comparison to parent compound magnolol (-7.3) and Inhibitor N3 (-5.9). These encouraging results suggest further

biological investigation as these novel derivatives could eventually lead to potential therapeutic agents for the treatment of cancer and COVID-19 diseases.

Future Aspects

The next step is to carry out further biological and biochemical activity investigations of all DBPO series such as evaluation of enzyme inhibitory activity against K-RAS, 6LU7, and 6M2Q, Biological evaluations (*In vitro*, *In vivo* testing), binding assays, and determination of pharmacological and toxicological profiles.

REFERENCES

(1) Garza, B.; Echeverria, A.; Gonzalez, F.; Castillo, O.; Eubanks, T.; Bandyopadhyay, D. Phytochemical Investigation of Magnolia Grandiflora Green Seed Cones: Analytical and Phytoceutical Studies. *Food Sci. Nutr.* **2019**, *7* (5), 1761–1767. https://doi.org/10.1002/fsn3.1016.

(2) Yu, S. X.; Yan, R. Y.; Liang, R. X.; Wang, W.; Yang, B. Bioactive Polar Compounds from Stem Bark of Magnolia Officinalis. *Fitoterapia* **2012**, *83* (2), 356–361. https://doi.org/10.1016/j.fitote.2011.11.020.

(3) Schühly, W.; Khan, S. I.; Fischer, N. H. Neolignans from North American Magnolia Species with Cyclooxygenase 2 Inhibitory Activity. *Inflammopharmacology* **2009,** *17* (2), 106–110. https://doi.org/10.1007/s10787-009-7013-y.

(4) Li, L. F.; Lu, J.; Li, X. M.; Xu, C. L.; Deng, J. M.; Qu, R.; Ma, S. P. Antidepressant-like Effect of Magnolol on BDNF up-Regulation and Serotonergic System Activity in Unpredictable Chronic Mild Stress Treated Rats. *Phyther. Res.* **2012**, *26* (8), 1189–1194. https://doi.org/10.1002/ptr.3706.

(5) Lee, Y. K.; Yuk, D. Y.; Kim, T. Il; Kim, Y. H.; Kim, K. T.; Kim, K. H.; Lee, B. J.; Nam, S. Y.; Hong, J. T. Protective Effect of the Ethanol Extract of Magnolia Officinalis and 4-O-Methylhonokiol on Scopolamine-Induced Memory Impairment and the Inhibition of Acetylcholinesterase Activity. *J. Nat. Med.* **2009**, *63* (3), 274–282. https://doi.org/10.1007/s11418-009-0330-z.

(6) Bang, K. H.; Kim, Y. K.; Min, B. S.; Na, M. K.; Rhee, Y. H.; Lee, J. P.; Bae, K. H. Antifungal Activity of Magnolol and Honokiol. *Arch. Pharm. Res.* **2000**, *23* (1), 46–49. https://doi.org/10.1007/BF02976465.

(7) Baschieri, A.; Pulvirenti, L.; Muccilli, V.; Amorati, R.; Tringali, C. Chain-Breaking Antioxidant Activity of Hydroxylated and Methoxylated Magnolol Derivatives: The Role of H-Bonds. *Org. Biomol. Chem.* **2017**, *15* (29), 6177–6184. https://doi.org/10.1039/c7ob01195d.

(8) Ranaware, A. M.; Banik, K.; Deshpande, V.; Padmavathi, G.; Roy, N. K.; Sethi, G.; Fan, L.; Kumar, A. P.; Kunnumakkara, A. B. Magnolol: A Neolignan from the Magnolia Family for the Prevention and Treatment of Cancer. *Int. J. Mol. Sci.* **2018**, *19* (8), 1–21. https://doi.org/10.3390/ijms19082362.

(9) Vivek-Ananth, R.P. .; Abhijit, R.; Nithin, R. . H. S. B. . A. S. I. S. I. of P. N. P.; To, Inhibitors of Human Proteases Key to SARS-CoV-2 infection. Molecules. 2020, 25, 3822. In Silico Identification Of. *Molecules* 2020, *25*, 3822.

(10) Bhowmik, D.; Nandi, R.; Jagadeesan, R.; Kumar, N.; Prakash, A.; Kumar, D. Identification of Potential Inhibitors against SARS-CoV-2 by Targeting Proteins Responsible for Envelope Formation and Virion Assembly Using Docking Based Virtual Screening, and Pharmacokinetics Approaches. *Infect. Genet. Evol.* **2020**, *84* (May), 104451. https://doi.org/10.1016/j.meegid.2020.104451.

(11) . Quideau S, Deffieux D, Duat-Casassus C, P. L. Plant Polyphenols: Chemical Properties, Biological Activity, and Synthesis. *Angew. Chem. Int. Ed.* **2011**, *50*, 586–621.

(12) Bringmann, G.; Gulder, T.; Gulder, T. A. M.; Breuning, M. Atroposelective Total Synthesis of Axially Chiral Biaryl Natural Products. *Chem. Rev.* **2011**, *111* (2), 563–639. https://doi.org/10.1021/cr100155e.

(13) Maioli, M.; Basoli, V.; Carta, P.; Fabbri, D.; Dettori, M. A.; Cruciani, S.; Serra, P. A.; Delogu, G. Synthesis of Magnolol and Honokiol Derivatives and Their Effect against Hepatocarcinoma Cells. *PLoS One* **2018**, *13* (2), 1–21. https://doi.org/10.1371/journal.pone.0192178.

(14) Hajduk P J, Bures M, Praestagaard J, F. S. W. Privileged Molecules for Protein Binding Identified from NMR Base Screening. *J Med Chem* **2000**, *43*, 3443–3447.

(15) Amblard, F.; Govindarajan, B.; Lefkove, B.; Rapp, K. L.; Detorio, M.; Arbiser, J. L.; Schinazi, R. F. Synthesis, Cytotoxicity, and Antiviral Activities of New Neolignans Related to Honokiol and Magnolol. *Bioorganic Med. Chem. Lett.* **2007**, *17* (16), 4428–4431. https://doi.org/10.1016/j.bmcl.2007.06.024.

(16) Poivre, M.; Duez, P. Biological Activity and Toxicity of the Chinese Herb Magnolia Officinalis Rehder & E. Wilson (Houpo) and Its Constituents. *J. Zhejiang Univ. Sci. B* **2017**, *18* (3), 194–214. https://doi.org/10.1631/jzus.B1600299.

(17) Li, M.; Zhang, F.; Wang, X.; Wu, X.; Zhang, B.; Zhang, N.; Wu, W.; Wang, Z.; Weng, H.; Liu, S.; Gao, G.; Mu, J.; Shu, Y.; Bao, R.; Cao, Y.; Lu, J.; Gu, J.; Zhu, J.; Liu, Y. Magnolol Inhibits Growth of Gallbladder Cancer Cells through the P53 Pathway. *Cancer Sci.* **2015**, *106* (10), 1341–1350. https://doi.org/10.1111/cas.12762.

(18) Zhang, J.; Chen, Z.; Huang, X.; Shi, W.; Zhang, R.; Chen, M.; Huang, H.; Wu, L. Insights on the Multifunctional Activities of Magnolol. *Biomed Res. Int.* **2019**, *2019*. https://doi.org/10.1155/2019/1847130.

(19) Kanda, T.; Yokosuka, O.; Imazeki, F.; Fujiwara, K.; Nagao, K.; Saisho, H. Amantadine Inhibits Hepatitis A Virus Internal Ribosomal Entry Site-Mediated Translation in Human Hepatoma Cells. *Biochem. Biophys. Res. Commun.* **2005**, *331* (2), 621–629.

https://doi.org/10.1016/j.bbrc.2005.03.212.

(20) Sugrue, R. J.; Hay, A. J. Structural Characteristics of the M2 Protein of Influenza a Viruses: Evidence That It Forms a Tetrameric Channe. *Virology* **1991**, *180* (2), 617–624. https://doi.org/10.1016/0042-6822(91)90075-M.

(21) Smith JP. Treatment of Chronic Hepatitis C with Amantadine. *Dig. Dis. Sci.* 1997, *42* (8), 1681–1687.

(22) Abreu, G. E. A.; Aguilar, M. E. H.; Covarrubias, D. H.; Durán, F. R. Amantadine as a Drug to Mitigate the Effects of COVID-19. *Med. Hypotheses* **2020**, *140*, 109755. https://doi.org/10.1016/j.mehy.2020.109755.

(23) Smieszek, S. P.; Przychodzen, B. P.; Polymeropoulos, M. H. Amantadine Disrupts Lysosomal Gene Expression: A Hypothesis for COVID19 Treatment. *Int. J. Antimicrob. Agents* **2020**, *55* (6), 106004. https://doi.org/10.1016/j.ijantimicag.2020.106004.

(24) Kolocouris, A.; Tzitzoglaki, C.; Johnson, F. B.; Zell, R.; Wright, A. K.; Cross, T. A.; Tietjen, I.; Fedida, D.; Busath, D. D. Aminoadamantanes with Persistent in Vitro Efficacy against H1N1 (2009) Influenza A. *J. Med. Chem.* **2014**, *57* (11), 4629–4639. https://doi.org/10.1021/jm500598u.

(25) Pereira, B. B. Challenges and Cares to Promote Rational Use of Chloroquine and Hydroxychloroquine in the Management of Coronavirus Disease 2019 (COVID-19) Pandemic: A Timely Review. *J. Toxicol. Environ. Heal. - Part B Crit. Rev.* **2020**, *23* (4), 177–181. https://doi.org/10.1080/10937404.2020.1752340.

(26) Eng, E. O.; Chew, J. S. W.; Jin, P. L.; Chua, R. C. S. In Vitro Inhibition of Human Influenza A Virus Replication by Chloroquine. *Virol. J.* **2006**, *3*, 3–5. https://doi.org/10.1186/1743-422X-3-39.

(27) Keyaerts, E.; Vijgen, L.; Maes, P.; Neyts, J.; Ranst, M. Van. In Vitro Inhibition of Severe Acute Respiratory Syndrome Coronavirus by Chloroquine. *Biochem. Biophys. Res. Commun.* **2004**, *323* (1), 264–268. https://doi.org/10.1016/j.bbrc.2004.08.085.

(28) Yao, X.; Ye, F.; Zhang, M.; Cui, C.; Huang, B.; Niu, P.; Liu, X.; Zhao, L.; Dong, E.; Song, C.; Zhan, S.; Lu, R.; Li, H.; Tan, W.; Liu, D. In Vitro Antiviral Activity and Projection of Optimized Dosing Design of Hydroxychloroquine for the Treatment of Severe Acute Respiratory Syndrome Coronavirus 2 (SARS-CoV-2). *Clin. Infect. Dis.* **2020**, *71* (15), 732–739. https://doi.org/10.1093/cid/ciaa237.

(29) Fox, R. I. Mechanism of Action of Hydroxychloroquine as an Antirheumatic Drug. *Semin Arthritis Rheum.* **1993**, *23*, 82–91. https://doi.org/doi: 10.1016/s0049-0172(10)80012-5.

(30) Siegel, R.; Ma J, Zou, Z.; Jemal, A. Cancer Statistics, 2014. *CA Cancer J Clin.* **2014**, *64* (1), 9–29. https://doi.org/10.3322/caac.21208.

(31) Siegel, R.L.; Miller, K. D. . J. A. Cancer Statistics, 2016. *CA Cancer J Clin.* **2016**, *66* (1), 7–30. https://doi.org/10.3322/caac.21332.

(32) Tang, H.; Zhang, Y.; Li, D.; Fu, S.; Tang, M.; Wan, L.; Chen, K.; Liu, Z.; Xue, L.; Peng, A.; Ye, H.; Chen, L. Discovery and Synthesis of Novel Magnolol Derivatives with Potent Anticancer Activity in Non-Small Cell Lung Cancer. *Eur. J. Med. Chem.* **2018**, *156*, 190–205. https://doi.org/10.1016/j.ejmech.2018.06.048.

(33) DeSantis, C. E.; Lin, C. C.; Mariotto, A. B.; Siegel, R. L.; Stein, K. D.; Kramer, J. L.; Alteri, R.; Robbins, A. S.; Jemal, A. Cancer Treatment and Survivorship Statistics, 2014. *CA. Cancer J. Clin.* **2014**, *64* (4), 252–271. https://doi.org/10.3322/caac.21235.

(34) Holohan, C.; Van Schaeybroeck, S.; Longley, D. B.; Johnston, P. G. Cancer Drug Resistance: An Evolving Paradigm. *Nat. Rev. Cancer* **2013**, *13* (10), 714–726. https://doi.org/10.1038/nrc3599.

(35) Yun, C. W.; Lee, S. H. The Roles of Autophagy in Cancer. *Int. J. Mol. Sci.* **2018**, *19* (11), 1–18. https://doi.org/10.3390/ijms19113466.

(36) Xu, T.; Zheng, Z.; Guo, Y.; Bai, L. P. Semisynthesis of Novel Magnolol-Based Mannich Base Derivatives That Suppress Cancer Cells via Inducing Autophagy. *Eur. J. Med. Chem.* **2020**, *205*, 112663. https://doi.org/10.1016/j.ejmech.2020.112663.

(37) Sivilotti, L.; Nistri, A. GABA Receptor Mechanisms in the Central Nervous System. *Prog. Neurobiol* **1991**, *36*, 35.

(38) Bormann, J. The "ABC" of GABA Receptors. *Trends Pharmacol. Sci.* **2000**, *21* (1), 16–19. https://doi.org/10.1016/S0165-6147(99)01413-3.

(39) Sigel, E.; Steinmann, M. E. Structure, Function, and Modulation of GABAA Receptors. *J. Biol. Chem.* **2012**, *287* (48), 40224–40231. https://doi.org/10.1074/jbc.R112.386664.

(40) Möhler, H. The GABA System in Anxiety and Depression and Its Therapeutic Potential. *Neuropharmacology* **2012**, *62* (1), 42–53. https://doi.org/10.1016/j.neuropharm.2011.08.040.

(41) Fuchs, A.; Baur, R.; Schoeder, C.; Sigel, E.; Müller, C. E. Structural Analogues of the Natural Products Magnolol and Honokiol as Potent Allosteric Potentiators of GABAA Receptors. *Bioorganic Med. Chem.* **2014**, *22* (24), 6908–6917. https://doi.org/10.1016/j.bmc.2014.10.027.

(42) Pootoolal, J.; Neu, J.; Wright, G. D. Glycopeptide Antibiotic Resistance. *Annu. Rev. Pharmacol.* **2002**, *42*, 381–408. https://doi.org/10.1146/annurev.pharmtox.42.091601.142813.

(43) Raad, I. I.; Hanna, H. A.; Hachem, R. Y.; Dvorak, T.; Arbuckle, R. B.; Chaiban, G.; Rice, L. B. Clinical-Use-Associated Decrease in Susceptibility of Vancomycin-Resistant Enterococcus Faecium to Linezolid: A Comparison with Quinupristin-Dalfopristin. *Antimicrob. Agents Chemother.* **2004**, *48* (9), 3583–3585. https://doi.org/10.1128/AAC.48.9.3583-3585.2004.

(44) Wang, G.; Ella-Menye, J. R.; Sharma, V. Synthesis and Antibacterial Activities of Chiral 1,3-Oxazinan-2-One Derivatives. *Bioorganic Med. Chem. Lett.* **2006**, *16* (8), 2177–2181. https://doi.org/10.1016/j.bmcl.2006.01.072.

(45) Jada, S.; Reddy Doma, M.; Singh, P. P.; Kumar, S.; Malik, F.; Sharma, A.; Khan, I. A.; Qazi, G. N.; Kumar, H. M. S. Design and Synthesis of Novel Magnolol Derivatives as Potential Antimicrobial and Antiproliferative Compounds. *Eur. J. Med. Chem.* **2012**, *51*, 35–41. https://doi.org/10.1016/j.ejmech.2011.12.039.

(46) MacEdo, B.; Kaschula, C. H.; Hunter, R.; Chaves, J. A. P.; Van Der Merwe, J. D.; Silva, J. L.; Egan, T. J.; Cordeiro, Y. Synthesis and Anti-Prion Activity Evaluation of Aminoquinoline Analogues. *Eur. J. Med. Chem.* 2010, *45* (11), 5468–5473. https://doi.org/10.1016/j.ejmech.2010.07.054.

(47) Solomon, V. R.; Haq, W.; Srivastava, K.; Puri, S. K.; Katti, S. B. Synthesis and Antimalarial Activity of Side Chain Modified 4-Aminoquinoline Derivatives. **2007**, 394–398. https://doi.org/10.1021/jm061002i.

(48) Papanastasiou, I.; Tsotinis, A.; Kolocouris, N.; Prathalingam, S. R.; Kelly, J. M. Design , Synthesis , and Trypanocidal Activity of New Aminoadamantane Derivatives. **2008**, 1496–1500. https://doi.org/10.1021/jm7014292.

(49) Zoidis, G.; Tsotinis, A.; Kolocouris, N.; Kelly, J. M.; Prathalingam, S. R. Design and Synthesis of Bioactive 1 , 2-Annulated Adamantane Derivatives. **2008**, 3177–3185. https://doi.org/10.1039/b804907f.

(50) Chiba, S.; Nagawa, Y.; Yui, T. Electroencephalographic studies of 2-methyl-4-amino-6-methoxy-s-triazine (CV399)]. *pharmacologica Japonica*, **1970**, 66, *76-82*. PubMed: 5464140

(51) Lambert, J. B.; Zhao, Y.; Wu, H.; Tse, W. C.; Kuhlmann, B. The allyl leaving group approach to tricoordinate silyl, germyl, and stannyl cations. *Journal of the American Chemical Society*, **1999**, *121*(21), 5001-5008.

(52) Sponsel, V.M.; Macmillan, J. Metabolism of gibberellin A29 in seeds of Pisum sativum. *Planta.* **1978**, 144, *69-78.* PubMed: 24408646

(53) H. M. Flint, A. B. Bořkovec, D. L. Palmer, Fumigation: A New Method of Chemosterilizing the Pink Bollworm, Environmental Entomology, **1974**, 3,1, 172–176, https://doi.org/10.1093/ee/3.1.172

(54) Ryan, Quigley. L-Pyroglutamic Acid Benefits Side Effects and Dosage. **2020** https://community.bulksupplements.com/l-pyroglutamic-acid/

(55) Santa Cruz Biotechnology. N-Benzooxazol-2-yl-guanidine (CAS 39123-82-5) https://www.scbt.com/p/n-benzooxazol-2-yl-guanidine-39123-82-5

(56) Dijs I. J.; Ochten, V.; Van, H.L.; Walree, C. A.; Geus, J. W.; Jenneskens, L. W.; Alkyl sulphonic acid surface-functionalised silica as heterogeneous acid catalyst in the solvent-free liquid-phase addition of acetic acid to camphene. Journal of Molecular Catalysis A: *Chemical*, **2002**,188(1-2), 209-224

(57) Milipore sigma, peer-reviewed papers. 1-(4-methylphenyl)-3-buten-ol. Web 11/29/20 https://www.sigmaaldrich.com/catalog/product/aldrich/551198?lang=en&region=US

(58) Mark Williams. 17 June 2019. Chebi|143868 1,3,8-Trihydroxy-4-methyl-2,7-diprenylxanthone. https://www.ebi.ac.uk/chebi/searchId.do?chebiId=CHEBI:143868

(59) Kewn, S.; Wang, L.H.; Hoggard, P.G.; Rousseau, F.; Hart, R.; Macneela, J.P.; Khoo, S.H.; Back, D.J. Enzymatic assay for measurement of intracellular DXG triphosphate concentrations in peripheral blood mononuclear cells from human immunodeficiency virus type-1- infected patients. *Antimicrob. Agents Chemothe.*, **2003**, 47(1), 255-261.

(60) Ito, J., Kanno, Y.; Hatanaka, T. *U.S. Patent No. 10,428,274*. **2019**. Washington, DC: U.S. Patent and Trademark Office.

(61) Mastryukov, S. Structure of the 3,3-dimethyl-3-silathietane molecule according to data from gas-phase electron diffraction analysis with consideration of vibrational effects. *Journal of Structural Chemistry*, **1988**, *28*(5), 674–679. https://doi.org/10.1007/BF00752047

(62) Nagy, P. L., Roth, J., Szilvassy, Z., Tory, K., Brownstein, M., Takács, K., Kolonics, A. *U.S. Patent Application No. 14/748,150,* **2015**

(63) Allen, D. G., Raston, C. L., Skelton, B. W., White, A. H., & Wild, S. B. Synthesis and resolution of an asymmetric arsonium cation. Crystal and molecular structures of (R)-Benzyl (methyl)(4-methylphenyl)(naphthalen-1-yl)-arsonium bromide and hexafluorophosphate. *Aust. J. Chem*., **1984**, *37*(6), 1171-1181.

(64) Institute, U. *NSC370380*, **2003**, Unilever Center for Molecular Informatics, Cambridge University.

(65) Effmert, U.; Kalderas, J.; Warnke, R.; Piechulla, B. Volatile mediated interactions between bacteria and fungi in the soil. *J. chem. ecol*. **2012**, 38(6):665-703

(66) Ito, J.; Kanno, Y.; Hatanaka, T. *U.S. Patent No. 10,428,274*. **2019**, Washington, DC: U.S. Patent and Trademark Office.

(67) Tang, W. Gossypol acetate induced apoptosis of pituitary tumor cells by targeting the BCL-2 via the upregulated microRNA miR-15a. *Int. J. Clin. Exp. Med*., **2015**, 8(6), 9079–9085

(68) Shainyan, B. A., & Kleinpeter, E. Conformational preferences of Si–Ph, H and Si–Ph, Me silacyclohexanes and 1, 3-thiasilacyclohexanes. Additivity of conformational energies in 1, 1-disubstituted heterocyclohexanes. *Tetrahedron*, **2012**, *68*(1), 114-125.

(69) Cowman, C. 1H NMR of glycosaminoglycans and hyaluronic acid oligosaccharides in aqueous solution: The amide proton environment. *Arch. Biochem. Biophys*, **1984**, 230(1), 203–212. https://doi.org/10.1016/0003-9861(84

(70) Gaikwad, D.D.; Chapolikar, A.D.; Devkate, C.G.; Warad, K.D.; Tayade, A.P.; Pawar, R.P.; Domb, A.J. Synthesis of indazole motifs and their medicinal importance: An overview.
Eur. J. Med. Chem. **2015**, 90, 707–731.

(71) Dong, J.Y.; Zhang, Q.J.; Wang, Z.T.; Huang, G.; Li, S.S. Recent advances in the development of indazole-based anticancer agents. *Chem. Med. Chem.*, **2018**, 13, 1490–1507.

(72) Wan, Y.C.; He, S.Z.; Li, W.; Tang, Z.L. Indazole derivatives: Promising anti-tumor agents. Anti-Cancer Agents. *Med. Chem*, **2018**, 18.

(73) Zhang, S.G, Liang, C.G, Zhang, W.H. Recent Advances in Indazole-Containing Derivatives:Synthesis and Biological Perspectives. *Molecules*, **2018**, 23(11), 2783 doi:10.3390/molecules23112783
https://www.ncbi.nlm.nih.gov/pmc/articles/PMC6278422/

(74) McGall, G.; Kuimelis, G.R. Silane Mixtures. United States, Patent Application Publication, **2007**, Pub. No.: US 2007/0275411 A1.

(75) Vineyard, B. D., & Godt Jr, H. C. A Study of the Reaction of Boric Acid with Amines: Hydroxyboroxin-Amine Salts. *Inorg. Chem.*,**1964**, 3(8), 1144-1147.

(76) Dabhi, A.S.; Bhat, S.R.; Shah, M.J. Voglibose: An Alpha Glucosidase Inhibitor. J. Clin. *Diagn* Res., **2013**, 7(12): 3023-3027.

(77) Fensome, A.; Adams, W. R.; Adams, A. L.; Berrodin, T. J.; Cohen, J.; Huselton, C.; Melenski, E. G. Design, synthesis, and SAR of new pyrrole-oxindole progesterone receptor modulators leading to 5-(7-fluoro-3, 3-dimethyl-2-oxo-2, 3-dihydro-1 H-indol-5-yl)-1-methyl-1 H-pyrrole-2-carbonitrile (WAY-255348). *J. Med. Chem*., **2008**, 51(6), 1861-1873.

(78) Pettijohn, Ted M. Compositions useful for olefin polymerization and processes therefore and therewith. U.S. Patent No. 5,622,906. **1997**.

(79) Friedel, H.A, Fitton, A. Flupirtine A Review of its Pharmacological Properties, and Therapeutic Efficacy in Pain States. *Drugs*, **1993**, 45(4), 548-569.

(80) Liu, X. F.; Li, X. Y.; Qiao, C.; Fu, H. C.l.; He, L. N.; Betaine catalysis for hierarchical reduction of CO2 with amines and hydrosilane to form formamides, animals, and methylamines. *Angew. Chem. Int. Ed*., **2017**, 56(26), 7425-7429.

(81) Pryor, W.A., and Porter, N.A. Suggested mechanisms for the production of 4-hydroxy-2-nonenal from the autoxidation of polyunsaturated fatty acids. *Free Radic. Biol. Med*., **1990**, 8, 541-543

(82) Esterbauer, H., Schaur, R.J., and Zoliner, H. Chemistry and biochemistry of 4-hydroxynonenal, malonaldehyde, and related aldehydes. *Free Radic. Biol. Med*., **1991**,11, 81-128

(83) Sodum, R.S.; Chung, F.L. 1, N-2-ethenodeoxyguanosine as a potential marker for DNA adduct formation by trans-4-hydroxy-2-nonenal. *Cancer Res.*, **1988**, 48, 320-323

(84) https://www.lsbio.com/biochemicals/4-oxo-2-nonenal-d3-cas-1313400-91-7-ls-h6150/6150

(85) Näsström, T.; Fagerqvist, T.; Barbu, M.; Karlsson, M.; Nikolajeff F.; Kasrayan, A.; Ekberg M.; Lannfelt, L.; Ingelsson, M.; Bergström, J. The lipid peroxidation products 4-oxo-2-nonenal and 4-hydroxy-2-nonenal promote the formation of α-synuclein oligomers with distinct biochemical, morphological, and functional properties. *Free Radic. Biol. Med*, **2011**, 50, 428–437. doi:10.1016/j.freeradbiomed.2010.11.027.

(86) Altman, M. D.; Andresen, B. M.; Brubaker, J. D.; Childers, M. L.; Donofrio, A.; Fischmann, T.; Maclean, J. K. **2018**, U.S. Patent No. 9,969,749. Washington, DC: U.S. Patent and Trademark Office.

(87) Bakthavatchalam, R.; Blum, C. A.; Brielmann, H.; Caldwell, T. M.; De Lombaert, S.; Hodgetts, K. J.; Zheng, X. U.S. Patent No. 7,074,799. **2006**, Washington, DC: U.S. Patent and Trademark Office.

(88) Maling, H.M.; Eichelbaum, F.M.; Saul, W.; Sipes, I.G.; Brown, E. A.; Gillette, J.R. Nature of the protection against carbon tetrachloride-induced hepatotoxicity produced by pretreatment with dibenamine (N-(2-chloroethyl)dibenzylamine). *Biochem. Pharmacol.*, **1974**, 23, 10, 1479-1491.

(89) Schayer, R.W.; Kennedy, H.; and Smiley, R. 1953, effect of dibenamine (*N*-(2-chloroethyl)dibenzylamine) on the metabolism of radioactive epinephrine. *J. Biol. Chem.*, **1953**, 202, 39-43.

(90) Burns, John A.; Butler, James C.; Moran, John; Whitesides, George, M. Selective Reduction of Disulfides by Tris (2 carboxyethyl) phosphine. *J. Org. Chem*., **1991**, 56, 8, 2648–2650. doi:10.1021/jo00008a014.

(91) Wortmann, L., Lücking, U., Lefranc, J., Briem, H., Koppitz, M., Eis, K., ... & Wilhelm, B. O. N. E. **2018**, U.S. Patent No. 9,993,484. Washington, DC: U.S. Patent and Trademark Office.

(92) Jiyou, L.; Yiquan, X.; Guzhi, S.; Heling, S.; Xinhua, Maolin, Jin.; Boqin, Y.; Wang, M. Inhibitory effect of glycyrrhiza uralensis fish and chelidonium majus l on gastrocarcinogenesis induced by n-methyl- N' - nitro- N'- nitrosoguanidine. *Chin.* J. Cancer, **1992**, 4 (2) 10-12.

(93) Xie, Z.; Yu, L.; Yu, H.; Deng, Q. Application of a fluorescent derivatization reagent 9-chloromethyl anthracene on determination of carboxylic acids by HPLC. *J. Chromatogr. Sci*., **2012**, 50, 6, 464-468

(94) Colletti, S. L.; Stanton, M. G. 2016, U.S. Patent No. 9,402,816. Washington, DC: U.S. Patent and Trademark Office

(95) Igal, A.R.; Wang, P.; Coleman, R.A. Triacsin C blocks de novo synthesis of glycerolipids and cholesterol esters but not recycling of fatty acid into phospholipid: evidence for functionally separate pools of acyl-CoA. *Biochem. J.*, **1997**, 324, 529–534

APPENDIX

APPENDIX

NMR and IR Spectras for novel DBPO series

1. *5,5'-diallyl-[1,1'-biphenyl]-2,2'-diol* **Magnolol**

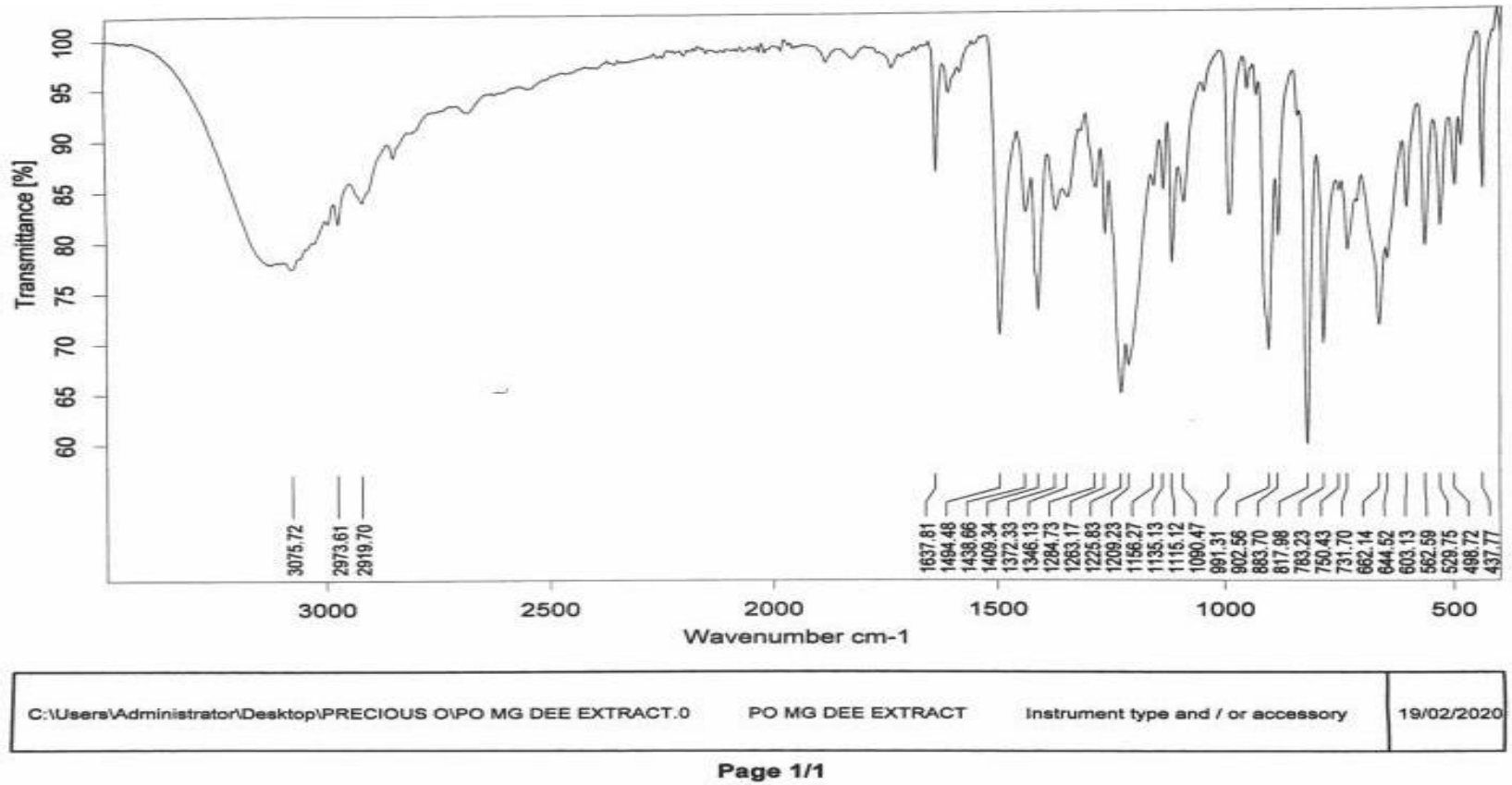

Figure 30. FTIR of magnolol

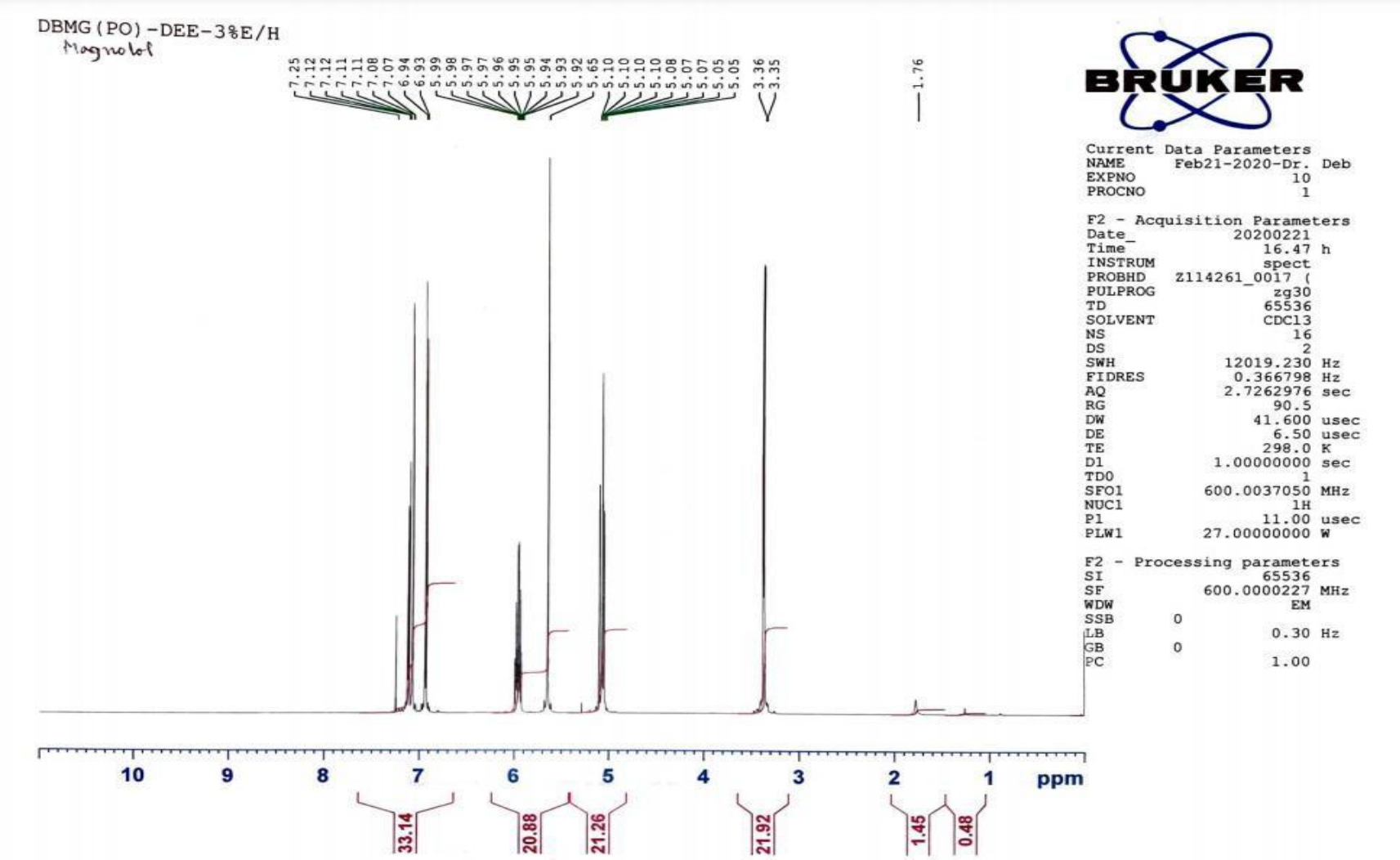

Figure 31. Proton NMR of magnolol

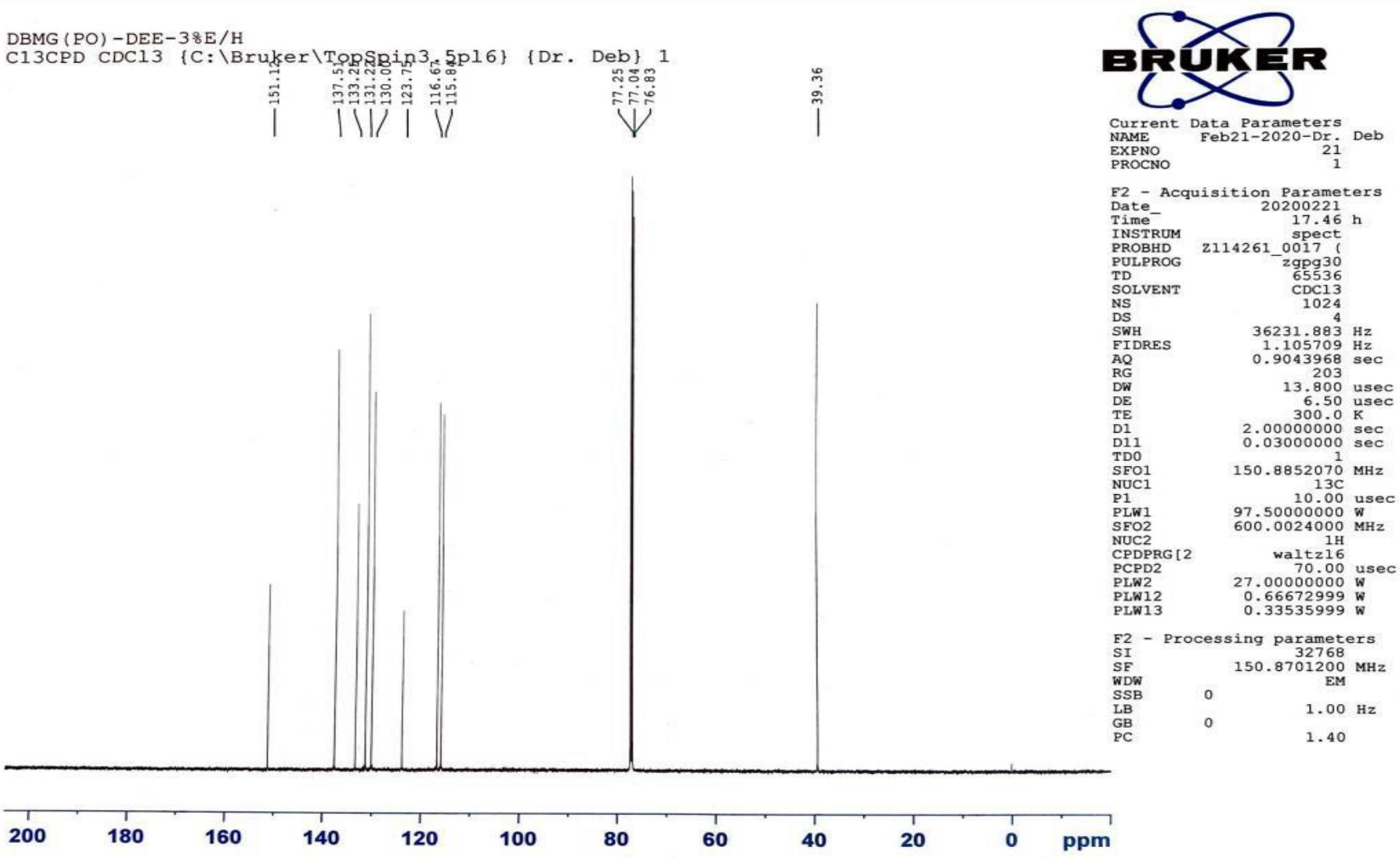

Figure 32. 13 carbon NMR of magnolol

2. *5,5'-diallyl-[1,1'-biphenyl]-2,2'-diyl dimethanesulfonate* **DBMGPO-1**

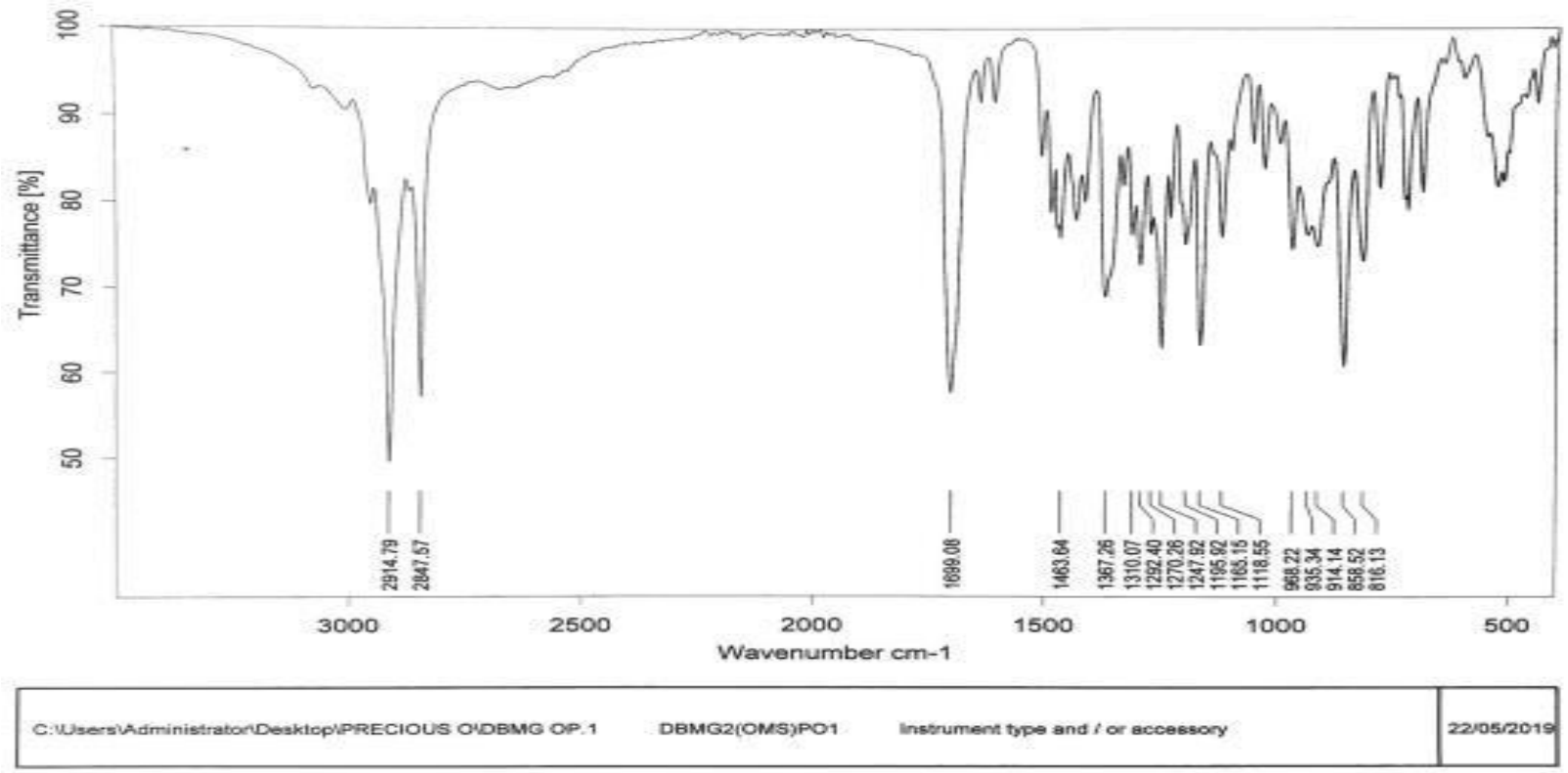

Figure 33. FTIR of **DBMGPO-1**

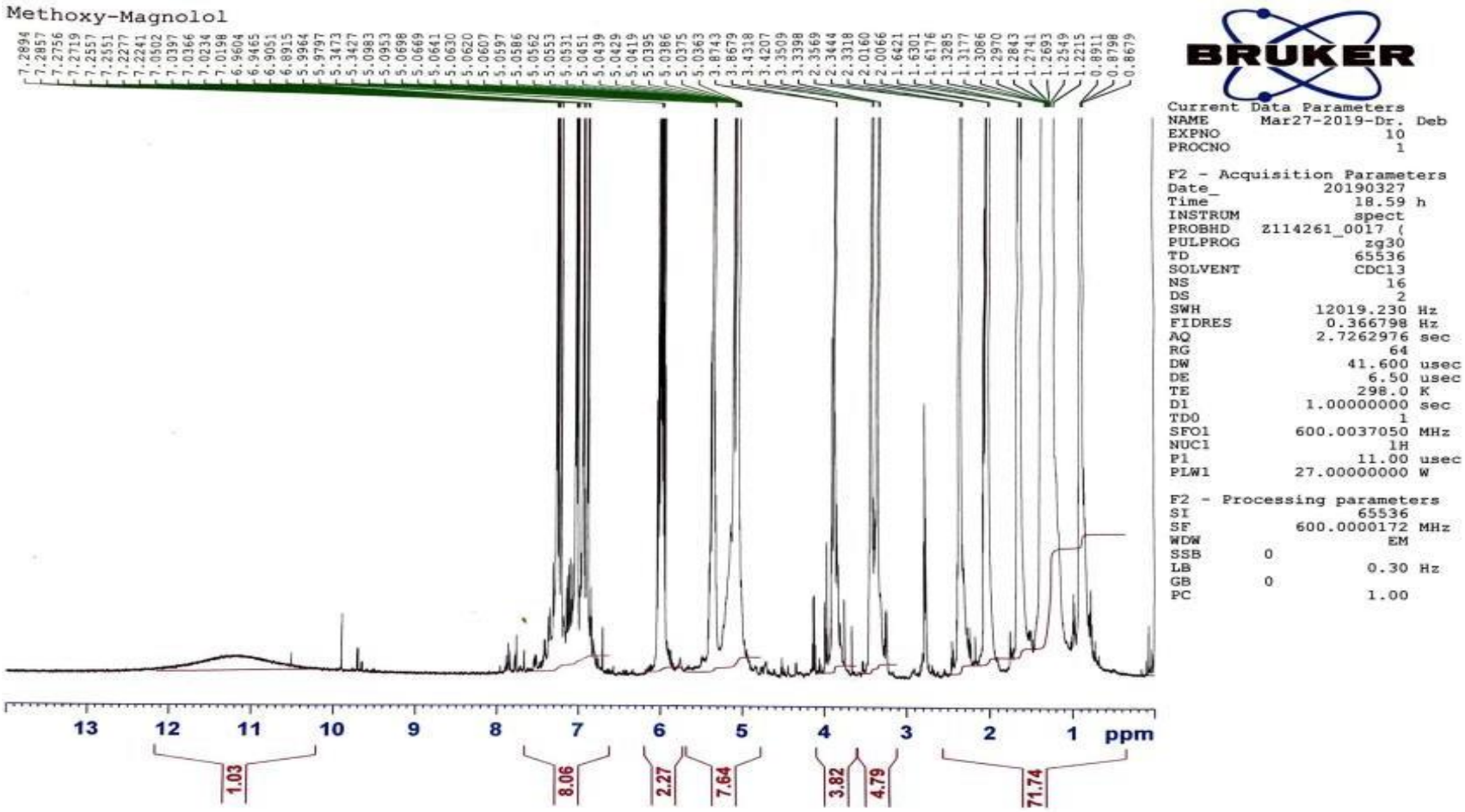

Figure 34. Proton NMR of **DBMGPO-1**

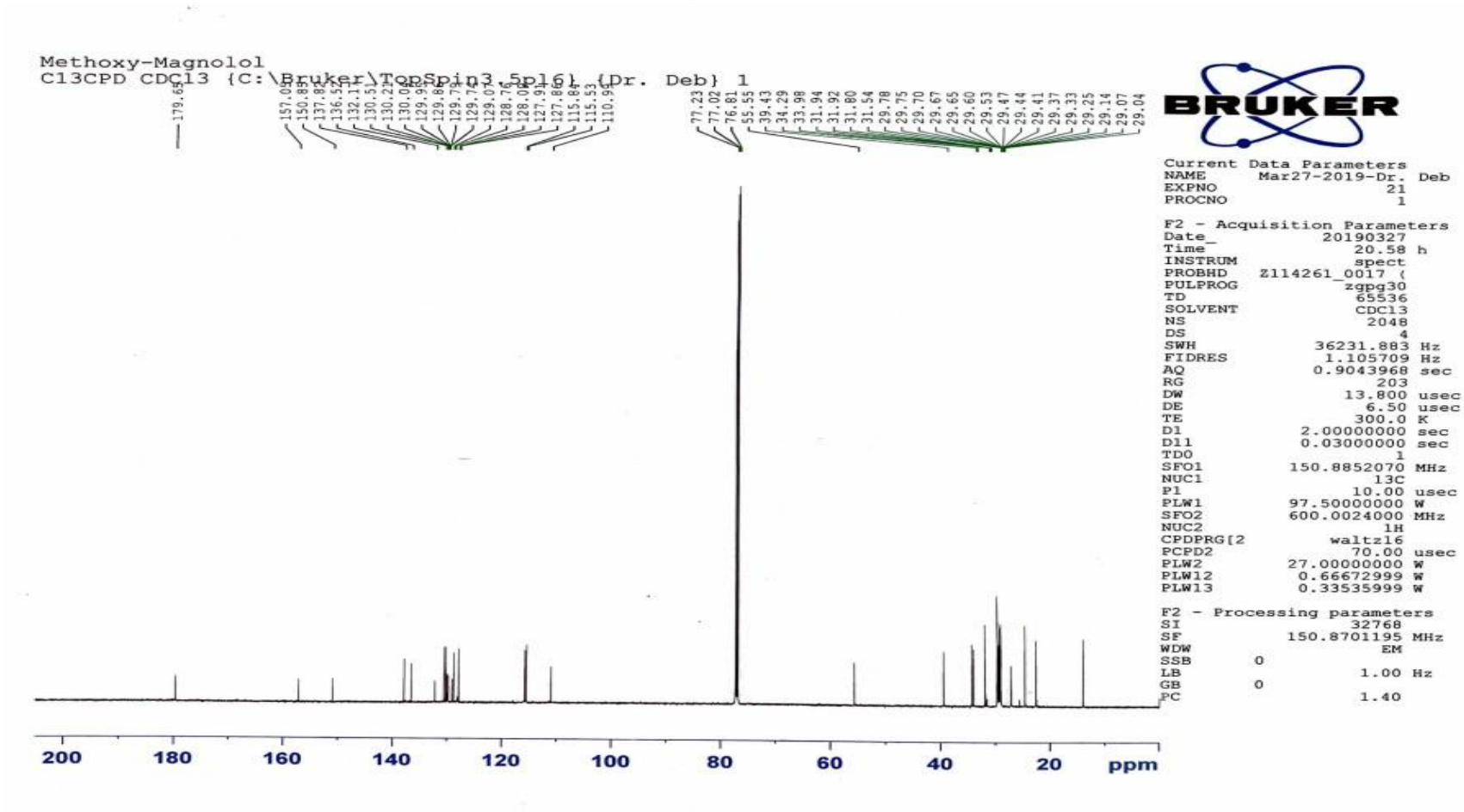

Figure 35. 13 carbon NMR of **DBMGPO-1**

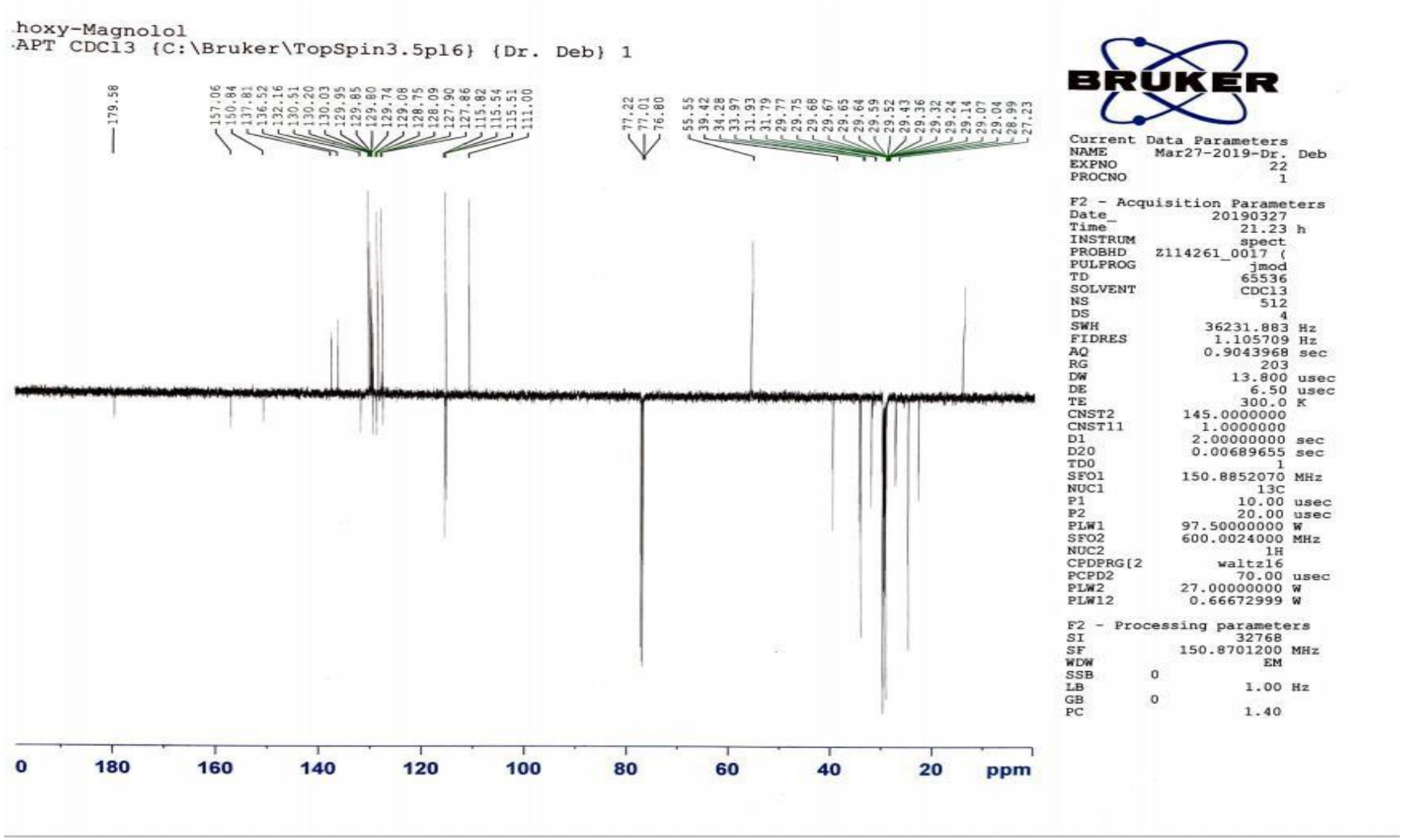

Figure 36. APT NMR of **DBMGPO-1**

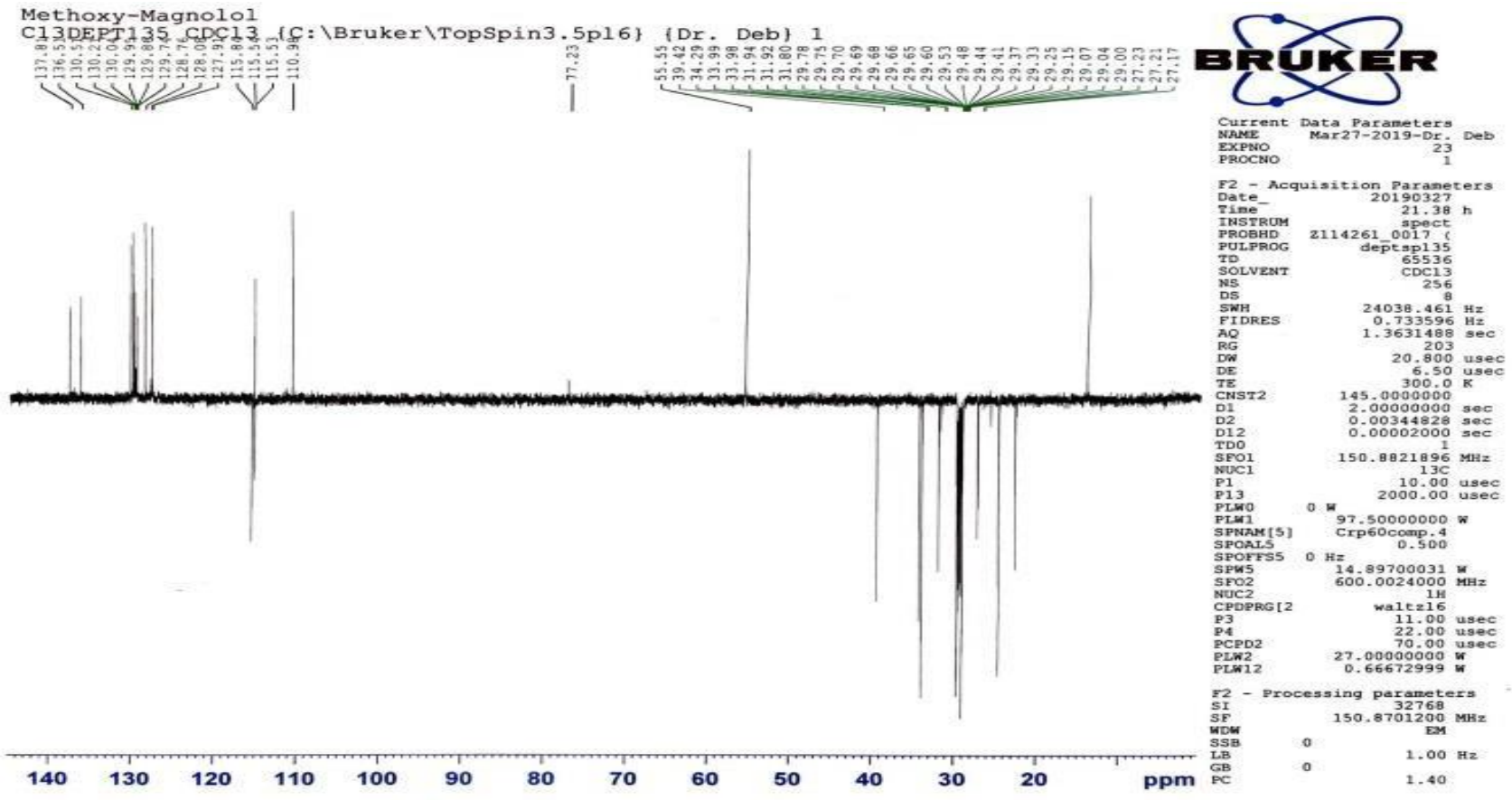

Figure 37. DEPT 135 NMR of **DBMGPO-1**

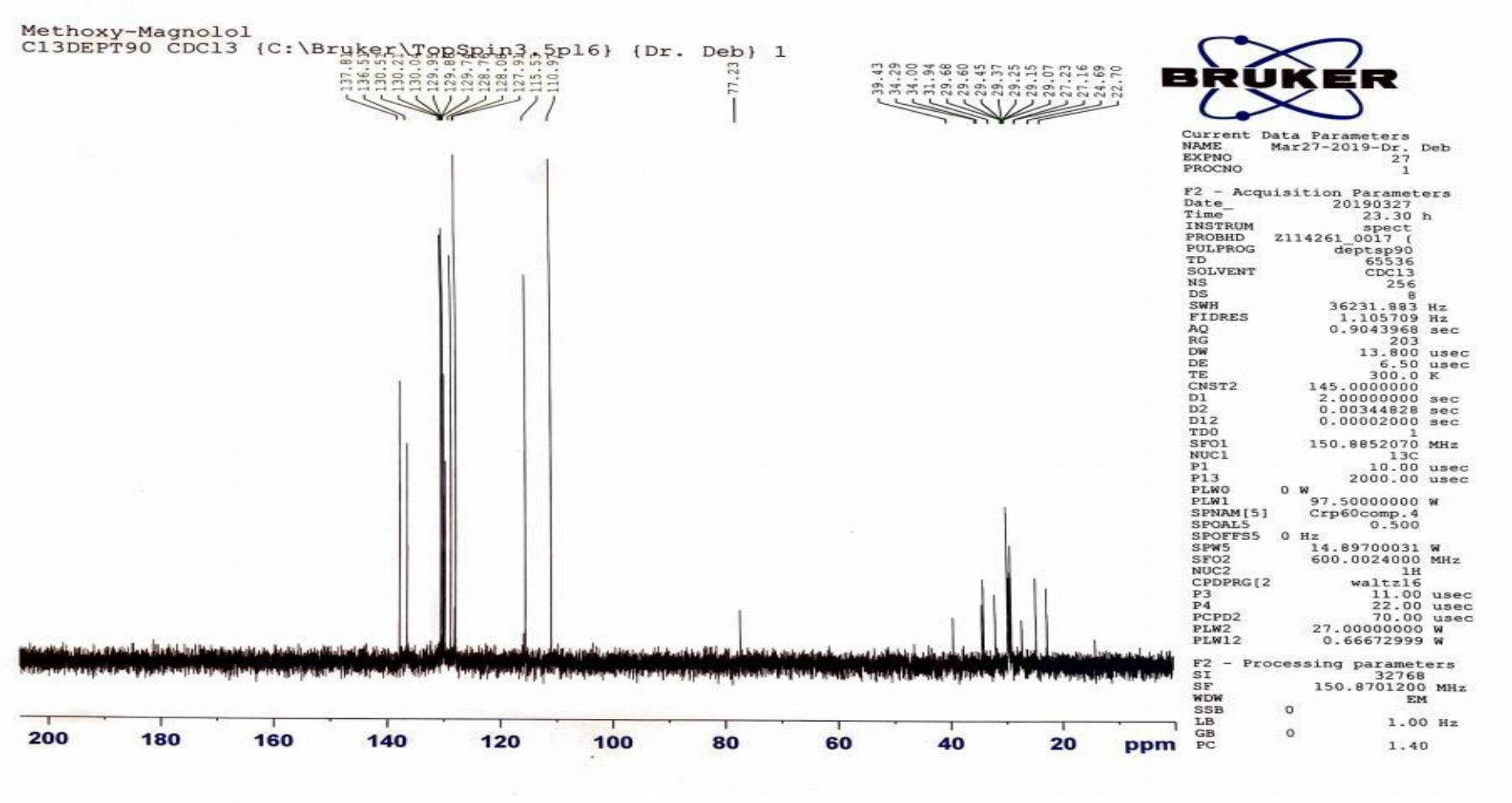

Figure 38. DEPT 90 NMR of **DBMGPO-1**

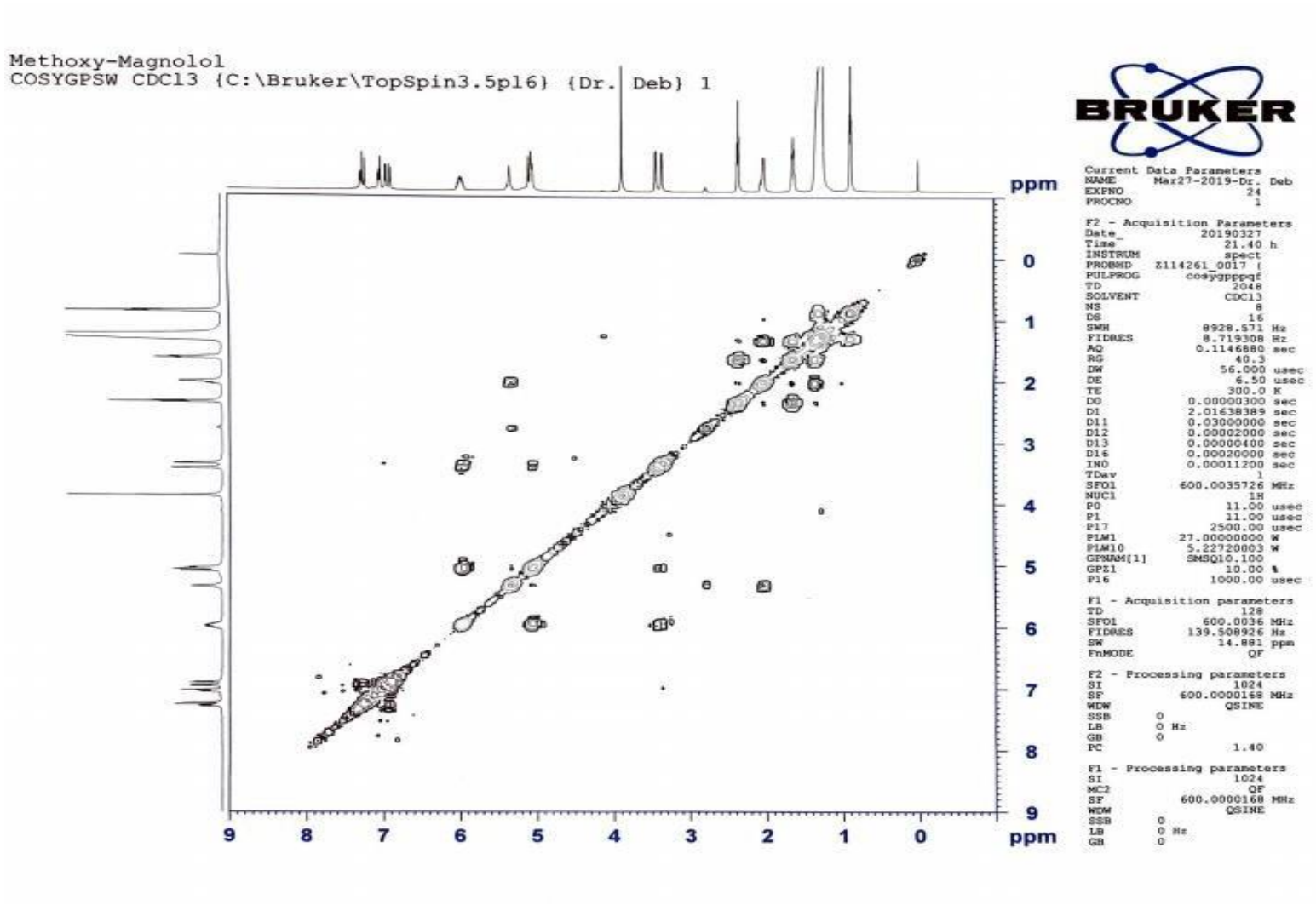

Figure 39. COSY NMR of **DBMGPO-1**

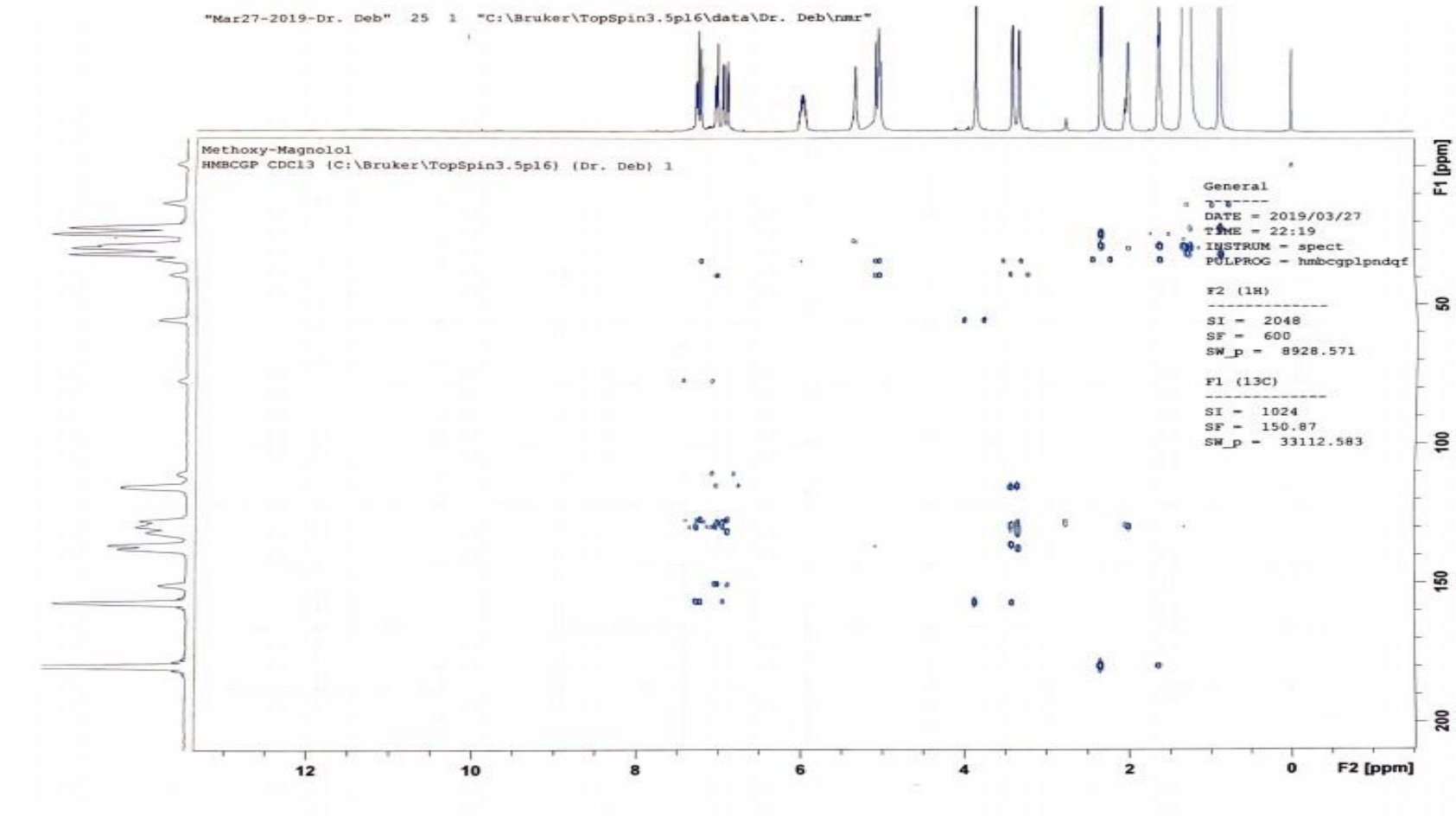

Figure 40. HMBC NMR of **DBMGPO-1**

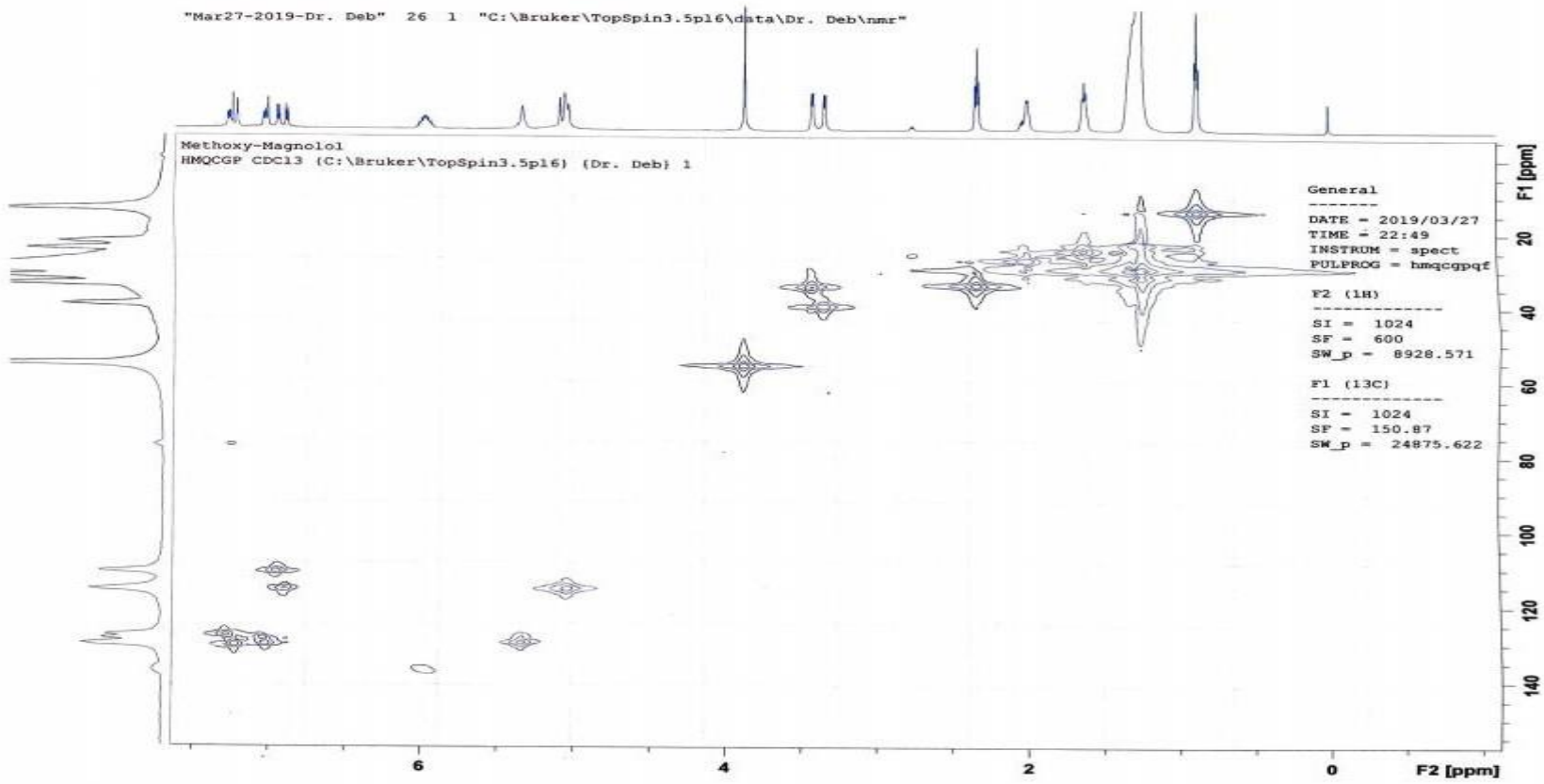

Figure 41. HMQC NMR of **DBMGPO-1**

3. *5,5'-diallyl-[1,1'-biphenyl]-2,2'-diyl bis(4-fluorobenzenesulfonate)* **DBMGPO-2**

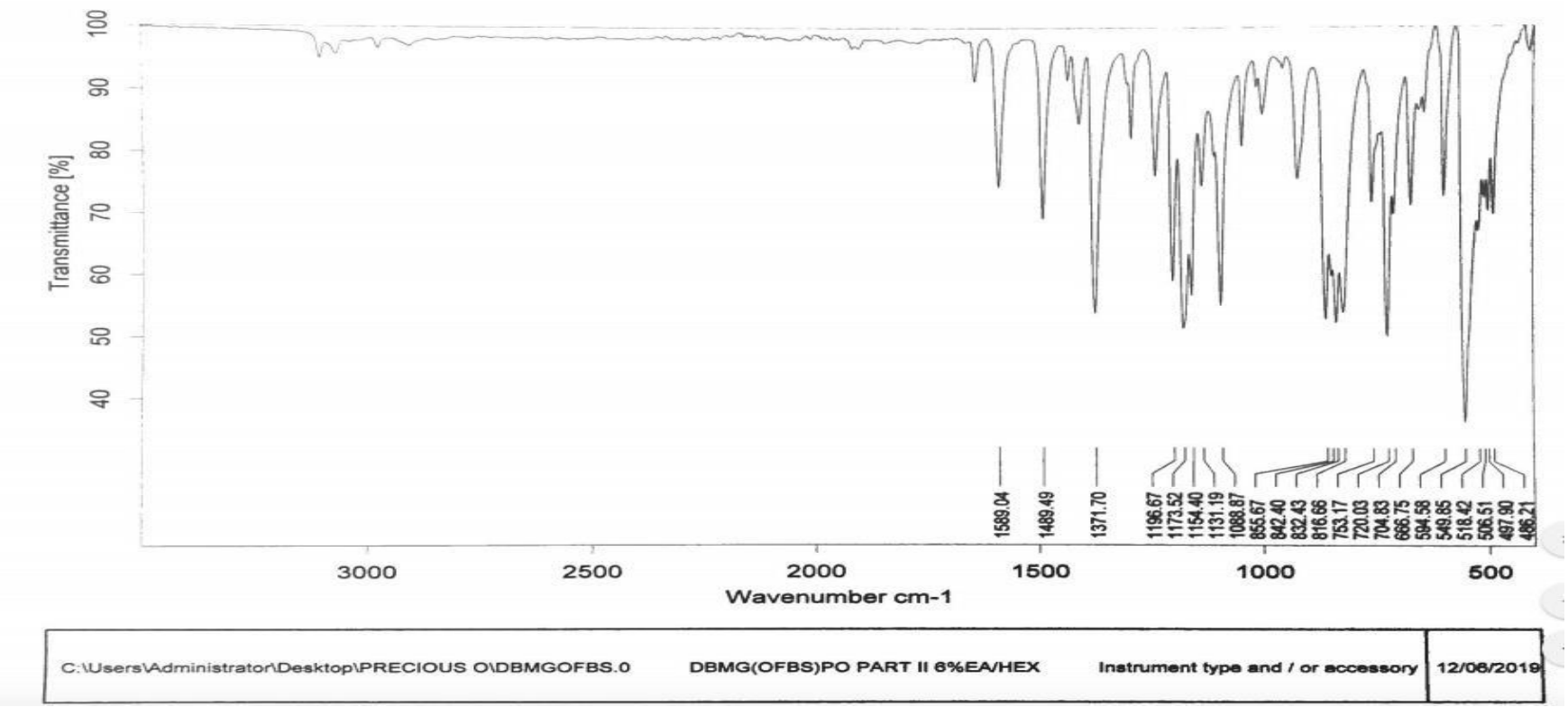

Figure 42. FTIR **DBMGPO-2**

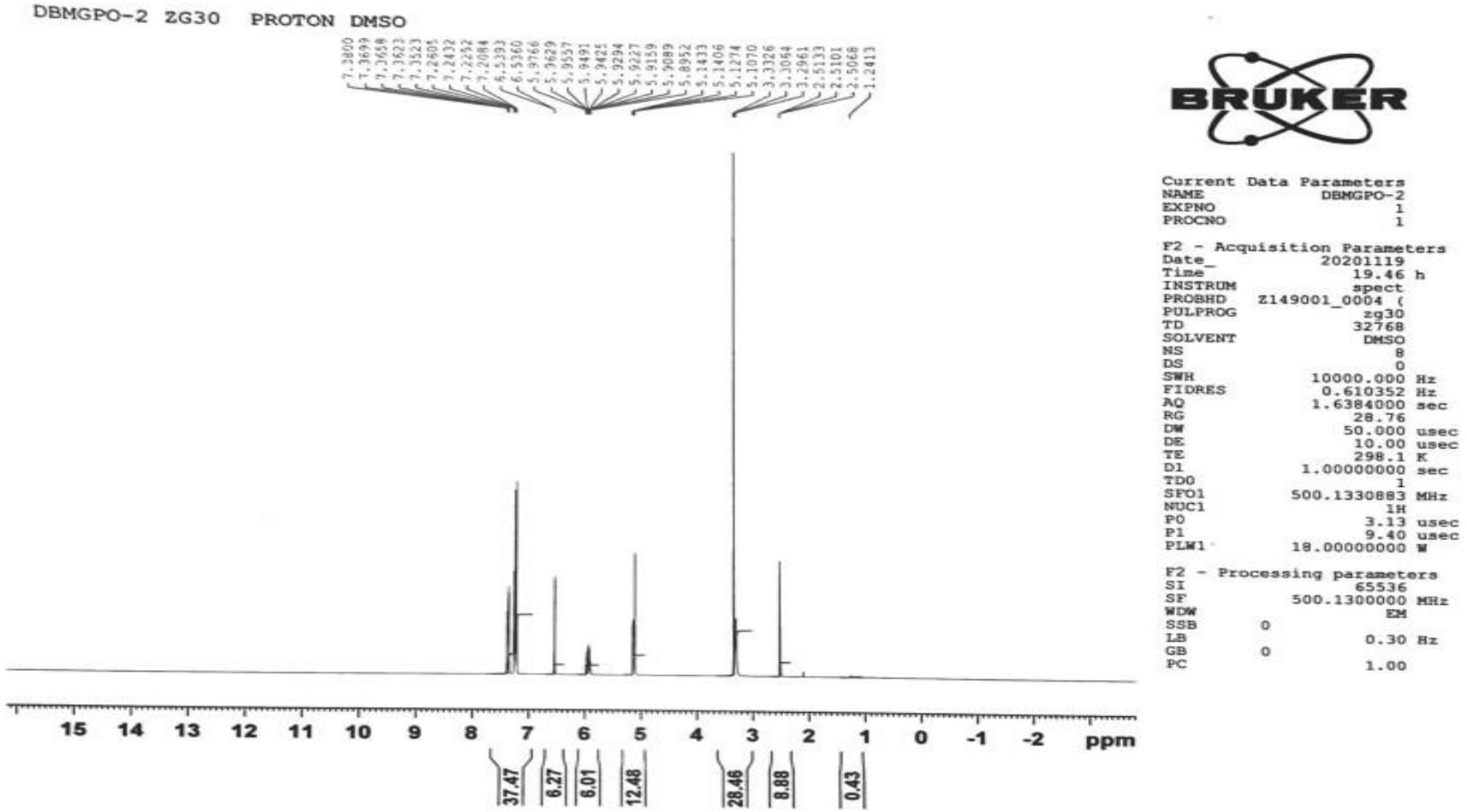

Figure 43. Proton NMR DBMGPO-**2**

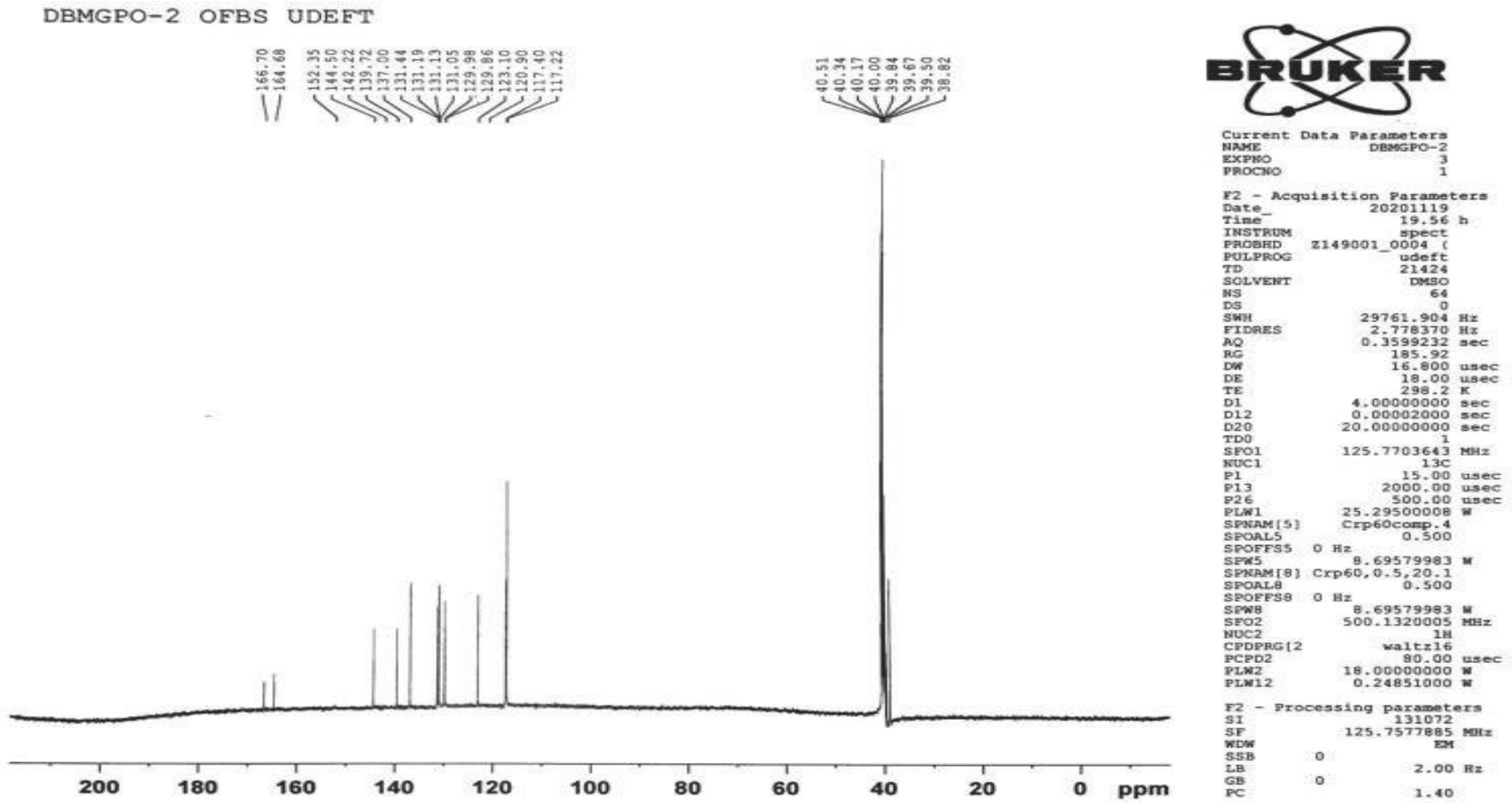

Figure 44. 13 carbon NMR **DBMGPO-2**

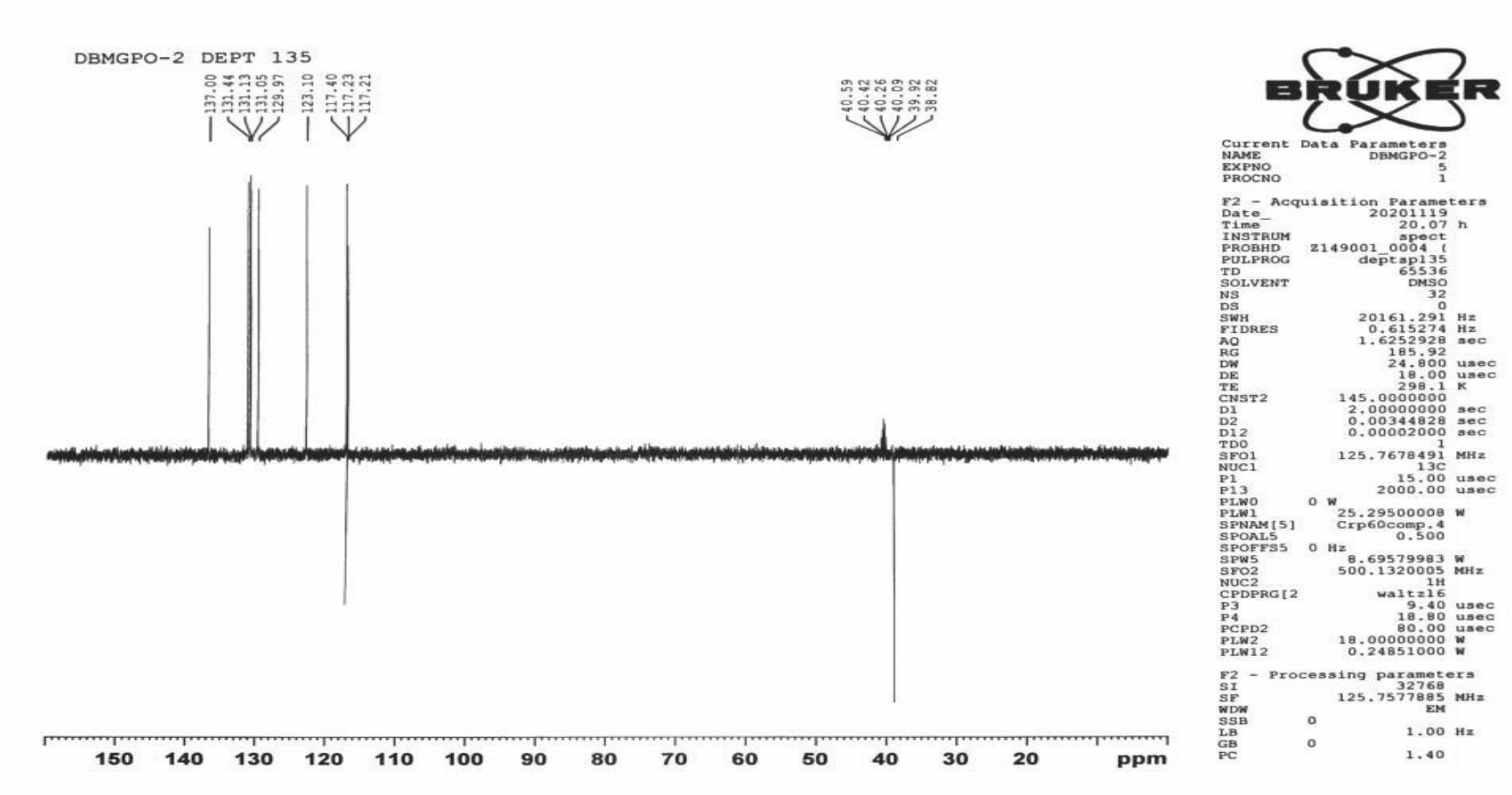

Figure 45. 13 carbon DEPT 135 NMR **DBMGPO-2**

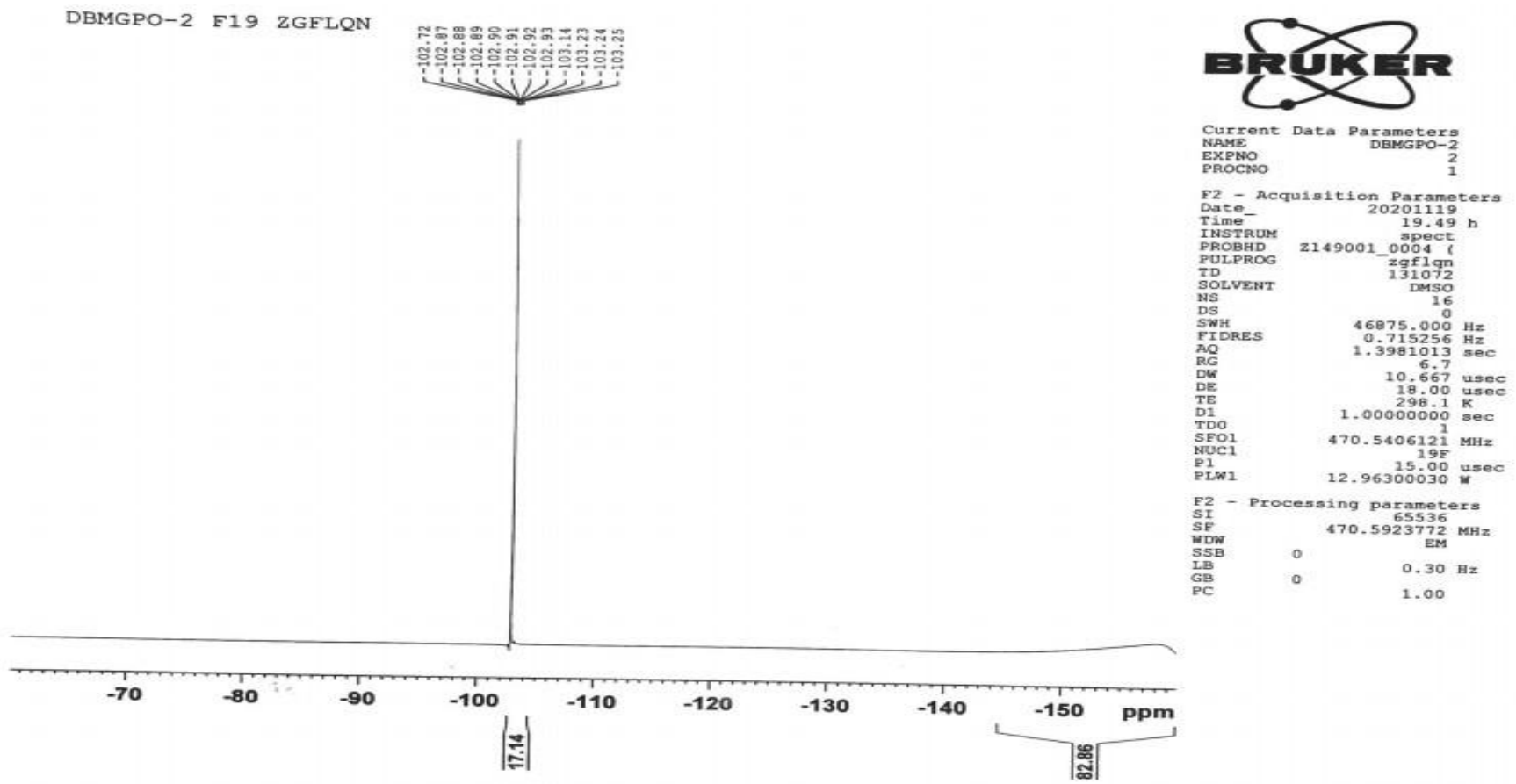

Figure 46. 19F NMR **DBMGPO-2**

4. *5,5'-diallyl-[1,1'-biphenyl]-2,2'-diyl bis(4-nitrobenzenesulfonate)* **DBMGPO-3**

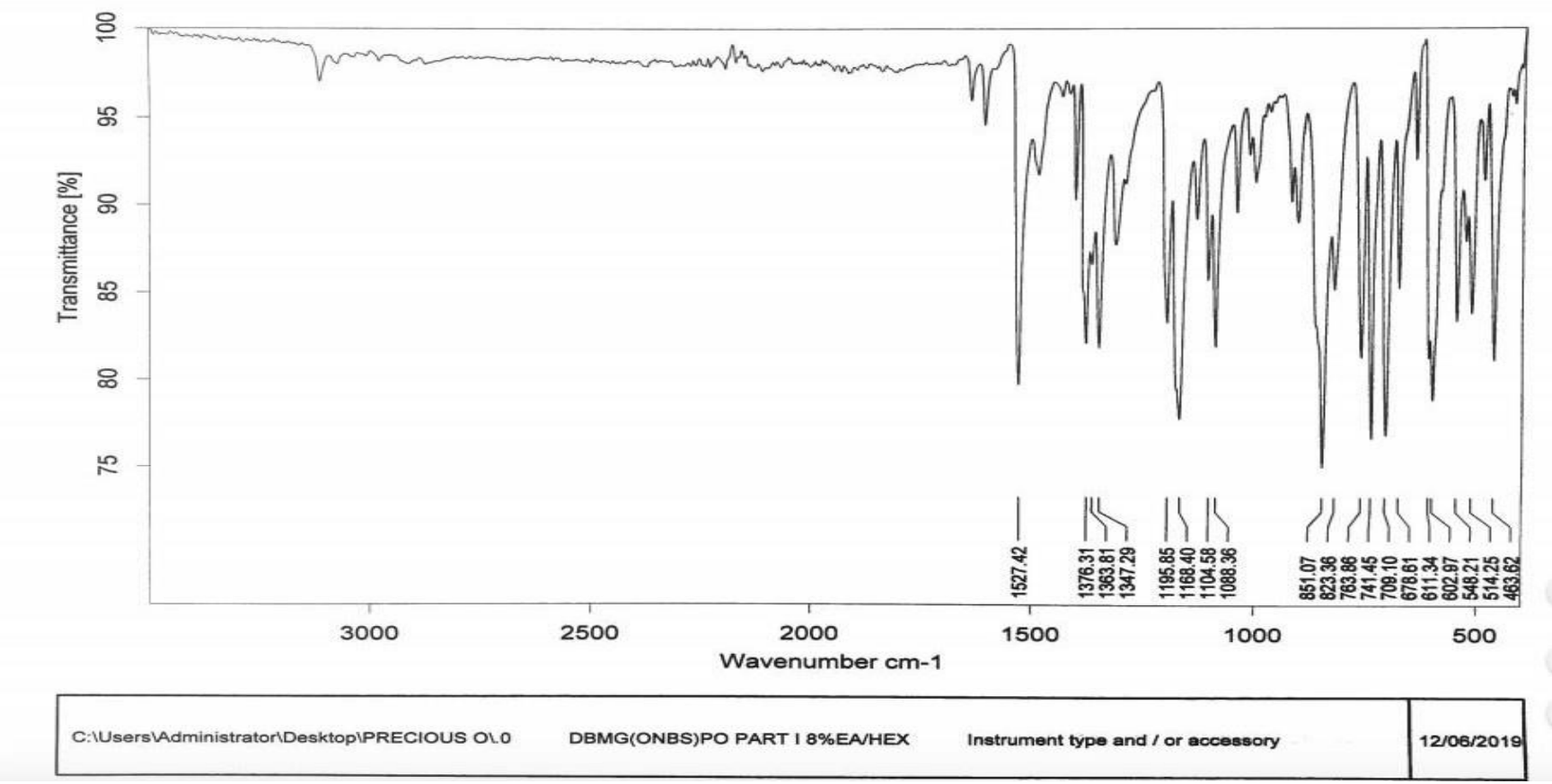

Figure 47. FTIR **DBMGPO-3**

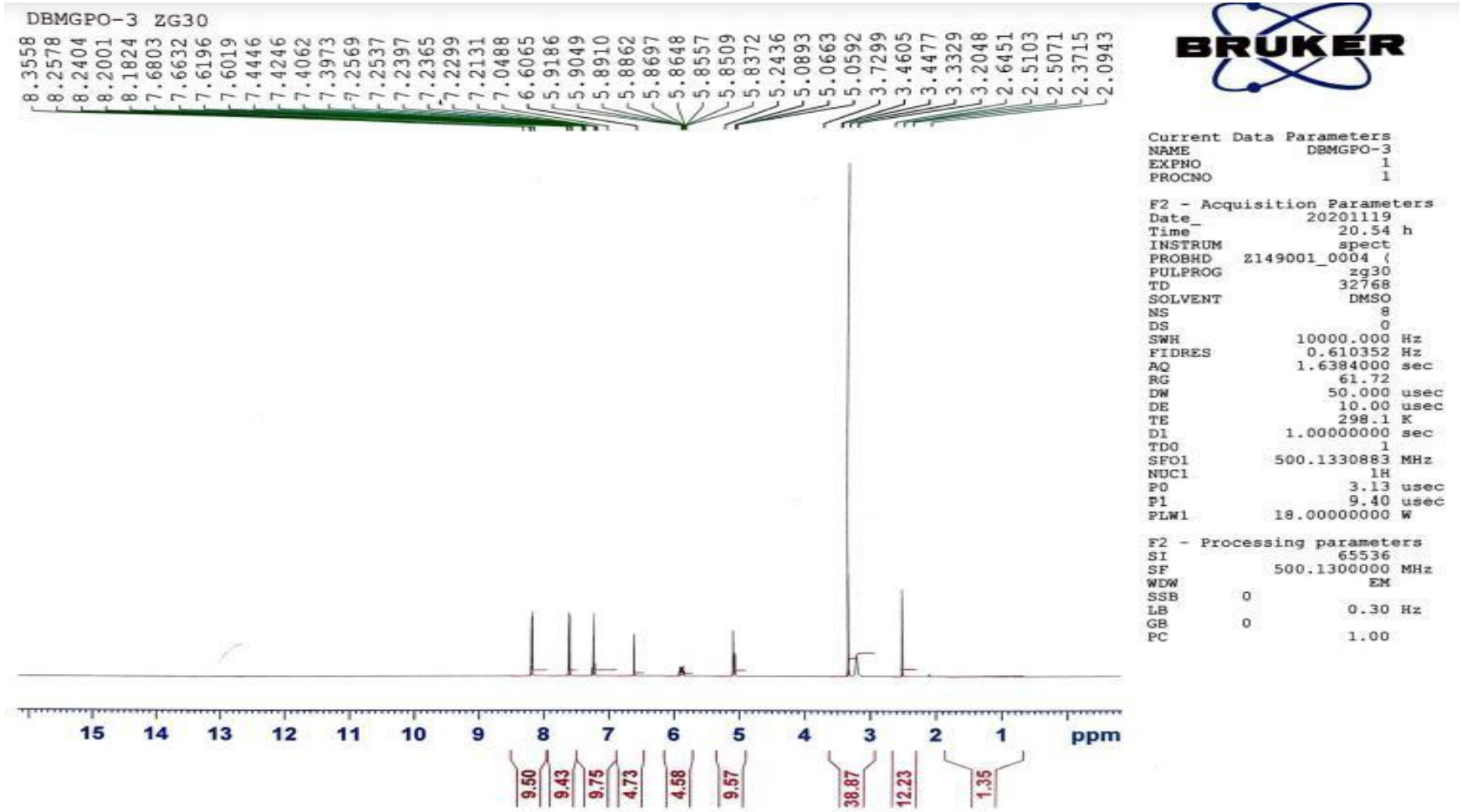

Figure 48. PROTON NMR **DBMGPO-3**

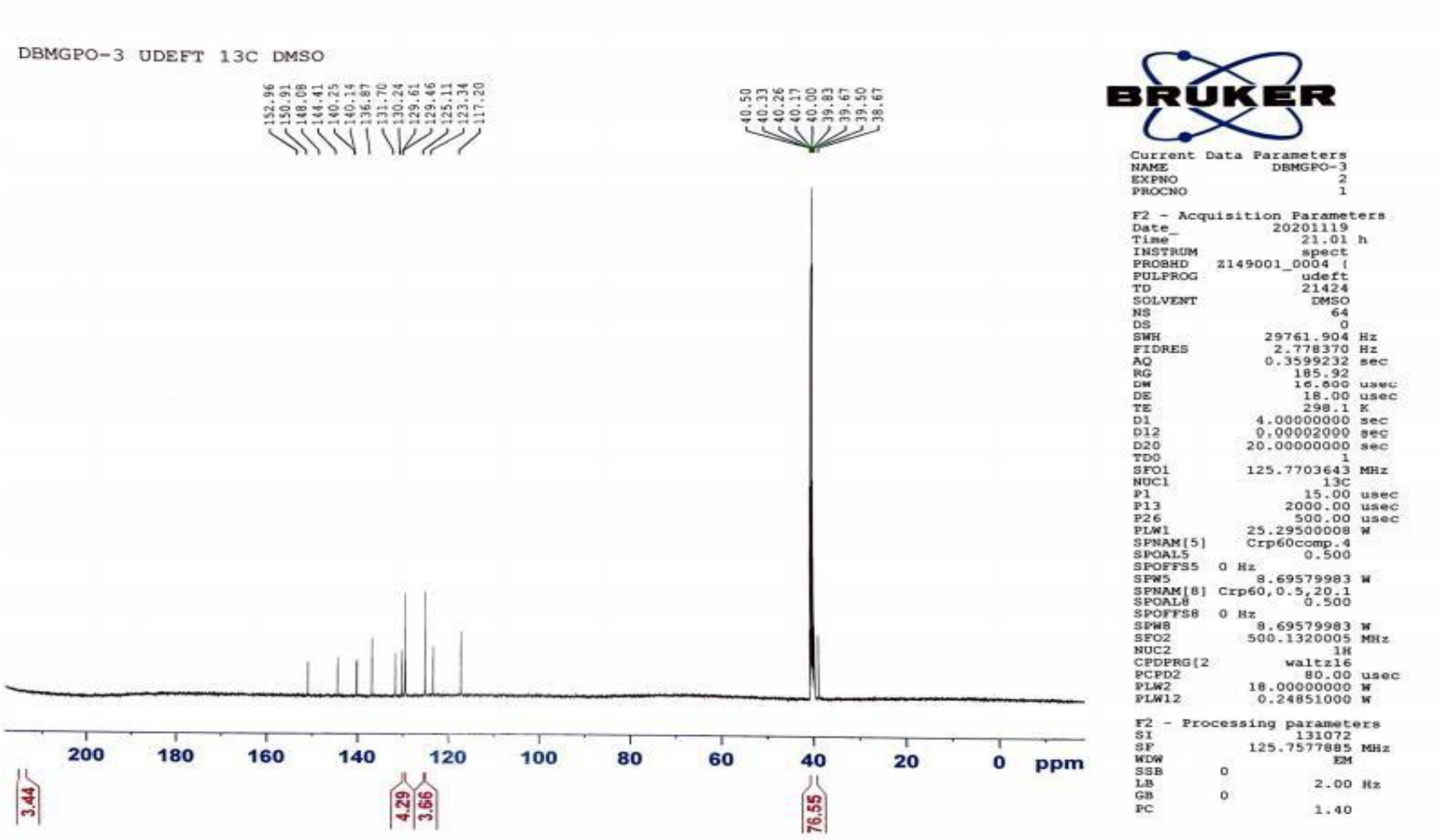

Figure 49. 13 carbon NMR **DBMGPO-3**

5. *5,5'-diallyl-[1,1'-biphenyl]-2,2'-diyl bis(3,5-bis(trifluoromethyl)benzenesulfonate)* **DBMGPO-4**

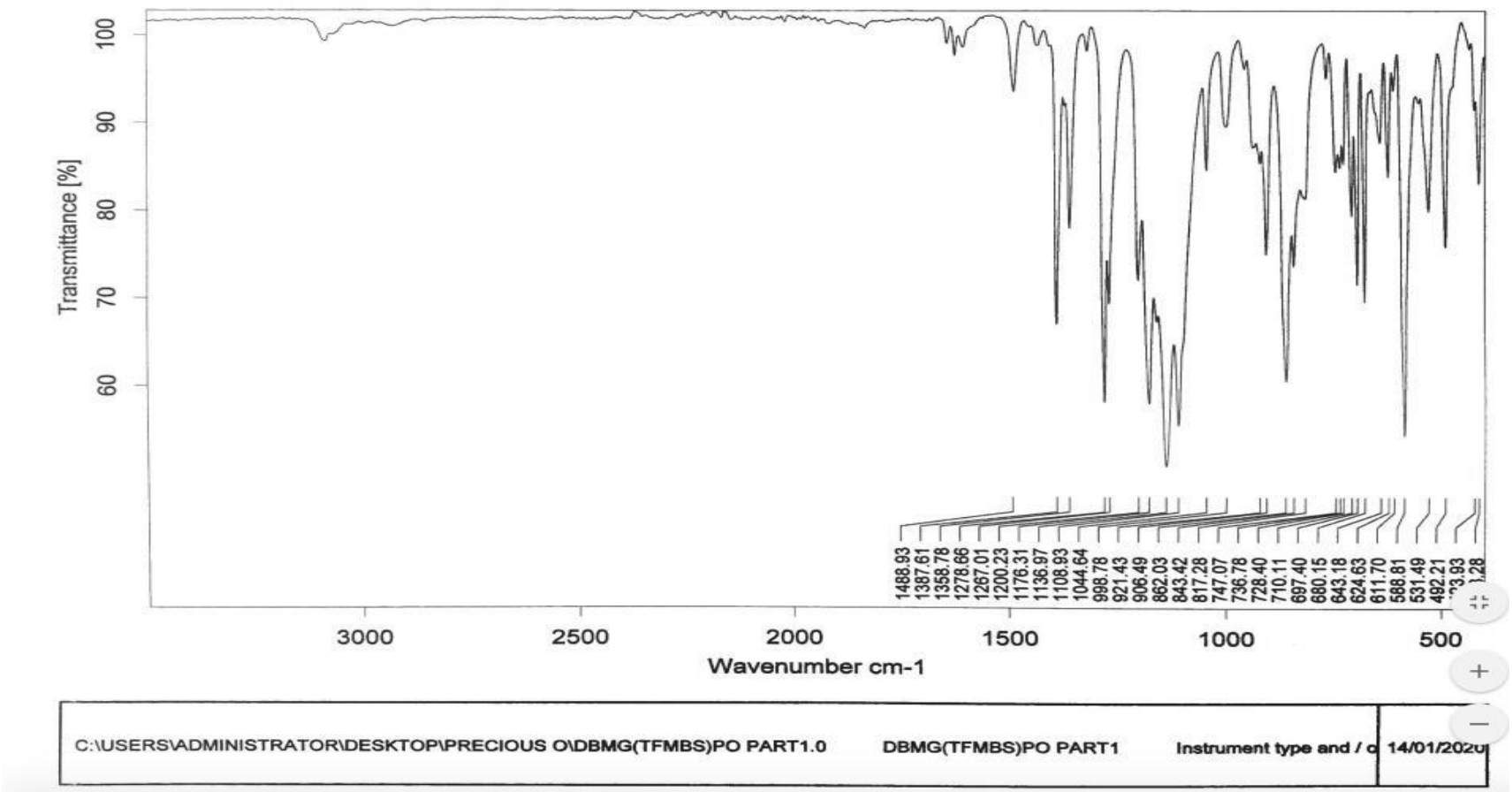

Figure 50. FTIR **DBMGPO-4**

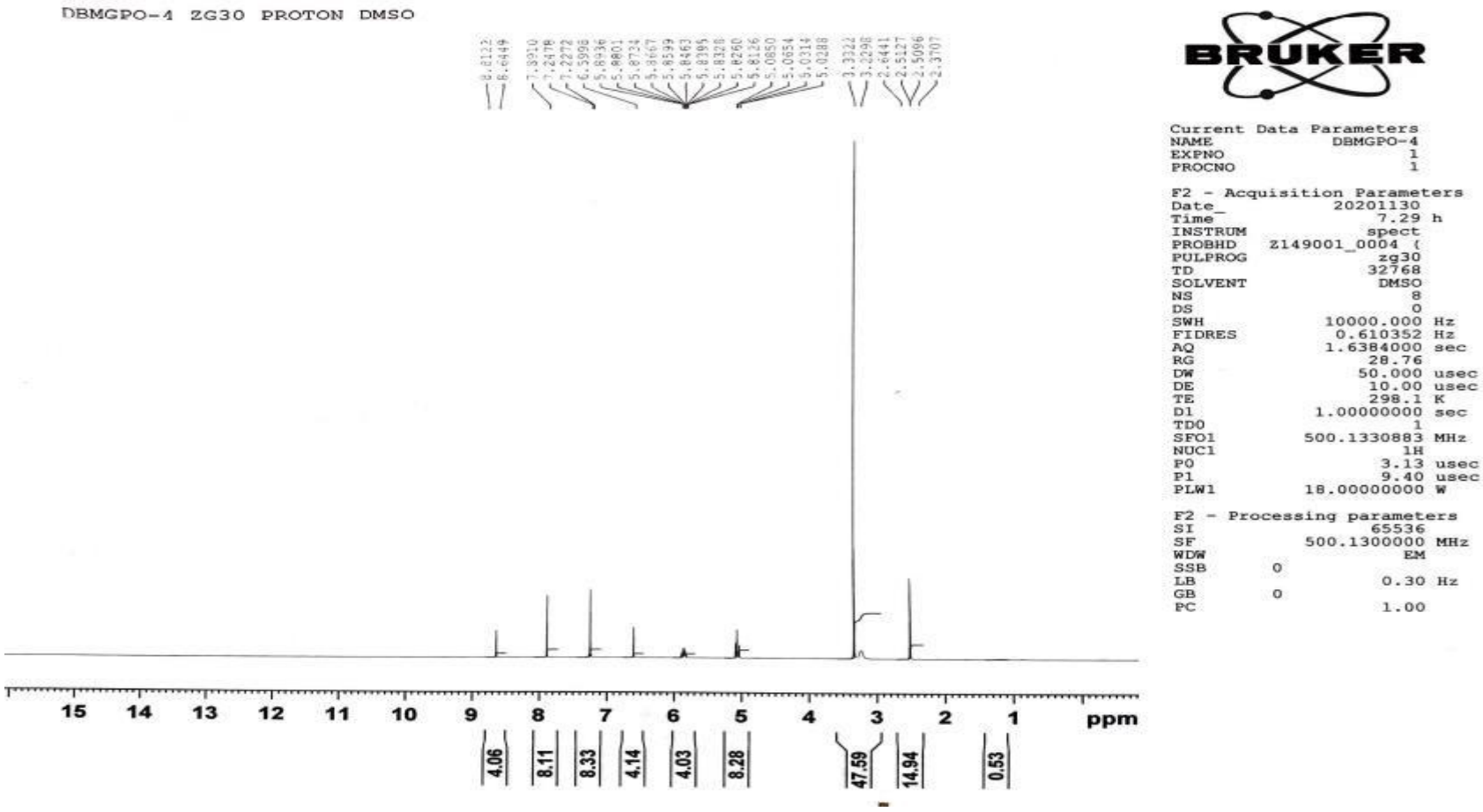

BRUKER

```
Current Data Parameters
NAME                  DBMGPO-4
EXPNO                        1
PROCNO                       1

F2 - Acquisition Parameters
Date_                 20201130
Time                      7.29 h
INSTRUM                  spect
PROBHD     Z149001_0004 (
PULPROG                  zg30
TD                      32768
SOLVENT                  DMSO
NS                           8
DS                           0
SWH                10000.000 Hz
FIDRES             0.610352 Hz
AQ                 1.6384000 sec
RG                       28.76
DW                      50.000 usec
DE                      10.00 usec
TE                      298.1 K
D1                 1.00000000 sec
TD0                          1
SFO1             500.1330883 MHz
NUC1                        1H
P0                       3.13 usec
P1                       9.40 usec
PLW1              18.00000000 W

F2 - Processing parameters
SI                       65536
SF               500.1300000 MHz
WDW                         EM
SSB          0
LB                       0.30 Hz
GB           0
PC                       1.00
```

Figure 51. Proton NMR **DBMGPO-4**

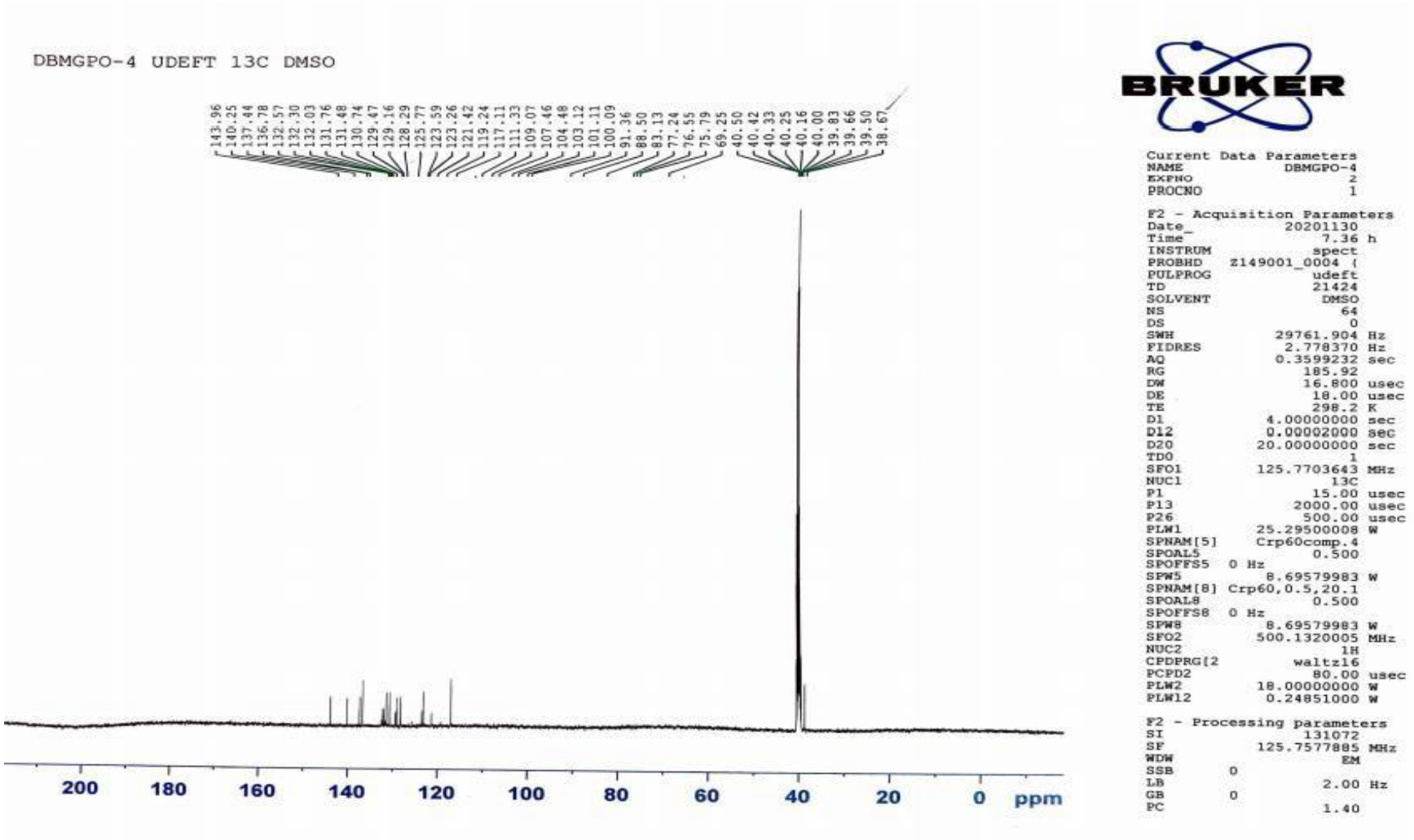

Figure 52. 13 carbon NMR **DBMGPO-4**

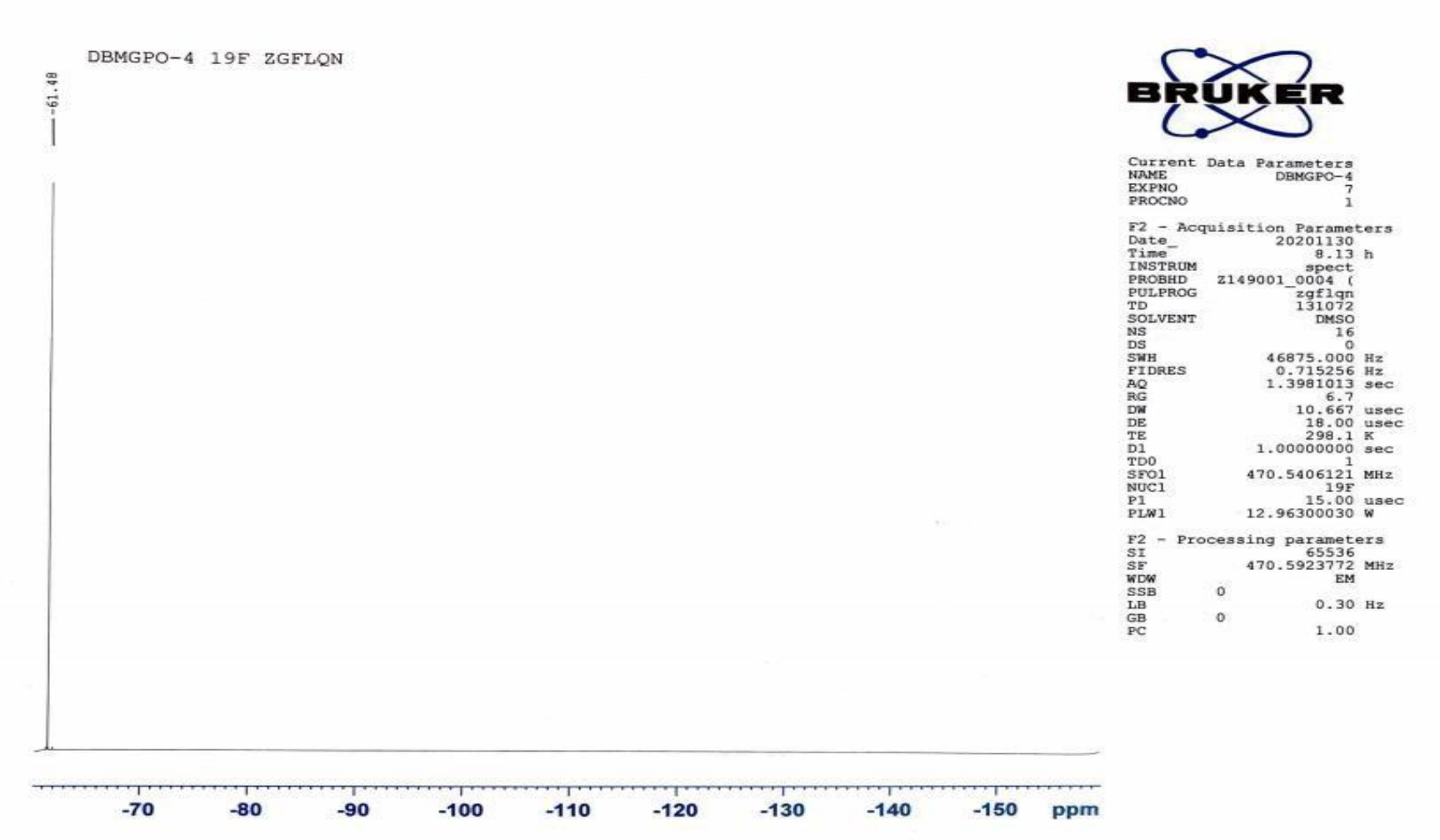

Figure 53. 19F NMR **DBMGPO-4**

6. *5,5'-diallyl-[1,1'-biphenyl]-2,2'-diyl bis(pyrrolidine-1-sulfonate)* **DBMGPO-6**

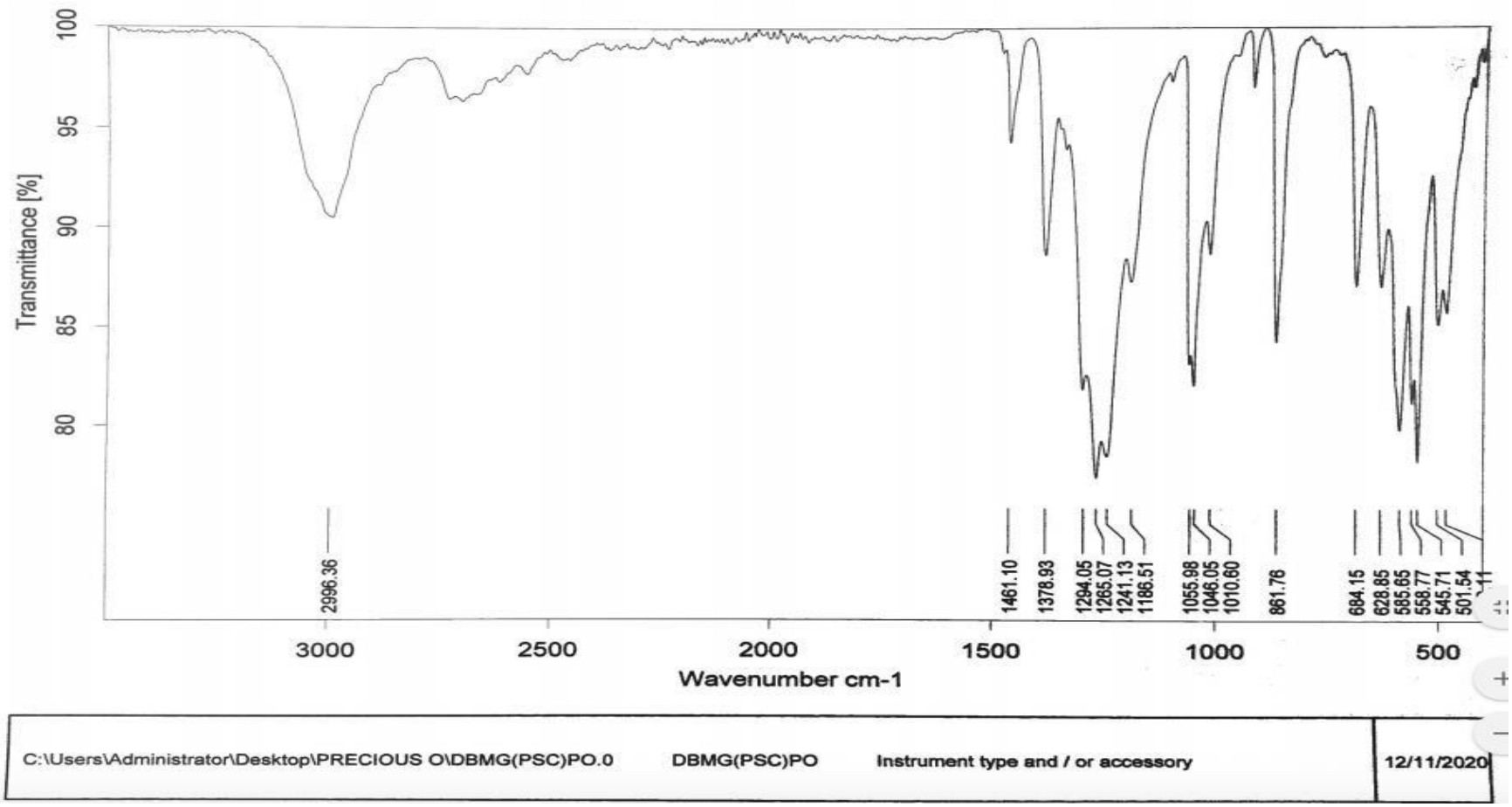

Figure 54. FTIR **DBMGPO-6**

7. *5,5'-diallyl-[1,1'-biphenyl]-2,2'-diyl bis(morpholine-4-sulfonate)* **DBMGPO-7**

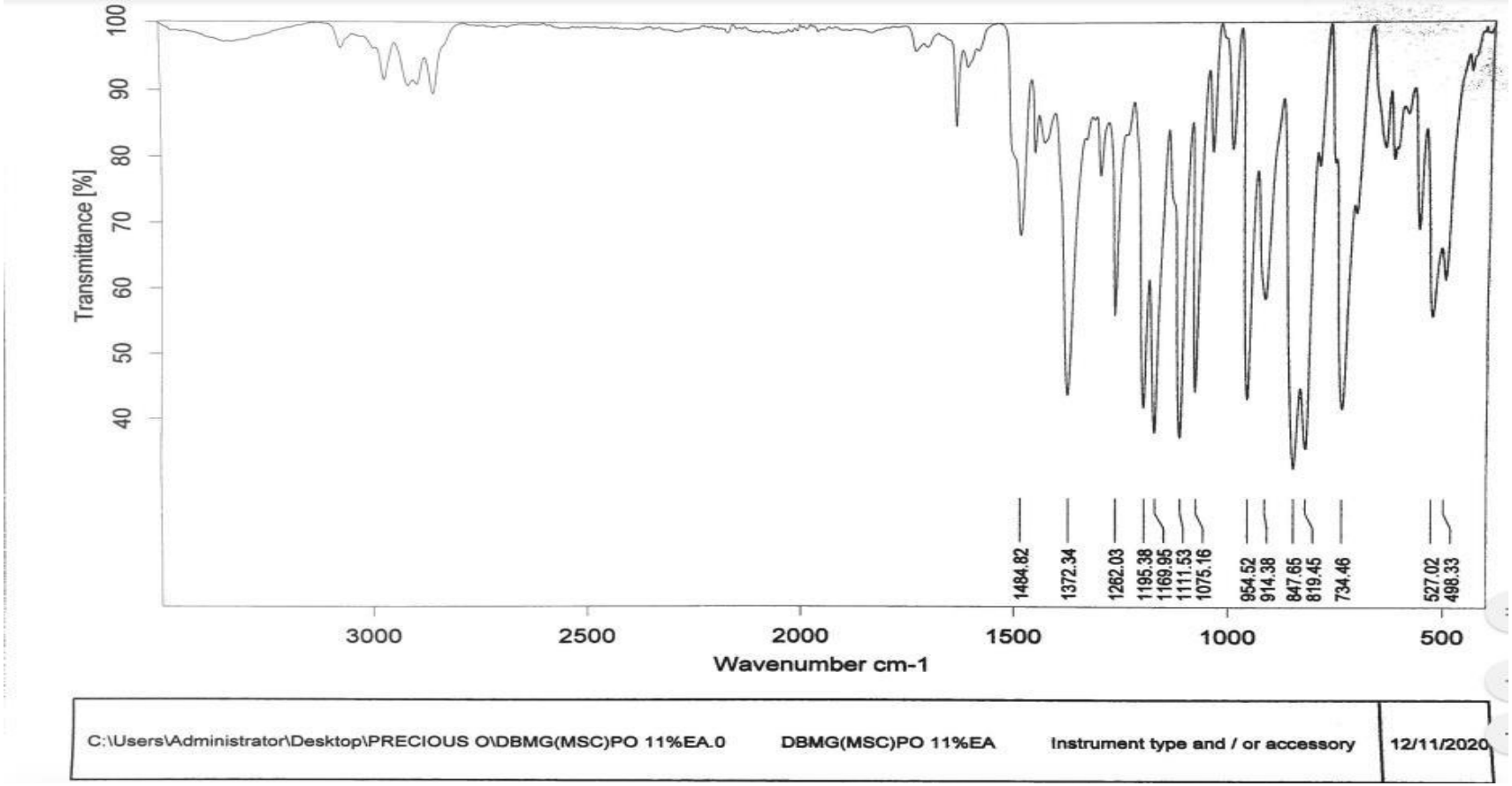

Figure 55. FTIR **DBMGPO-7**

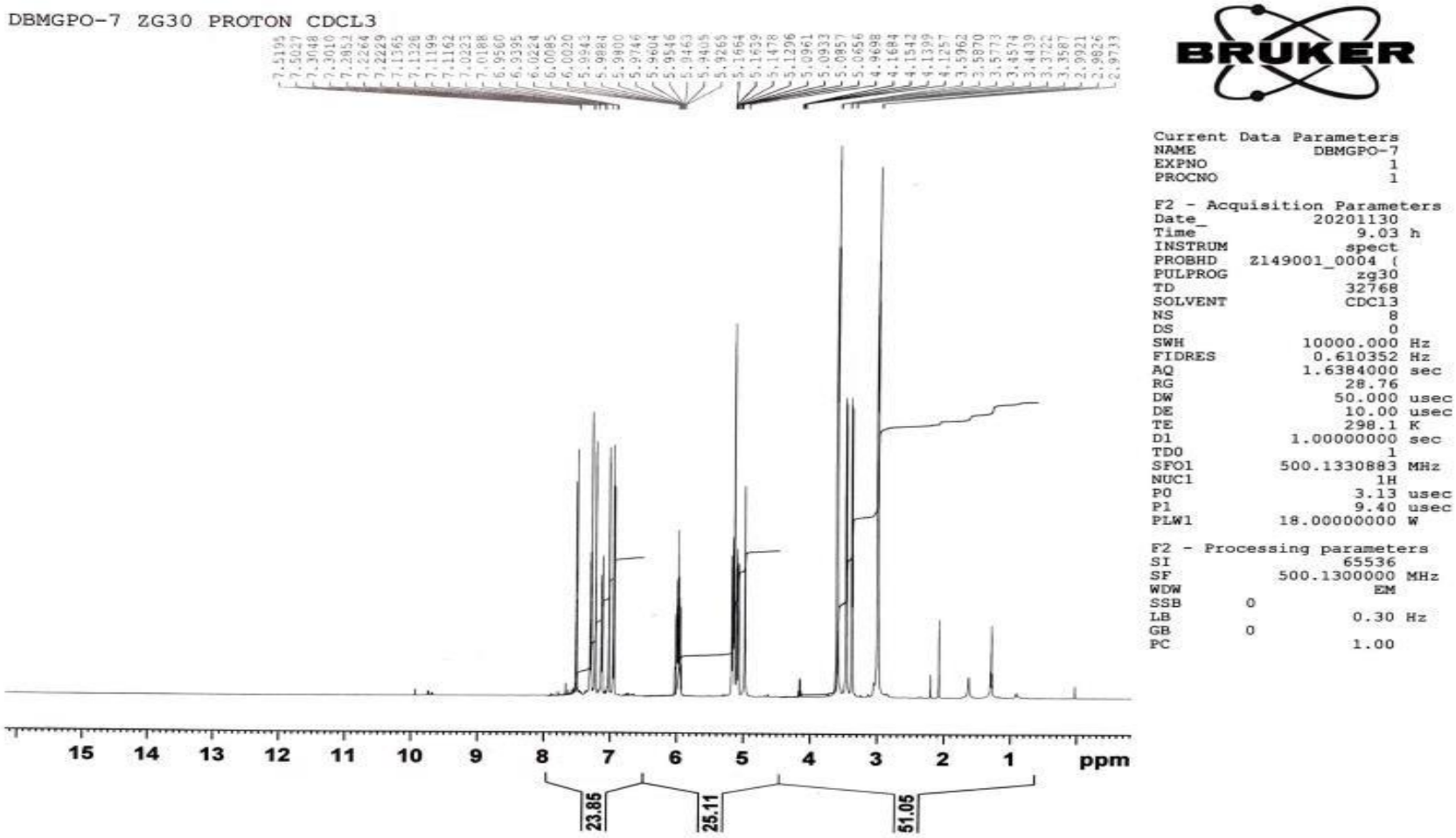

Figure 56. Proton NMR **DBMGPO-7**

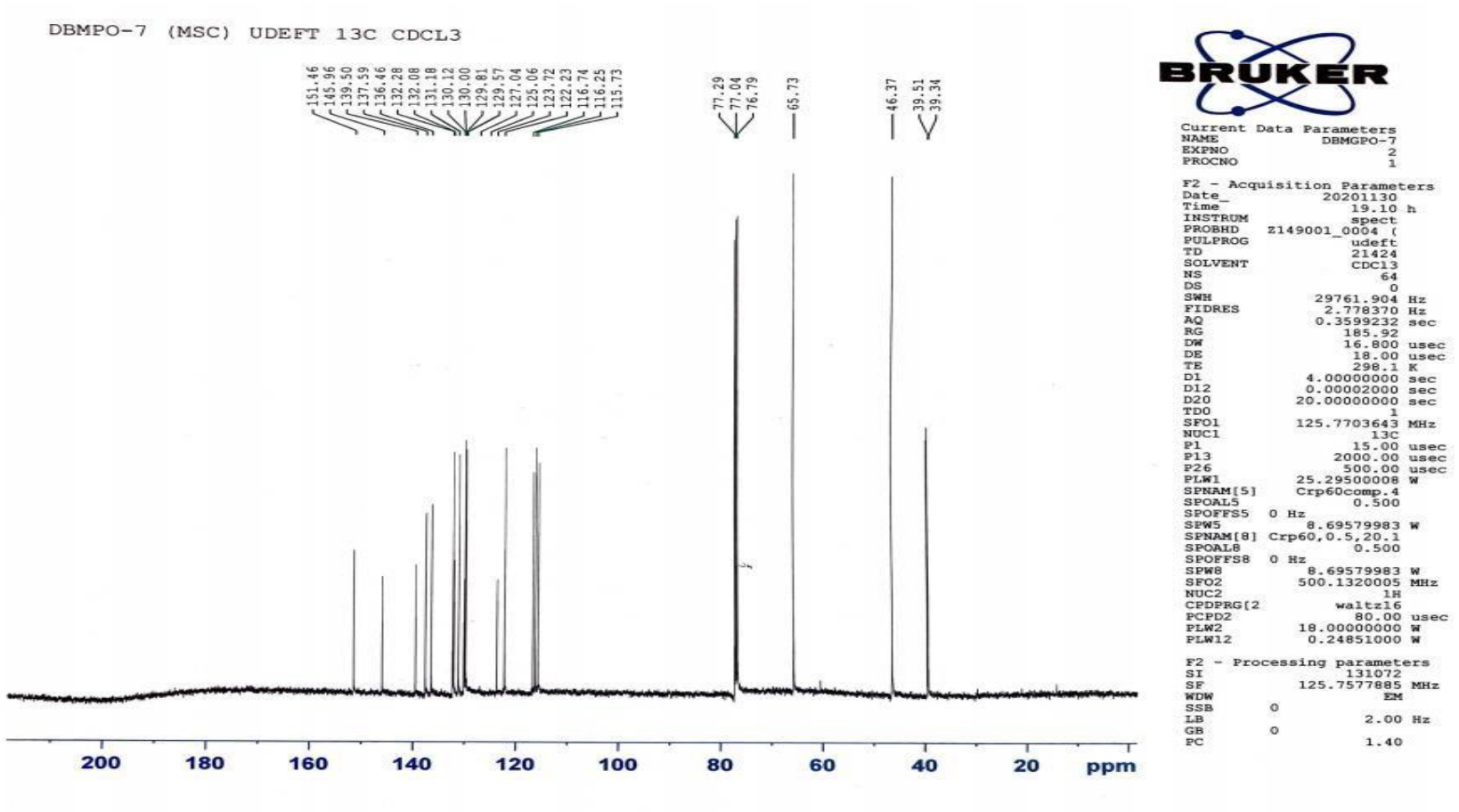

Figure 57. 13 carbon NMR **DBMGPO-7**

8. *5,5'-diallyl-[1,1'-biphenyl]-2,2'-diyl bis(3-cyanoazetidine-1-sulfonate)* **DBMGPO- 8**

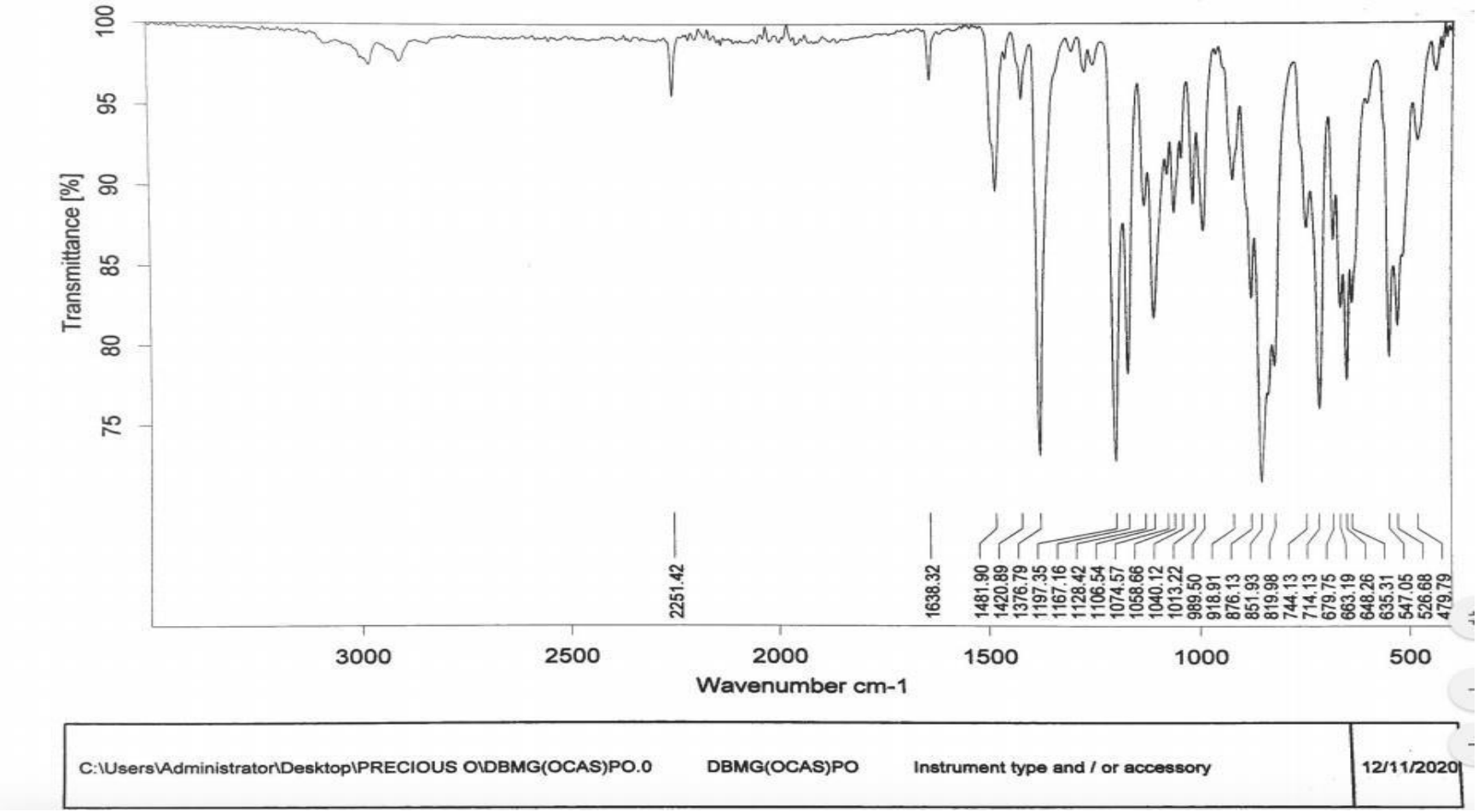

Figure 58. FTIR **DBMGPO-8**

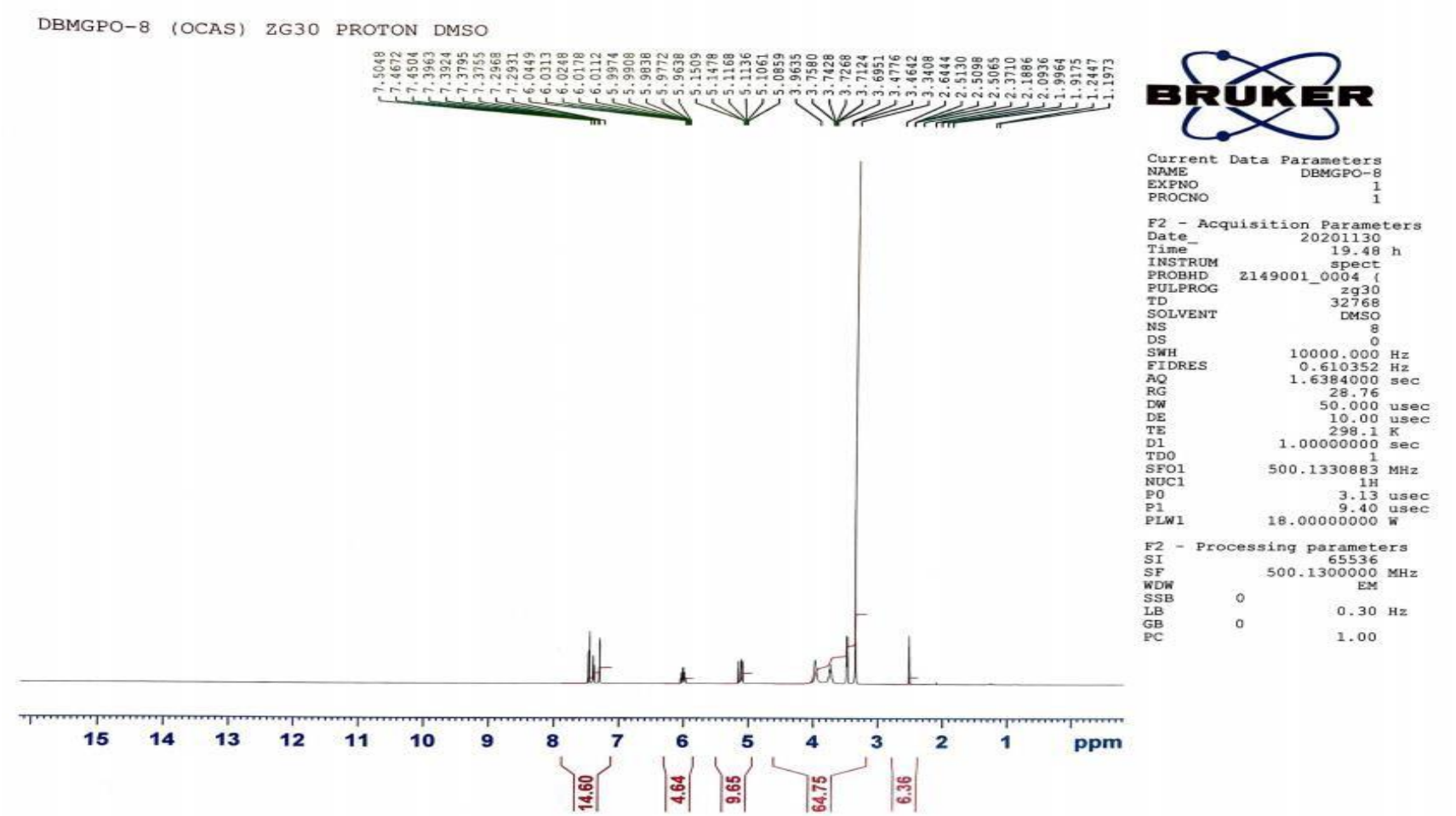

Figure 59. Proton NMR **DBMGPO-8**

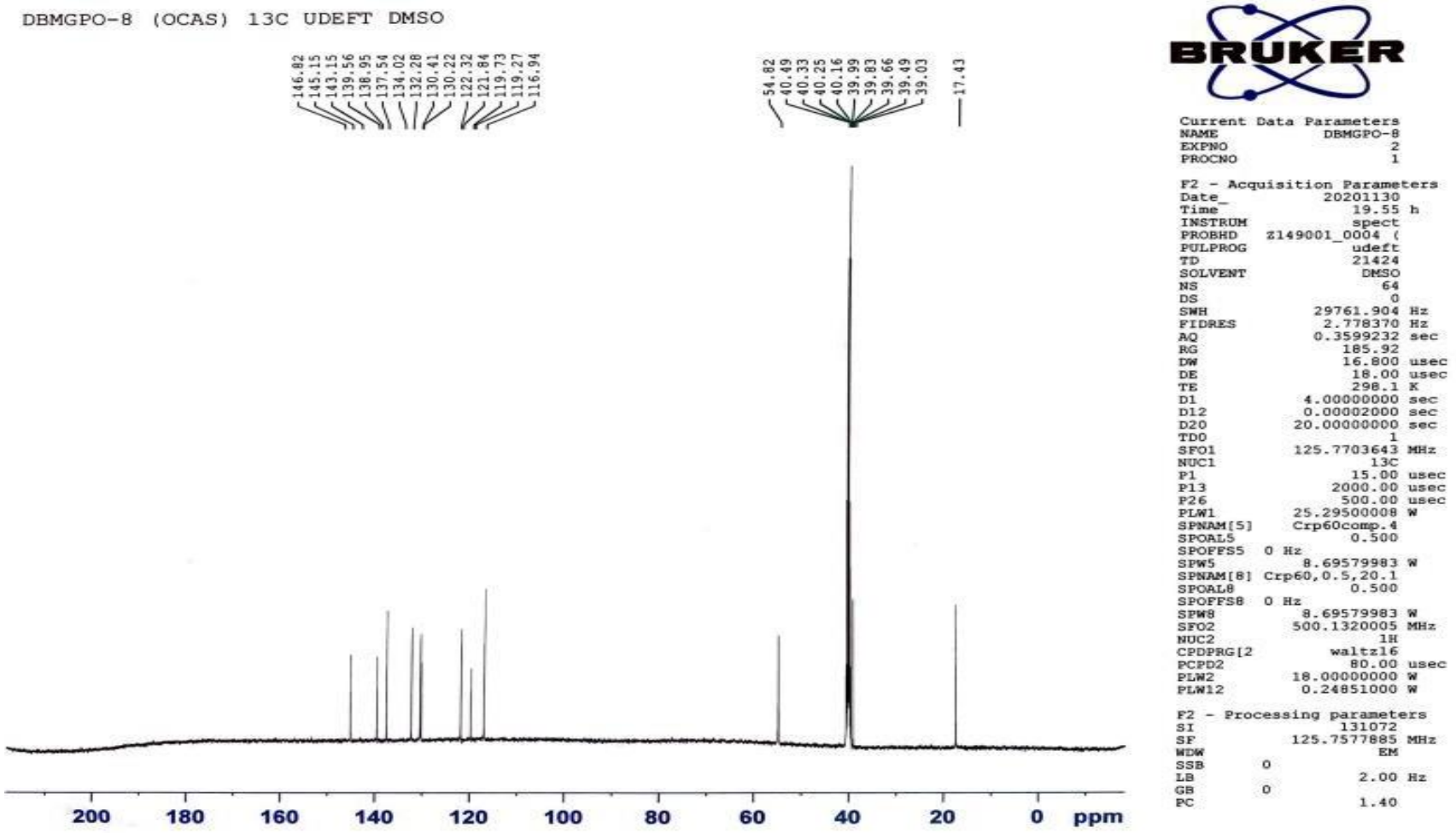

Figure 60. 13 carbon NMR **DBMGPO-8**

9. *(1s,3r,5R,7S)-3-aminoadamantan-1-yl 3-cyanoazetidine-1-sulfonate* **DBADAPO-1A**

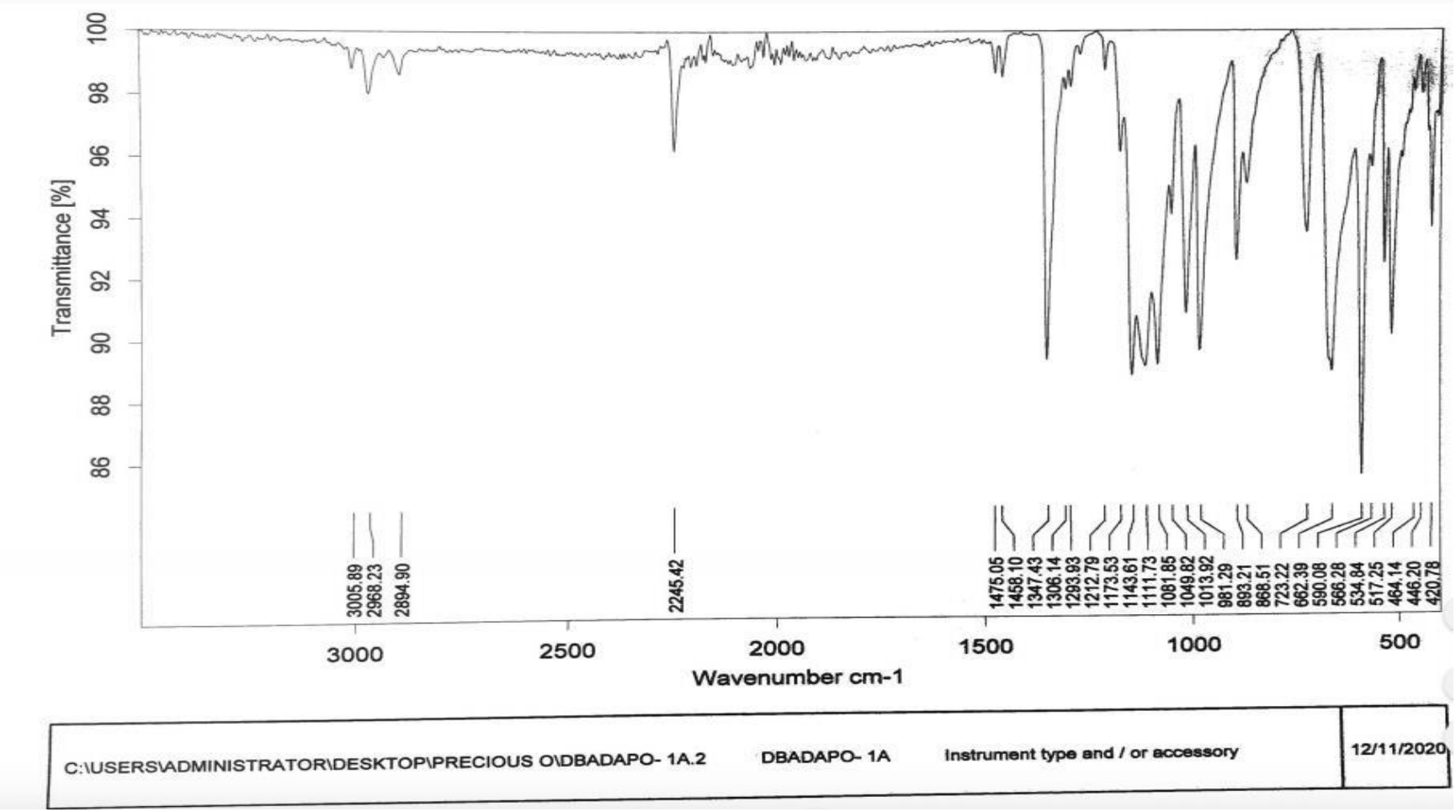

Figure 61. FTIR **DBADAPO-1A**

10. *(1s,3r,5R,7S)-3-(3-cyanoazetidine-1-sulfonamido) adamantan-1-yl 3-cyanoazetidine-1-sulfonate* **DBADAPO-1B**

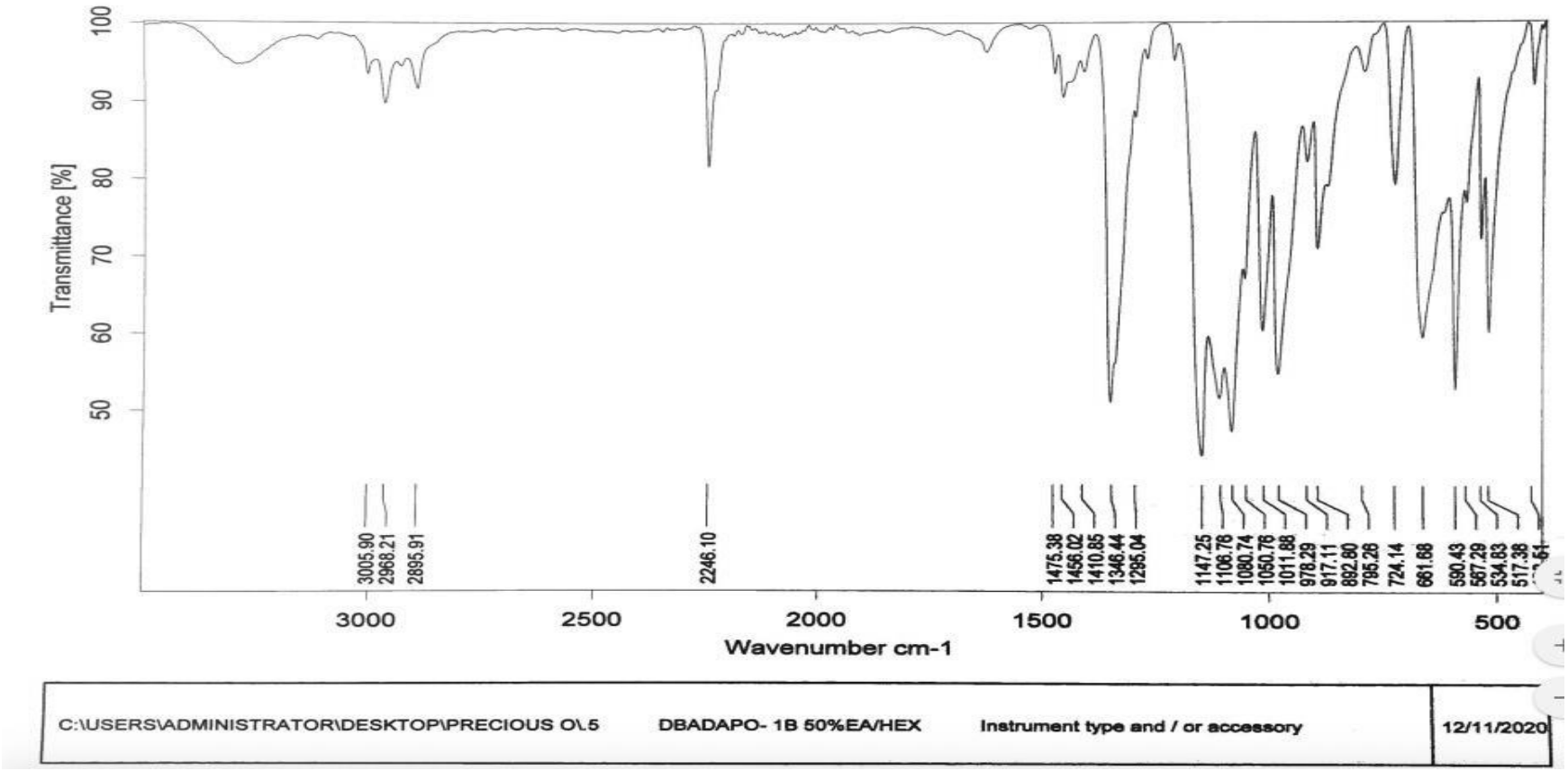

Figure 62. FTIR **DBADAPO-1B**

11. *1s,3r,5R,7S)-3-(3-cyano-N-((3-cyanoazetidin-1-yl)sulfonyl)azetidine-1-sulfonamido) adamantan-1-yl 3-cyanoazetidine-1-sulfonate*
DBADAPO-1C

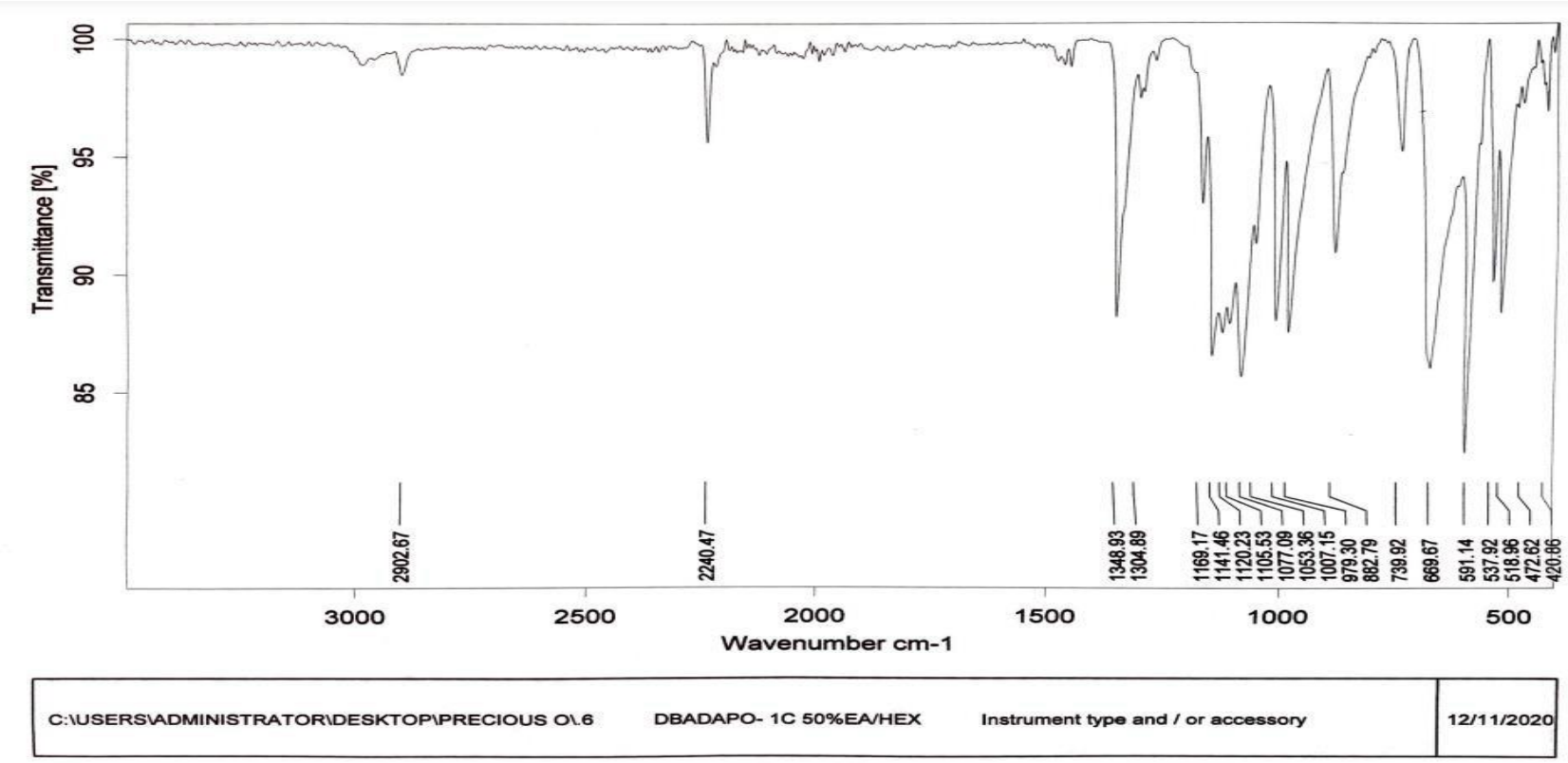

Figure 63. FTIR **DBADAPO-1C**

12. *N-(7-chloroquinolin-4-yl)-3-cyanoazetidine-1-sulfonamide* **DBQPO-1A**

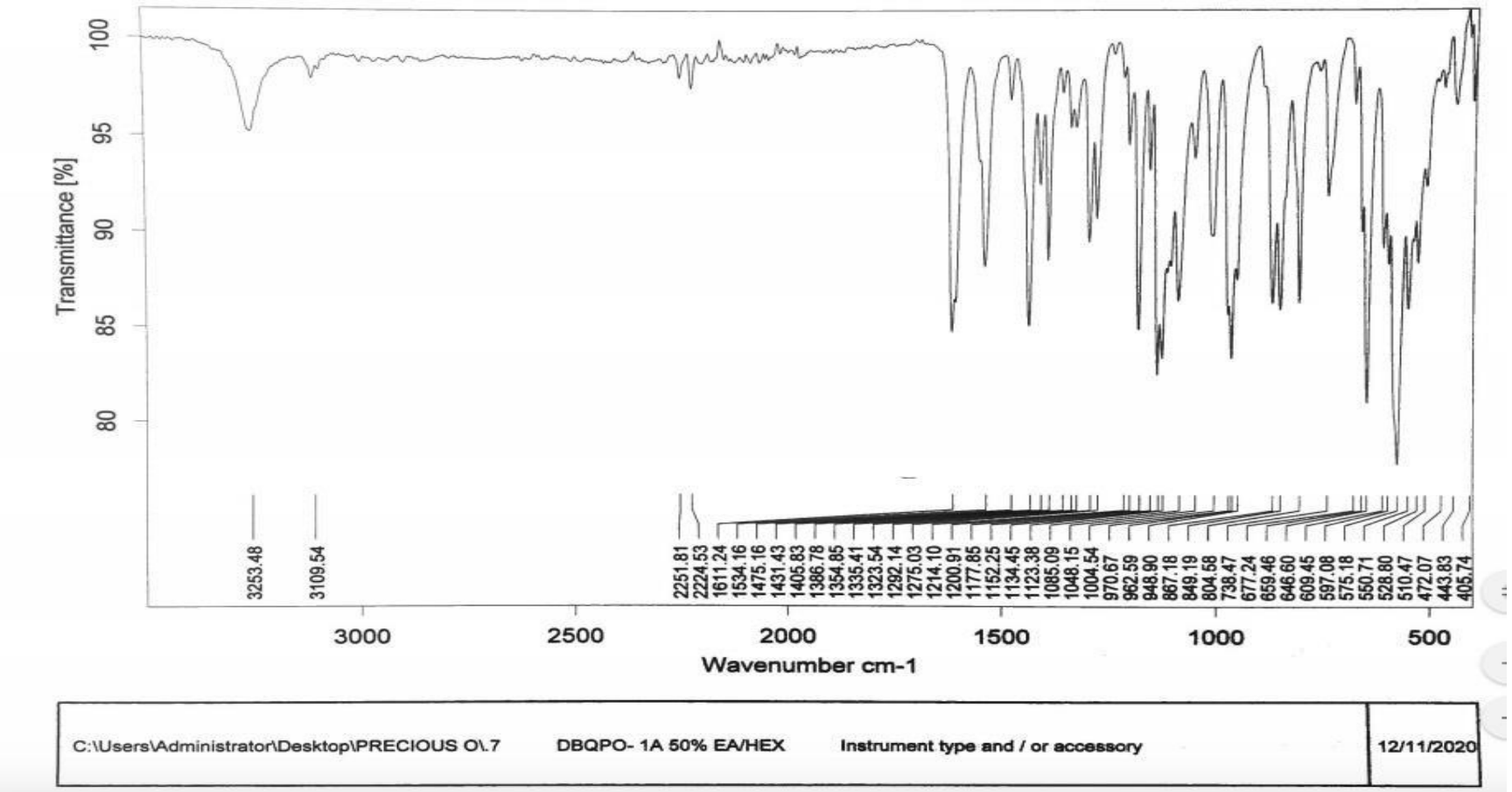

Figure 64. FTIR **DBQPO-1A**

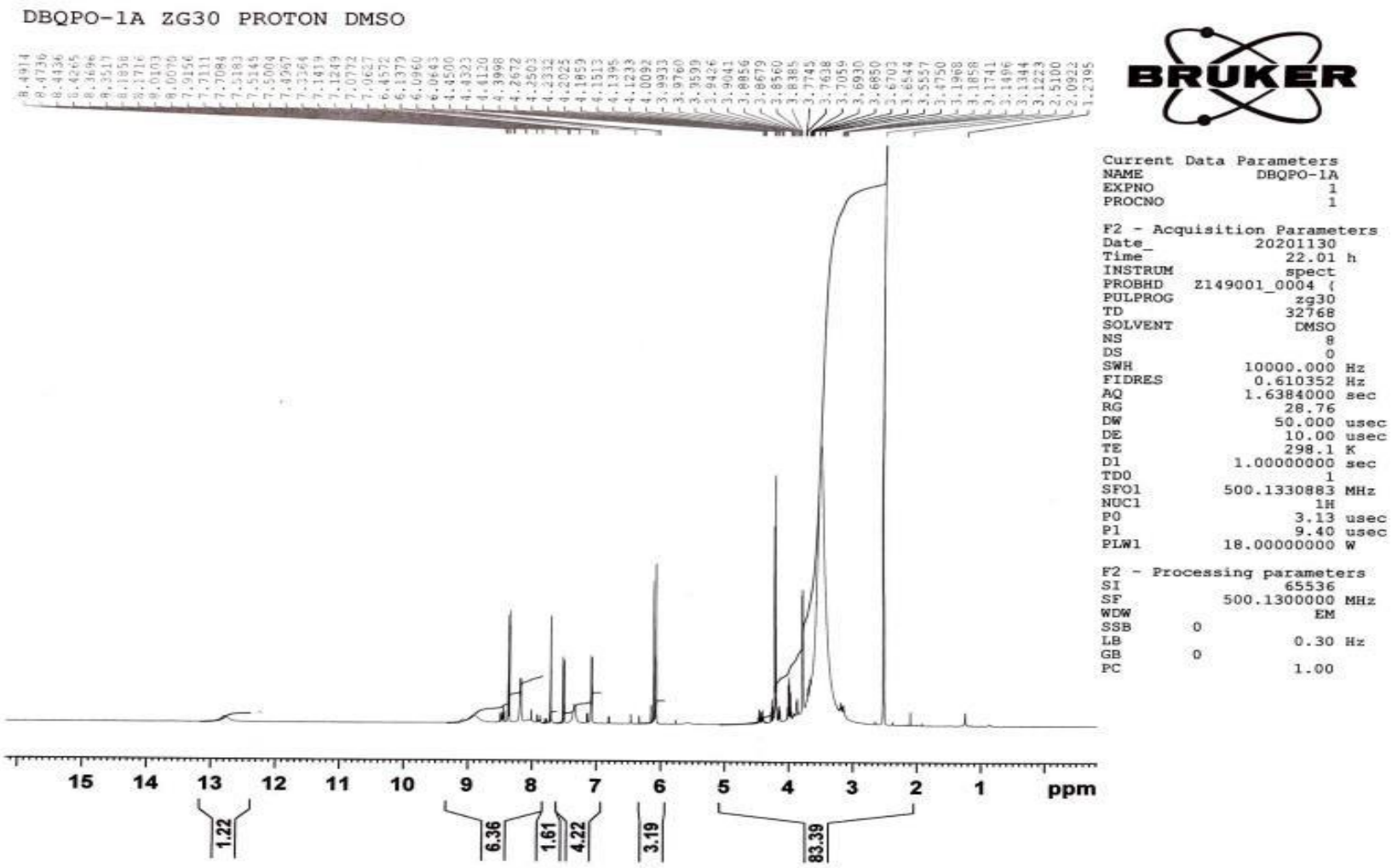

Figure 65. Proton NMR **DBQPO-1A**

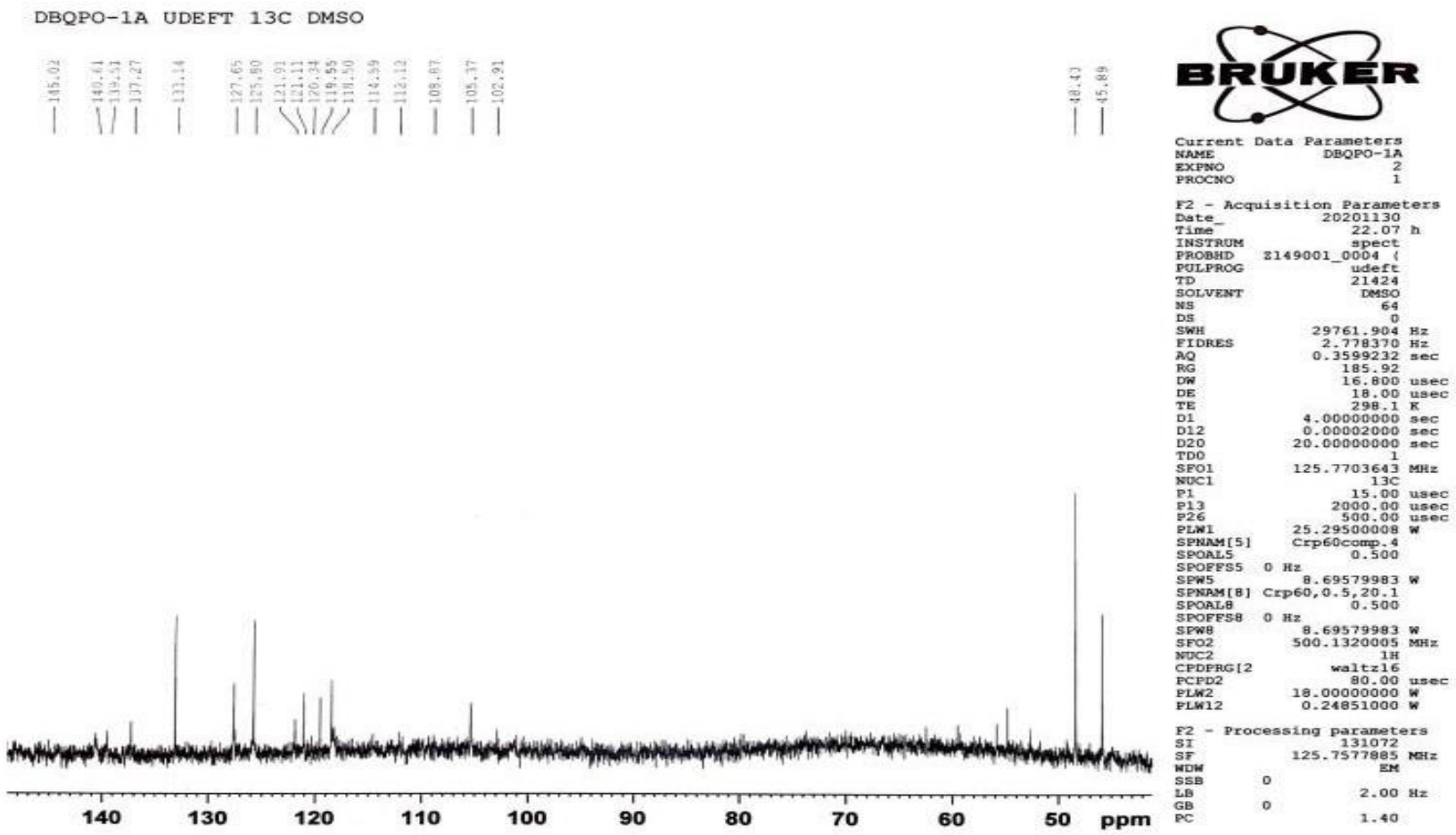

Figure 66. 13 carbon NMR **DBQPO-1A**

13. *N-(7-chloroquinolin-4-yl)-3-cyano-N-((3-cyanoazetidin-1-yl)sulfonyl)azetidine-1-sulfonamide* **DBQPO-1B**

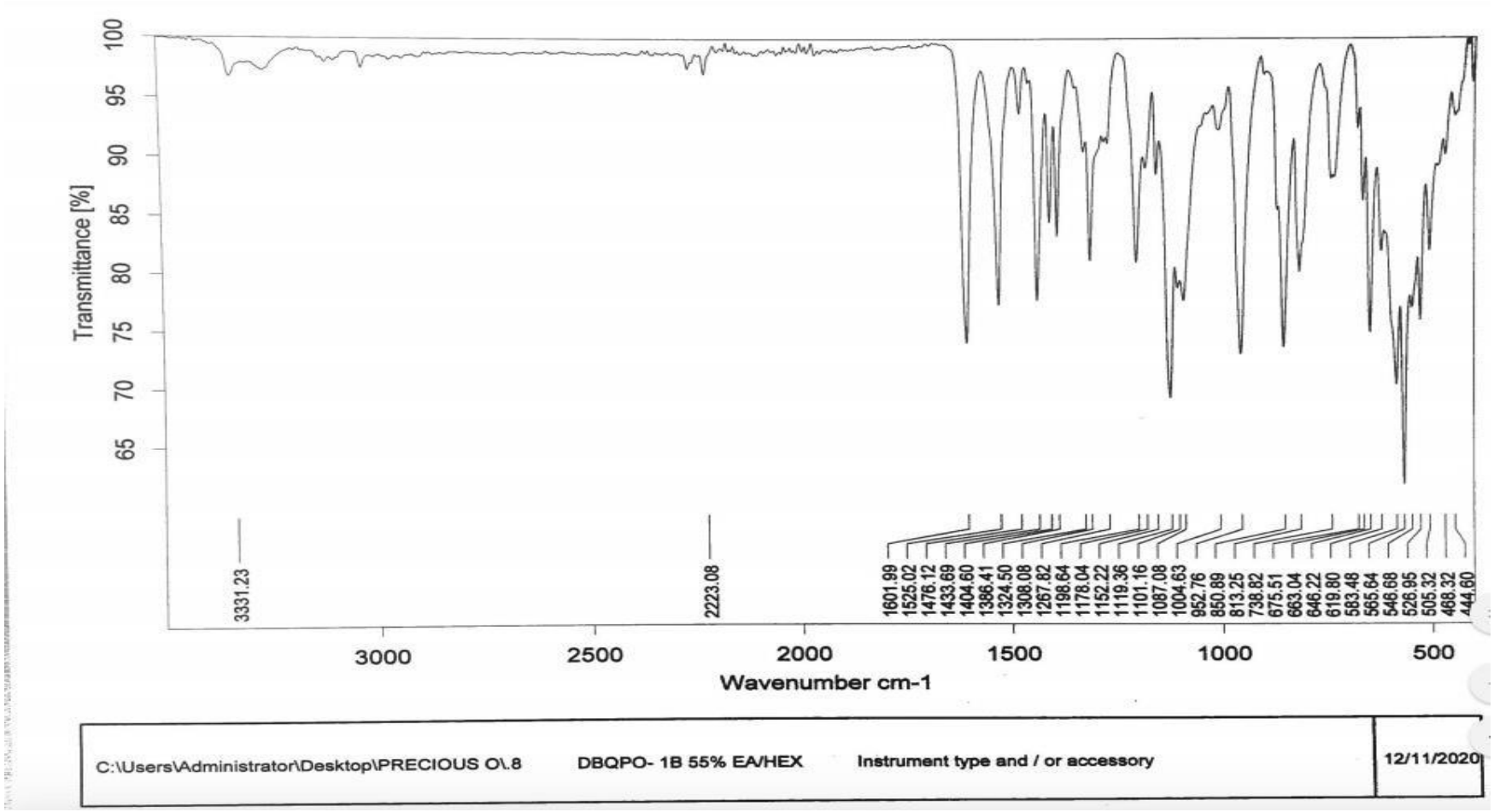

Figure 67. FTIR **DBQPO-1B**

14. *N-(7-chloroquinolin-4-yl)-4-(trifluoromethyl)benzenesulfonamide* **DBQPO- 2A**

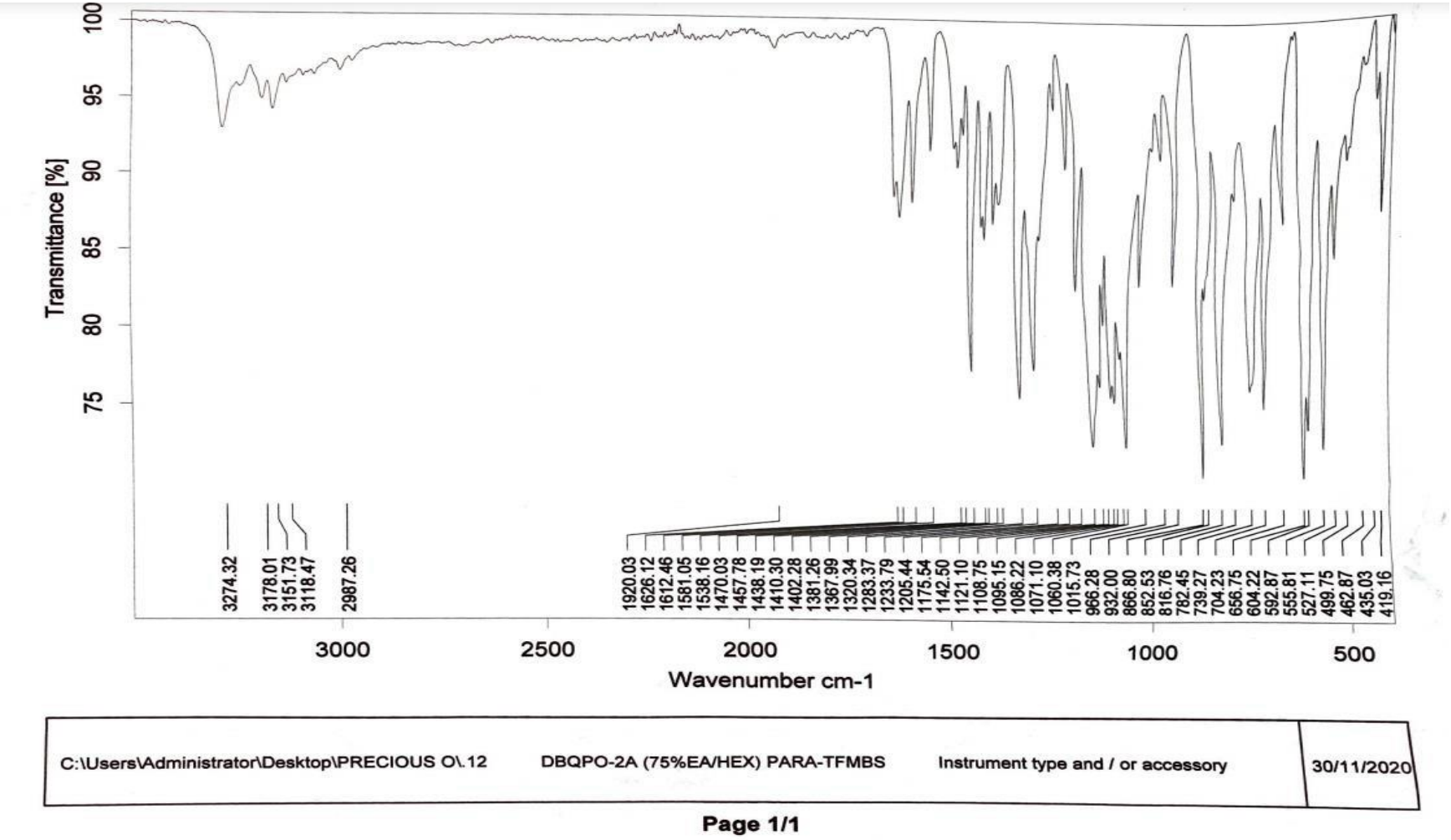

Figure 68. FTIR **DBQPO-2A**

15. *N-(7-chloroquinolin-4-yl)-4-(trifluoromethyl)-N-((4-(trifluoromethyl)phenyl)sulfonyl)* benzenesulfonamide **DBQPO- 2B**

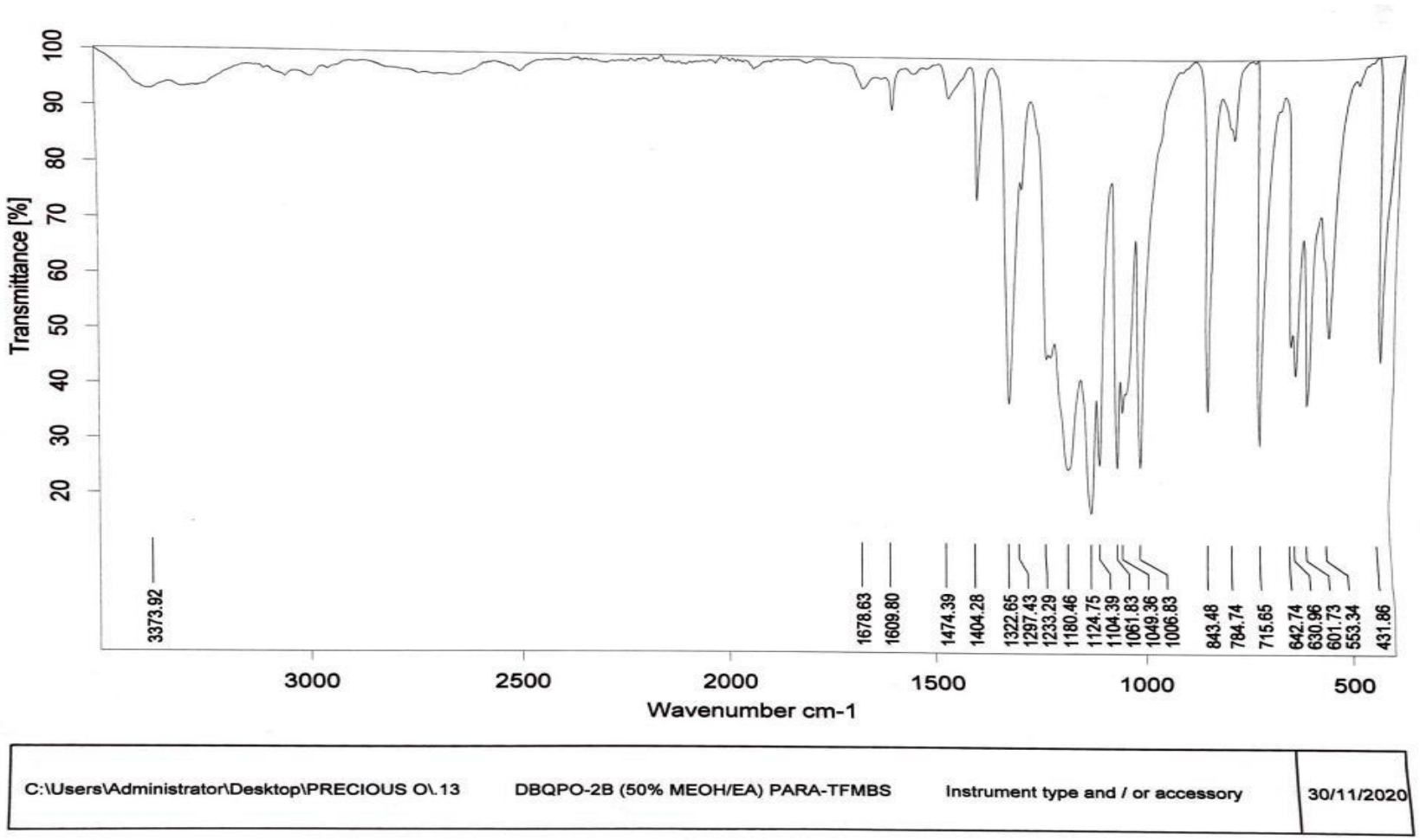

Figure 69. FTIR **DBQPO-2B**

BIOGRAPHICAL SKETCH

Precious Makuo Okwuchukwu started her master's program at the University of Texas Rio Grande Valley in 2019. She received a Bachelor of Science degree (2015) in Pharmacy from SRM Institute of Science and Technology in India. She practiced as a pharmacist in Nigeria for four years before deciding to pursue her master's degree in chemistry. During her master's program, she worked as a research assistant under the supervision of Dr. Debasish Bandyopadhyay. She receives a Master of Science degree in Chemistry in December of 2020. She can be reached at: okwuchukwupreciousm@gmail.com